Nanofibers and Nanoporous Metal Oxides for Gas Sensing Applications

A thesis submitted in fulfilment of the requirements for the degree of Doctor of Philosophy

Rosmalini Ab Kadir

BEng. Electrical

MSc. Microelectronics

School of Electrical and Computer Engineering

College of Science Engineering and Health

RMIT University

March 2015

Declaration

I certify that except where due acknowledgement has been made, the work is that of the author alone; the work has not been submitted previously, in whole or in part, to qualify for any other academic award; the content of the thesis/project is the result of work which has been carried out since the official commencement date of the approved research program; any editorial work, paid or unpaid, carried out by a third party is acknowledged; and, ethics procedures and guidelines have been followed.

Rosmalini Ab Kadir

9 July 2015

Acknowledgements

First and foremost, I would like to express my heartfelt gratitude to Professor Kourosh Kalantar-zadeh as my first supervisor for his excellent supervision and encouragement during my PhD candidature. I greatly benefited from his keen scientific insight and persistently offered assistance on my experiments and research papers. He always engaged me in new ideas and his passion for research was a great inspiration for me throughout my PhD candidature. I would also like to thank my second supervisor Dr. Sharath Sriram for his valuable knowledge, ideas and discussions towards my candidature. I would also like to thank the various members in the group:, Dr. Rozina Abdul Rani, Dr. Ahmad Sabirin, Dr Jianzhen Ou, Dr Sumeet Walia, Dr. David Yao, Dr Adam Chrimes, Dr Sivacarendran Balendhran, Dr. Majid Nour, Ms Pyshar Yi, Mr. Wei Zhang, Mr. Kyle Berean and Ms Manal Al Saif. They provided a friendly and cooperative environment and also insightful comments on my work.

Appreciation also goes out to the RMIT Microelectronics and Materials Technology Centre (MMTC) technical staffs, specifically, Mr. Yuxun Cao, Mr. Paul Jones and Ms Chi Ping as well as Mr. Philip Francis and Dr. Matthew Field from the RMIT Microscopy and Microanalysis Facility (RMMF) for all assistance throughout my candidature. I am grateful for the funding sources that allowed me to pursue my studies. My research would not have been possible without the financial support from the Malaysia Ministry of Education (MOE) and MARA University of Technology. I would also like to acknowledge the additional financial support and conference funding from the School of Electrical and Computer Engineering (SECE) and School of Graduate Research (SGR), RMIT.

Not to forget, I would also like to extend my appreciation to close friend: Ms Nurul Huda, Ms Faradila, Ms Siti Hajar, Ms Nurhazlin Khairudin, Ms Yusnira Husaini, Ms Robi'atun Adayiah Awang, Ms Syazilawati, Ms Khadijah, Ms Sarah and Ms Dharma Aryani and families for their support during ups and downs of this PhD journey. My dearest friends, who are far but yet so close, ladies of 96, Sekolah Menengah Sains Tengku Muhammad Faris Petra, thank you very much for your prayers and encouragements.

A special contribution to my husband, Syed Nasaruddin Syed Idris for his understanding and great supports when I needed it most. Your prayers for me were what sustained me thus far. To my beloved daughters, Syarifah Nur Insyirah and Syarifah Nur Fatini, hats off to both of you for understanding a busy mum like me. Special thanks to sisters: Ros Hidayu, Roshatikah, Amira Shafiniey and Anis Suraya for their willingness to take turns to accompany me here in Melbourne. Finally, I am also very grateful to my parents, Ab Kadir Haron and Rozan Yusoff as well as the whole family for their constant love and pray without which, I would have never reached so far.

Dedication

To Abang, Kakak, Adik, Ma and Abah the whole family, for their love and support.

Abstract

Air pollution is one of the greatest problems that the world facing is facing today. The World Health Organization (WHO) has provided air quality guidelines, which represent the most widely agreed and up-to-date assessments of air pollutants on human health, recommending stringent thresholds for air quality. This consequently signifies the need to develop gas sensors with the specifications that meet WHO targets. Additionally, gas sensors are also used in variety of other applications such as in many industrial surveillance and processes, automotive, aviation and food industries, medical analysis and diagnostics as well as homeland security and defense.

Gas sensing using semiconducting oxides has had considerable progress to date. It has been demonstrated that the key factors for developing efficient semiconducting gas sensors is to make use of selected metal oxides after engineering their morphologies and crystallographies. It is well-known that nanostructured metal oxides are generally superior in performance due to their high specific surface area. This increased surface area facilitates the reactive adsorption/desorption of different gas species onto the sensitive metal oxide layer and thus, augments performance of the sensors. Additionally nanostructuring can help in tuning of the electronic band structure of the metal oxide sensing layer, enhancing both selectivity and sensitivity. Hence, searching for the right nanostructured metal oxides with high specific surface area and controllable structures for effective gas sensing is an important research goal nowadays. Nanostructuring can be carried out *via* obtaining various nano morphologies. Many studies, however, have focused on creating nanofibers and nanopores as these morphologies are recognized to be amongst the most efficient for gas sensing applications.

Due to the aforementioned justifications, the author of this PhD thesis became involved in the investigation of three different metal oxide nanofibers and nanopores metal oxides, which are tin oxide (SnO_2) nanofibers, niobium oxide (Nb_2O_5) and tungsten trioxide (WO_3) nanopores in both nanoporous and nanofibrious structures. There are many different types of gas sensors including those based on conductometric, Schottky and optical templates. In this research, the PhD candidate explored these three templates and investigated their performances when nanofibers and nanopores SnO_2, Nb_2O_5 and WO_3 sensitive layers are incorporated with them. To develop the nanostructured sensing films, the author chose electrospinning and anodization synthesis methods which are the most compatible for forming nanofibrious and nanoporous structures.

In the first stage, the PhD candidate demonstrated hydrogen (H_2) gas sensors based on hollow and filled well-aligned electrospun SnO_2 nanofibers, operating at a low temperature of 150 °C. SnO_2 nanofibers with diameters ranging from 80 to 400 nm were successfully synthesized in which the diameters of the nanofibers were controlled by adjusting the concentration of polyacrylonitrile in the solution for electrospinning. The presence of this polymer resulted in the formation of granular walls for the nanofibers. The PhD candidate innovatively investigated the correlation between nanofibers morphology, structure, oxygen vacancy contents and the gas sensing performances. X-ray photoelectron spectroscopy analysis revealed that the granular hollow SnO_2 nanofibers, which showed the highest responses, contained a significant number of oxygen vacancies, which were favorable for gas sensor operating at low temperatures.

In the second stage of this research, the PhD candidate developed nanoporous Nb_2O_5 Schottky diode based ethanol (C_2H_5OH), H_2 and methane (CH_4) sensors. In this project, 1 μm thick Nb_2O_5 nanoporous films were successfully synthesized *via* an

anodization method at elevated temperatures using mixed solution of ethylene glycol, ammonium fluoride (NH_4F) and little amount of water. The fabricated sensors consist of a fairly ordered nano-vein like porous Nb_2O_5. Subsequently, platinum (Pt), palladium (Pd) and gold (Au) were sputtered as both Schottky contacts and catalysts for the comparative studies. The sensing behaviours were studied in terms of the Schottky barrier height variations and properties of the metal catalysts. Based on the results obtained, it was concluded that sensor with the Pd catalyst offered the best performance. The better performance of the Pd-Nb_2O_5 gas sensor was attributed to the properties of Pd catalyst, allowing more efficient breakdown of ethanol molecules and better solubility of the H atoms, which resulted in the highest Schottky barrier change.

In the third stage, the PhD candidate focused on developing nanoporous Nb_2O_5 optical based H_2 sensors. In this work the anodization solution was modified to allow the process at much higher tempertures and shorter durations which resulted in continous and high density nanoporous films in comparison to the stage two. The nanoporous Nb_2O_5 films was prepared by the anodic oxidation of niobium (Nb) sputtering-deposited onto fluorine doped tin oxide (FTO). Thin Pt layer was deposited as a catalyst capable of splitting H_2 molecules. The measurements were conducted over a range of temperatures starting from room temperatures to 100 °C. The compact nanoporous networks with high active surface areas demonstrated excellent absorbance changes at 100 °C with the response factor of 12.1 %.

In the last stage, the PhD candidate explored Schottky diode based C_2H_5OH and H_2 gas sensors fabricated *via* anodization of tungsten (W) foil to form nanoporous WO_3 films. The anodization was conducted using ethylene glycol (98% purity) mixed with ammonium fluoride (NH_4F) and small amount of water. The process resulted in highly ordered and large surface to volume ratio WO_3 films. Utilizing these nanoporous

structures, Schottky diode-based gas sensors were developed by depositing Pt catalytic contact. Analysis of the current–voltage (I–V) characteristics and dynamic responses of the sensors indicated that these devices exhibited the largest voltage shift towards H_2 gas as compared to C_2H_5OH at an optimum operating temperature of 200 °C.

In summary, the PhD candidate believes that the studies carried out in the process of this research provided an in-depth vision regarding the fabrication and performance of nanofibers and nanoporous metal oxide based gas sensors.

List of Symbols

A	contact area
A^{**}	Richardson constant
Abs_{air}	absorbance in air
Abs_{gas}	absorbance in gas
C	concentration
d	diameter
δ	polymer scaling exponent
E_g	band gap energy
Φ_B	Schottky barrier height at zero bias
Φ_{BAir}	Schottky barrier height in air
Φ_{BEth}	Schottky barrier height ethanol
Is	saturation current
$I–V$	current-voltage
k	Boltzmann's constant
λ	lambda
M_w	molecular weight
n	ideality factor
q	electron charge
R_{air}	resistance in air
R_{gas}	resistance in gas
T	temperature
V	applied voltage

V_{air}	voltage in air
V_F	forward voltage
V_{gas}	voltage in gas

List of Abbreviations

AFM	atomic force microscopy
DI	deionized
DMF	dimethylformamide
FTO	fluorine doped tin oxide
GADDS	general area detector diffraction system
HBEC	high binding energy component
LBEC	low binding energy component
MFC	mass flow control
PAN	polyacrylonitrile
PECS	precision etching coating system
PMMA	poly(methyl methacrylate)
PVP	polyvinyl pyrrolidone
RF	radio frequency
RF	response factor
SBH	Schottky barrier height
SCCM	standard cubic centimeter per minute
SEM	scanning electron microscopy
SR	sensor response
TEM	transmission electron microscopy
XPS	x-ray photoemission spectroscopy
XRD	x-ray diffraction

List of Figures

List of Tables

Table of Contents

Chapter 1

Introduction

1.1 Motivation

Nanostructured metal oxides such as tin oxide (SnO_2), zinc oxide (ZnO), molybdenum oxide (MoO_3), niobium pentoxide (Nb_2O_5) and tungsten trioxide (WO_3) have received significant attention as gas sensing devices [1-10]. This is due to their low cost, small physical size, simple crystal structure, ease of integration, excellent stability, high sensitivity, rapid response and online sensing [11]. The application field spans from environmental monitoring, industrial surveillance and process, automative and aviation industries, homeland security, medical analysis and diagnostics [11-17]. Many efforts have been carried out in the quest for developing gas sensors with better sensing properties such as low operating temperature, rapid response and recovery time, high sensitivity and stability [18]. The sensing performances were strongly influenced by the morphology, porosity, surface energy, stochiometry and large surface-to-volume ratio of the sensing films [19]. Thus, this PhD project aims at improving gas sensing performance of metal oxide based devices by nanostructuring and tuning the properties of the sensitive materials.

The one dimensional (1D) nanostructures such as nanofibers, nanowires and nanobelts have shown great potentials to increase performance of metal oxide based sensors [18, 20-25]. With large surface-to-volume ratios and Debye length comparable to their dimensions, 1D structures were proven to be an excellent candidate for gas sensing instead of their solid flat films or bulk counterparts, providing more available surface sites for the target molecule absorption and desorption, while affecting the

whole body of the sensitive structure [26]. The directional morphology of 1D metal oxides provide low scattering pathways for electron transfer. These configuration are also advantageous to achieve high and quick gas response *via* effective and rapid diffusion of target gas species onto the whole sensing surface [27] .

Nanoporous metal oxides are another attractive platforms for gas sensing with enhanced performance [28-30]. These structures have been reported to show very high and rapid responses to gas, which are attributed to their large surface area and porous architecture, respectively [31]. The whole nanoporous films can be influenced by the adsorbed molecules as the target gases can penetrate into the entire films. This maximizes the interaction of the exposed surface of the nanostructured films with the gas species and consequently further increase the sensor sensitivity. The compatibility of the Debye length with the crystallite dimensions of the nanoporous films is also another important factor affecting the gas sensor response.

In this PhD research, the author focuses on (a) SnO_2 nanofibers, (b) Nb_2O_5 and (c) WO_3 nanoporous gas sensing devices.

(a) Since the first discovery of SnO_2 gas sensor by Taguchi in 1962, it has become one of the most investigated materials for developing metal oxide gas sensors [32]. SnO_2 based gas sensors generally operate at high temperatures and it is also known that their stoichiometry and their morphologies have drastic effects on the sensing performance [33-35]. As a result, the PhD candidate focuses on tuning the morphologies and oxygen content of nanostructured SnO_2 in order to reduce the operating temperature and improve the sensor response. The 1D nanofiber morphology was chosen as such a morphology provides a great flexibility for engineering the stoichiometry and morphological aspects [35-38]. Electrospinning method was chosen as it offers the capability of producing hollow/filled fibers of different diameters and

also provides a base for altering the stoichiometry *via* changing the precursors in the process [39-43]. In this work, the sensing films were fabricated *via* electrospinning method using polyacrylonitrile polymers as the precursor solution which result in filled and hollow SnO_2 nanofibers with granular walls containing oxygen vacancies. The author of this thesis hypothesized that such structures and properties will potentially improve the sensor performance.

(b) Nb_2O_5 is a metal oxide with unique properties that can offer certain opportunities for developing semiconducting and optical gas sensors. Nb_2O_5 based gas sensors with varieties of morphologies such as nanowires, nanorods, nanobelts, and nanoparticles as well as nanoporous films have been developed and investigated [44-48]. Among them, nanoporous Nb_2O_5 have attracted increasing research interest due to its large surface areas and porosities as well as high degree of tunability [44]. This metal oxide can be both intercalated and reduced upon exposure to hydrogen containing molecules [45]. This produces changes in electronic band structure that can be efficiently used for constructing gas sensors. In this PhD work, several different anodization methods are designed and applied by the author of this thesis for producing highly ordered nanoporous Nb_2O_5 films. These methods produce films with properties of fairly confined paths for direct electron transfer, large surface areas as well as structural dimensions comparable to the Debye length for enhancing the gas sensing capabilities of the films [46-48].

Nb_2O_5 nanoporous films are used for developing Schottky and optical based sensors that covers two major sections of this PhD research. Schottky based sensors using anodized Nb_2O_5 had not been shown for gas sensing applications at the time that this PhD researched commenced. As such, the author of this thesis set an aim for developing such Schottky based gas and vapour sensors. Subsequently the PhD

candidate focused on developing optical gas sensors based on nanoporous Nb_2O_5. Nb_2O_5 has been investigated for its good performance as an electrochromic material, showing alteration in its optical properties as a result of controlled H^+ intercalation [45, 49, 50]. As a result, the author postulated that nanoporous Nb_2O_5 can also be potentially incorporated as optical-based gas sensing devices for sensing gas molecules that contain hydrogen atoms.

(c) Beside SnO_2 and Nb_2O_5, WO_3 is one of the key materials for gas sensing applications, especially for atoms that can intercalate this metal oxide [5, 10]. Nanoporous WO_3 can enhance gas sensing performance due to the increased surface area for reactions [51-53]. There are many reports on conductometric type and optical based WO_3 gas sensor [54-58]. However, nanoporous WO_3 Schottky based gas sensors have received relatively little attention despite the excellent performances ascribe to the porosity of the incorporated films. Accordingly, the PhD candidate focuses her investigation on investigating nanoporous WO_3 Schottky based gas sensor. In this work, anodization is used for forming highly ordered nanoporous WO_3 with the advantages of high surface-to-volume ratio, directional pathways and nanostructures with dimensions smaller than Debye lengths.

1.2 Objectives

1.2.1 Investigation of electrospun granular hollow SnO_2 nanofibers hydrogen gas sensors operating at low temperatures

Since late 1950s, many types of metal oxide materials have been investigated for gas sensing applications [32, 59, 60]. By adapting nanostructured morphologies many advantages can be added to metal oxide semiconductors [4, 61]. This includes high surface-to-volume ratio and scales which are comparable to length [62]. Among the

nanostructures, 1D material are of particular interest due to their directional morphology that augments the carrier transport and that the whole bulk of the materials can be readily affected by the gas molecules. Therefore, tremendous effort has been focused on investigating the synthesis, characterization and gas sensing performances of 1D metal oxides including ZnO, WO_3, TiO_2, In_2O_3, MnO_2, Fe_2O_3, CuO and SnO_2 [58, 63-65].

Among these metal oxides, SnO_2 has appeared to be the most popular material for gas sensing. SnO_2 is a stable *n*-type semiconductor with a wide direct band gap (E_g = 3.6 eV), high conductivity, tunable morphology and crystallinity, chemical stability as well as excellent gas sensitivity. Subsequently, a number of processing routes have been employed to synthesize variety of 1D SnO_2 nanostructures in the forms of nanobelts, nanotubes, nanorods, nanowires, and nanofibers [23, 66-72].

Thermal evaporation method has been widely used in order to produce SnO_2 nanobelts [23, 71, 73, 74]. Additionally, SnO_2 nanobelts have been synthesized *via* sputtering techniques [75]. SnO_2 nanobelts, prepared *via* these methods, decorated with Au catalyst, has widely employed for gas sensing applications [75-77]. Besides nanobelts, various morphologies of pristine and doped nanowires have been produced by thermal evaporation method [25, 78, 79]. Shen *et al.* have fabricated intrinsic as well as Pt and Pd doped SnO_2 nanowires for gas sensing [80, 81]. Koeck *et al*. have fabricated ultra-long single crystalline SnO_2 nanowires implementing spray pyrolysis method [82]. Moreover, nanotubular SnO_2 have been made by templating. SnO_2 nanotubes have been templated using anodic aluminum oxide membranes, [83] nanorods of other metal oxides [84], carbon nanotubes and polymeric fibers [85, 86].

A large numbers of reports demonstrated electrospinning method for producing SnO_2 nanofibers [22, 87-90]. Electrospinning has been recognized as an efficient and

cost effective synthesis route for SnO_2 nanofiber. The electrospinning process is simple, flexible and effective in producing superfine fibers with high surface-to-volume ratio. Advantageously, electrospinning method can produce nanofibers with diameters as small as tens of nanometers and lengths of up to several centimeters with controllable morphologies and large-scale production capabilities [40]. Hollow and solid nanofibers can be produced depending on the precursor solution and parameters utilized during electrospinning. Hollow SnO_2 fibers have been obtained using coaxial electrospinning. However, they are large in diameters, ranging from 400 nm to 750 nm, depending on the core of the coax in the electrospinning tip [89]. In addition, hollow fibers have been demonstrated by Choi *et al.* using polyvinylpyrrolidone and dimethylformamide. However, the gas sensors based on these fibers only operated at near 400 °C [91]. In order to enhance the performance of gas sensing, few groups had doped (to induce catalytic properties with Pd, Al or Pt) or fabricate composite electrospun SnO_2 nanofibers (for enhancing charge separation with ZnO, CuO, CeO_2, CO and In_2O_3) [21, 41, 92-101].

So far, 1D SnO_2 based devices have been employed for sensing of various gas species such as H_2, NO_2, C_2H_5OH, H_2S, CO and HCHO [24, 41, 79, 87, 89, 102-106]. Amongst these gas species, H_2 is one of the most prominent. It is a widely used gas in various industrial applications such as automotive industries, refining processes petroleum, fuel cells and biological systems [107-112]. However H_2 having the characteristics of being colorless, odorless, explosive and extremely flammable gas with a low explosive limit of 4 % in air is an important gas that should be constantly monitored in the aforementioned processes [113]. As such, H_2 gas sensing at low temperatures is essential. Semiconducting metal oxide based gas sensors usually operate in the temperature range of 200–500 °C [92, 102, 114-116]. Besides, a low

operating temperature also offers other advantages in terms of reducing energy consumption and improving the reliability and stability of the gas sensor.

In this thesis, the PhD candidate presents the outcomes of her investigation on the H_2 sensing properties of the SnO_2 nanofibers operating at low operating temperatures in Chapter 2. The SnO_2 hollow nanofibers were fabricated by a single nozzle electrospinning process using phase separated mixed polymer. The effects of varying the concentration of polymer, used in preparing the electrospinning solution, are investigated by studying the morphology and stoichiometry of SnO_2. Finally, the author discussed the correlation between nanofibers morphology, oxygen vacancy contents and the gas sensing performances.

1.2.2 Investigation of Nb_2O_5 Schottky based ethanol vapour sensors: Effect of metallic catalysts

Ethanol vapour sensors are in always in demand due to their significant applications in food, biomedical, transportation and chemical industries as well as health and safety [117, 118]. Ethanol is also commonly used as a fuel or a fuel additive. It is either utilized or appears as a by-product of many chemical processes and is a common solvent in many industries. Ethanol is employed in alcoholic beverages and is also a famous antiseptic. Obviously, sensing ethanol is of importance for all the aforementioned applications [119-121].

There are many types of ethanol vapour sensors based on different transducers such as conductometric, surface acoustic wave, electrochemical, optical and Schottky diode based [64, 122-126]. Amongst these transducers, Schottky diodes with nanostructured metal oxide sensing elements offer simplicity of fabrication; reliable robustness and high sensitivity towards ethanol vapour [127]. A Schottky diode-based

sensor generally consists of a metal-semiconductor contact. The most common choices of metals are catalytic type noble metals including gold (Au), platinum (Pt) and palladium (Pd) [128-132]. They catalyse the target gas molecules, while regain their metallic properties after the interaction. Additionally with their relatively large work functions, these metals are likely to form Schottky contacts at their interface with most of the metal oxide semiconductors [133]. Metal catalysts are employed in the chemical industry for numerous chemical reactions. They operate by interacting with the target molecules, lowering the activation barriers and hence increasing the rate of reactions. The metal catalysts also enhance the sensitivity and reduce response and recovery time of the sensor. Au, Pt and Pd in the Schottky diode based sensors enable catalytic decomposition of ethanol, which otherwise would not be possible on the oxide surface. After the adsorption of ethanol, the local electronic properties of the metal/metal oxide semiconductor changes that results in a change in the Schottky contact behaviour and this alteration is used as the sensing parameter [134, 135].

Metal oxides that have been widely investigated in Schottky diode based ethanol sensors include SnO_2, TiO_2, ZnO, WO_3, MoO_3 and Ga_2O_3 [55, 136-143]. Niobium oxide (Nb_2O_5) is an important but yet much less studied metal oxide for Schottky diode based ethanol sensing. It is a *n*-type semiconductor with a ~3.5 eV band gap that have shown to offer unique properties for developing highly efficient solar-cells, electrochromic devices and sensors [144-149]. Devices based on Nb_2O_5 have been reported for sensing of various gases and chemical components [4, 150-154]. Numerous methods have been established for fabricating Nb_2O_5 based gas sensing devices. For example, Hyodo *et al*. and Rozina *et al.* have used Nb_2O_5 prepared *via* an anodization method [4, 150], while Nb_2O_5 nanowires were synthesized by Wang *et al*. through thermal oxidation process for hydrogen gas sensing [151]. Nb_2O_5 thin films doped with

TiO_2 have also been developed *via* sputtering method for carbon monoxide gas sensing [153]. There are also investigations regarding the effect of the calcination temperature on gas sensing properties of Nb_2O_5 [152].

In this PhD work, the Nb_2O_5 Schottky diode based sensors, integrated with different catalytic metals, are developed and investigated. Three noble metals of Pt, Pd, and Au with different work functions of 5.7, 5.6 and 5.4 eV respectively, are employed [155]. The effects of Pt, Pd and Au on the ethanol sensing performances of the Schottky diode based sensors are fully studied and the outcomes of the investigations are presented in Chapter 3 of this thesis.

1.2.3 Investigation of Nb_2O_5 nanoporous anodized Nb_2O_5: an optically responsive system to hydrogen gas molecules

Metal oxide semiconductors such as WO_3, NiO and MoO_3 are known for their outstanding performance as electro and chemo chromic materials due to their unique properties [10, 156-164]. Developments of electrochromic devices and chemo chromic optical sensors have been prompted by their ability to reversibly change their transmittance, absorption and reflectance according to applied voltages and ambient conditions. These materials generally change their colour and transparency as a result of the intercalation of ionic species such as Li^+ and H^+, which alter their electronic band structure [165].

Amongst the intercalatable metal oxide semiconductors, Nb_2O_5 is one of the emerging but less studied oxides. Nb_2O_5 has been demonstrated to have excellent optical properties, outstanding electrochemical responses, chemical stability, corrosion resistance, and colouration changes [45, 166, 167]. Crystalline Nb_2O_5 has low electrical

conductivity of ~10^{-6} S cm^{-1}, which is at least two orders of magnitude smaller in comparison to its electrochromic metal oxide counterparts such as MoO_3 and WO_3 [168]. It has been shown that upon intercalation of ionic species, crystalline Nb_2O_5 exhibits a colour change from transparent to blue, while amorphous Nb_2O_5 changes into a brownish-grey colour [167]. Intercalation also results in optical modulation. However in electrochromic applications, the optical modulation performance of amorphous Nb_2O_5 films rapidly degrades compared to crystalline films [49, 169, 170].

Considering the aforementioned characteristics of crystalline Nb_2O_5, there are significant opportunities for developing optical gas sensing elements based on this metal oxide. A critical approach in creating effective Nb_2O_5 based gas sensors is to form nano morphologies of this material that allow facile adsorption and dissociation of target gas molecules. Nanostructured Nb_2O_5 materials have been fabricated using various methods in order to obtain high specific surface area and controllable structures. Liquid phase deposition methods such as hydrothermal and solvothermal routes have produced Nb_2O_5 with various morphologies comprising of nanobelts, nanospheres, nanosheets and nanorods [148, 171-175]. In addition, nanoporous, nanochannelled, nanoveined and nanocolumns of Nb_2O_5 have also been synthesised *via* electrochemical methods [4, 176-180]. Amongst these methods, anodization is a particularly interesting technique due to its capability of forming highly porous films. Such structures provide platforms for efficient gas molecule diffusion, resulting in a high optical response and therefore augment a sensors' performance.

In previous work, an enhanced coloration efficiency of 47.0 cm^2 C^{-1} for crystalline nanoporous anodic Nb_2O_5, which is to date the highest ever reported for any electrochromic Nb_2O_5 based system has been demonstrated [45]. In this PhD work, the PhD candidate demonstrated the possibility of intercalating a large amount of Li^+ ions

into nanoporous anodic Nb_2O_5, with high surface-to-volume ratios, at very low applied voltages. Based on the excellent electrochromic performance of these Nb_2O_5 structures, it is proposed that crystalline nanoporous anodic Nb_2O_5 can also be a suitable candidate for optical gas sensing. The breakdown of the hydrogen molecule onto the surface of nanoporous anodic Nb_2O_5, with or without the assistance of a catalyst, can be used for producing H^+ ions that intercalate the crystal. These H^+ ions can subsequently change the electronic band structure of nanoporous anodic Nb_2O_5 generating a different optical response. It is known that in metal oxides with a propensity for intercalation, Li^+ and H^+ ions generally reduce the bandgap and eventually produce semi-metallic compounds for strongly intercalated systems [181-185]. Consequently, it is proposed that hydrogen containing gas molecules are also able to reduce the energy bandgap of Nb_2O_5 to produce measureable optical modulations. However, the optical gas sensing properties of Nb_2O_5 have not been studied. Hydrogen gas (H_2) is an excellent model to investigate this hypothesis. The applications of H_2 gas span from industrial surveillance and processes to fuel cells, petroleum refining, airspace and biomedical systems [108, 110-113]. H_2 gas is a colorless, odorless, explosive and extremely flammable gas. Therefore, H_2 leakage monitoring is paramount for its safe production, storage, handling and use.

In this PhD work, the PhD candidates investigate the optical sensing performance of a nanoporous anodic Nb_2O_5 film in the presence of H_2. Nanoporous Nb_2O_5 films are prepared by anodization of Nb metal films, which are deposited using RF sputtering onto fluorine-doped tin oxide (FTO) glass substrates. Anodization of Nb using an electrolyte containing glycerol and dipotassium phosphate (K_2HPO_4) at elevated temperature has been demonstrated by Melody *et al.* to produce nanoporous Nb_2O_5 films [186]. This electrolyte composition has been identified as having low resistivity

and thermal stability that contributes to the formation of porous films [187]. It has been proved that anodization at high temperatures with the electrolyte of glycerol/dipotassium phosphate, accelerates the process and results in much more robust and highly ordered nanoporous films [187-190]. In this PhD work, the same electrolyte is used for the formation of the nanoporous anodic Nb_2O_5 films. Experiments are conducted in order to assess the crystalline and morphological properties of Nb_2O_5 films and to reveal the subsequent optical changes, which occur upon hydrogen gas molecule interactions with these films.

1.2.4 Investigations of anodized nanoporous WO_3 Schottky contact structure for hydrogen and ethanol sensing

Tungsten trioxide (WO_3) is a *n*-type semiconductor with a band gap reported in the range of 2.6 to 3.3 eV, which has a wide range of applications due to its excellent electrical and optical properties [10, 191-193]. Various WO_3 morphologies have been synthesized using different physical and chemical routes. Chemical routes including hydrothermal, solvothermal, anodization and thermal oxidation methods have been shown to result in various morphologies including nanowires, nanorods, nanosheets, nanoparticles, and nanoplatlets as well as nanoporous films [56, 156, 194-199]. The aforementioned structures have been studied for diverse applications such as electrochromic smart windows, batteries, catalysts, electronic devices and solar cells [56, 156, 194, 195, 199-203].

WO_3 is also one of the most interesting and most researched metal oxides for sensing gases such as hydrogen (H_2), hydrogen sulfide (H_2S), hydrocarbons, ethanol (C_2H_5OH), ammonia (NH_3), nitrogen oxide (NO_2, NO and N_2O) and

carbon oxide (CO) [33, 54, 55, 200, 201, 204]. Many of these investigations are focused on conductometric based gas sensors, and the application of WO_3 nanostructures in contact based systems, including Schottky diode based sensors, have received rather limited attention [205, 206]. The interaction of WO_3 with hydrogen atom containing molecules is generally the most efficient when it is of an intercalating nature. In this case, the intercalated H^+ ions are embedded into the crystal structure of WO_3 and the released electrons are transferred to the lowest-lying unoccupied energy levels of WO_3. Such an interaction changes the band structure of the WO_3 system and increases its conductivity, both of which can be well used for sensing applications of the hydrogen atom containing molecules [207].

The electron affinity of WO_3 is in the order of 3.2 to 4.0 eV [208]. As a result, a Schottky diode-based sensor can be developed by depositing a large work function noble metal such as platinum (Pt) (work function of 5.7 eV), gold (Au) (work function of 5.4 eV) and palladium (Pd) (work function of 5.6 eV) as the adjoining electrode [155]. In addition, these noble metals can act as excellent catalysts for enhancing the gas reactions and augmenting the overall performance of the sensor [130, 209]. The operating principles of the Schottky based sensors are primarily associated with the observation of the shifts in I–V curve caused by dissociation of the gas analyte on the catalytic metal surface which alters the Schottky barrier height at the metal-metal oxide interface [210-212]. This causes an effective change in the semiconductor work function, resulting in a voltage change across it. This consequently changes the current through the junction as well.

The gas sensing characteristics of the Schottky diode based are greatly influenced by the morphology and porosity of the structures at the contacts interface, the contact metal and the semiconducting materials [213]. The reduction of the components' morphologies to nano dimensions can also alter the behaviour of the systems [19]. Obviously, the alteration of surface energy, an increase in the surface-to-volume ratio, adjustments with relation to Debye length and stoichiometry of the semiconducting material are all important factors that affect the characteristics of the Schottky based sensors [7, 136, 137, 214, 215]. Additionally, the porosity of the semiconductor components enhances gas diffusion through the film and increases gas interaction and eventually adsorption of the gas molecules which can improve the sensor's performance [216, 217].

There are many reports regarding the development of nanoporous structures and thin films of metal oxides for improving the performance of gas sensors [4, 218-221]. One of the most extensively investigated methods to fabricate highly porous metal oxides is anodization. Anodization generally occurs by applying a voltage across two electrodes that include one made of the base metal forming the porous metal oxide and the other a reference electrode in a suitable electrolyte. Anodization can potentially offer a simple and efficient process to obtain films with large surface area, tunable pores sizes and highly ordered morphologies [222-225].

To the best of author's knowledge, there is no report in the literature regarding the synthesis of WO_3 Schottky-based gas sensors *via* an anodization approach. Therefore, in this PhD thesis, the PhD candidate demonstrates the performance of a WO_3 Schottky-based gas sensor prepared by anodization of W foil. The synthesis is performed in a mixed ethylene glycol-water solvent

containing a small amount of NH_4F at room temperature. The author studies and compares the performances of Schottky diode-based gas sensor towards hydrogen gas and ethanol vapour. The sensor performances such as voltage shift, response and recovery time are investigated and discussed in detail in Chapter 5.

1.3 Thesis organization

This thesis presents detailed outcomes for the investigation and development of gas sensors based on SnO_2 nanofibers as well as nanoporous Nb_2O_5 and WO_3. The aim is to fabricate sensors with enhanced performances such as large and rapid response, high selectivity and reproducibility as well as low operating temperatures. The proposed topics are investigated and presented in this PhD thesis as follows:

- Chapter 1 is an overview of the PhD candidate's motivation for being involved in the proposed research as well as the objectives and the organization of the thesis.
- Chapter 2 presents the investigations regarding the development of hydrogen gas sensor based on SnO_2 nanofibers. The nanofibers synthesized *via* an electrospinning method and the full characterization of this material is presented. The author presents the effect of structural and morphological changes of SnO_2 on hydrogen gas sensing.
- Chapter 3 outlines the fabrication process of nanoporous Nb_2O_5 films and the investigation of these films as the base for Schottky based gas sensors. The author presents the effect of Pt, Pd and Au catalysts on the sensors' performances in the presence of ethanol vapour. Furthermore, the selectivity of gas sensors towards methane and hydrogen gas is also presented in this chapter.

- Chapter 4 presents the synthesis and structural characterization details of nanoporous Nb_2O_5 films grown on FTO glass substrate. The gas sensing performances are investigated in the presence of hydrogen gas which is also presented in this chapter.
- Chapter 5 presents the investigations of the Schottky contact gas sensors based on WO_3 nanoporous films synthesized *via* an anodization method at room temperature. Their sensing performances in the presence of hydrogen gas and ethanol vapour are presented and fully discussed in this chapter.
- Chapter 6 presents the conclusions for the thesis, the recommendations for future work and the PhD candidate's achievements during this PhD project.

Reference

[1] M. Batzill and U. Diebold, "The surface and materials science of tin oxide," *Prog. Surf. Sci.,* vol. 79, pp. 47-154, 2005.

[2] N. Barsan, M. Schweizer-Berberich, and W. Gopel, "Fundamental and practical aspects in the design of nanoscaled SnO_2 gas sensors: a status report," *Fresen. J. Anal. Chem.,* vol. 365, pp. 287-304, 1999.

[3] L. Chambon, C. Maleysson, A. Pauly, J. P. Germain, V. Demarne, and A. Grisel, "Investigation, for NH_3 gas sensing applications, of the Nb_2O_5 semiconducting oxide in the presence of interferent species such as oxygen and humidity," *Sens. Actuators B Chem.,* vol. 45, pp. 107-114, 1997.

[4] R. A. Rani, A. S. Zoolfakar, J. Z. Ou, M. R. Field, M. Austin, and K. Kalantar-zadeh, "Nanoporous Nb_2O_5 hydrogen gas sensor," *Sens. Actuators B Chem.,* vol. 176, pp. 149-156, 2013.

[5] Y. Xu, Q. Tan, Z. Tang, Z. Zhang, and Z. Yuan, "WO_3-based gas sensors," *Prog. Chem.,* vol. 21, pp. 2734-2743, 2009.

[6] A. Gurlo, "Nanosensors: towards morphological control of gas sensing activity. SnO_2, In_2O_3, ZnO and WO_3 case studies," *Nanoscale,* vol. 3, pp. 154-165, 2011.

[7] J. Yu, S. J. Ippolito, W. Wlodarski, M. Strano, and K. Kalantar-zadeh, "Nanorod based Schottky contact gas sensors in reversed bias condition," *Nanotechnology,* vol. 21, 265502, 2010.

[8] M. Shafiei, J. Yu, R. Arsat, K. Kalantar-zadeh, E. Comini, M. Ferroni, *et al.*, "Reversed bias Pt/nanostructured ZnO Schottky diode with enhanced electric field for hydrogen sensing," *Sens. Actuators B Chem.,* vol. 146, pp. 507-512, 2010.

[9] J. Yu, M. Shafiei, W. Wlodarski, Y. X. Li, and K. Kalantar-Zadeh, "Enhancement of electric field properties of Pt/nanoplatelet MoO_3/SiC Schottky diode," *J. Phys. D Appl. Phys.*, vol. 43, 2010.

[10] H. Zheng, J. Z. Ou, M. S. Strano, R. B. Kaner, A. Mitchell, and K. Kalantar-zadeh, "Nanostructured tungsten oxide - Properties, synthesis, and applications," *Adv. Funct. Mater.*, vol. 21, pp. 2175-2196, 2011.

[11] A. Ponzoni, E. Comini, I. Concina, M. Ferroni, M. Falasconi, E. Gobbi, *et al.*, "Nanostructured metal oxide gas sensors, a survey of applications carried out at SENSOR Lab, Brescia (Italy) in the security and food quality fields," *Sensors*, vol. 12, pp. 17023-17045, 2012.

[12] A. D. Wilson, "Review of electronic nose technologies and algorithms to detect hazardous chemicals in the environment," in *First World Conference on Innovation and Computer Sciences*. vol. 1, A. Karahoca and S. Kanbul, Eds., ed, 2012, pp. 453-463.

[13] N. Yamazoe and N. Miura, "Environmental gas sensing," *Sens. Actuator B Chem.*, vol. 20, pp. 95-102, 1994.

[14] G. F. Fine, L. M. Cavanagh, A. Afonja, and R. Binions, "Metal oxide semi-conductor gas sensors in environmental monitoring," *Sensors*, vol. 10, pp. 5469-5502, 2010.

[15] K. Wetchakun, T. Samerjai, N. Tamaekong, C. Liewhiran, C. Siriwong, V. Kruefu, *et al.*, "Semiconducting metal oxides as sensors for environmentally hazardous gases," *Sens. Actuator B Chem.*, vol. 160, pp. 580-591, 2011.

[16] S. Capone, P. Siciliano, F. Quaranta, R. Rella, M. Epifani, and L. Vasanelli, "Analysis of vapours and foods by means of an electronic nose based on a sol-gel metal oxide sensors array," *Sens. Actuator B Chem.*, vol. 69, pp. 230-235, 2000.

[17] A. Berna, "Metal oxide sensors for electronic noses and their application to food analysis," *Sensors,* vol. 10, pp. 3882-3910, 2010.

[18] X.-J. Huang and Y.-K. Choi, "Chemical sensors based on nanostructured materials," *Sens. Actuator B Chem.,* vol. 122, pp. 659-671, 2007.

[19] C. Wang, L. Yin, L. Zhang, D. Xiang, and R. Gao, "Metal oxide gas sensors: sensitivity and influencing factors," *Sensors,* vol. 10, pp. 2088-2106, 2010.

[20] I.-D. Kim, A. Rothschild, B. H. Lee, D. Y. Kim, S. M. Jo, and H. L. Tuller, "Ultrasensitive chemiresistors based on electrospun TiO_2 nanofibers," *Nano Lett.,* vol. 6, pp. 2009-2013, 2006.

[21] X. Xu, J. Sun, H. Zhang, Z. Wang, B. Dong, T. Jiang, *et al.*, "Effects of Al doping on SnO_2 nanofibers in hydrogen sensor," *Sens. Actuator B Chem.,* vol. 160, pp. 858-863, 2011.

[22] Y. Zhao, X.-L. He, J.-P. Li, J. Jia, and X.-G. Gao, "Enhanced gas sensing properties of aligned porous SnO_2 nanofibers," *Chinese Phys. Lett.,* vol. 29, 2012.

[23] A. Kolmakov, D. O. Klenov, Y. Lilach, S. Stemmer, and M. Moskovits, "Enhanced gas sensing by individual SnO_2 nanowires and nanobelts functionalized with Pd catalyst particles," *Nano Lett.,* vol. 5, pp. 667-673, 2005.

[24] A. Kolmakov, Y. X. Zhang, G. S. Cheng, and M. Moskovits, "Detection of CO and O_2 using tin oxide nanowire sensors," *Adv. Mater.,* vol. 15, pp. 997-+, 2003.

[25] G. Sberveglieri, C. Baratto, E. Comini, G. Faglia, M. Ferroni, A. Ponzoni, *et al.*, "Synthesis and characterization of semiconducting nanowires for gas sensing," *Sens. Actuator B Chem.,* vol. 121, pp. 208-213, 2007.

[26] Y. Ma, Y. Qu, and W. Zhou, "Surface engineering of one-dimensional tin oxide nanostructures for chemical sensors," *Microchim. Acta,* vol. 180, pp. 1181-1200, Oct 2013.

[27] J. H. Lee, "Gas sensors using hierarchical and hollow oxide nanostructures: Overview," *Sens. Actuator B Chem.,* vol. 140, pp. 319-336, 2009.

[28] T. K. Kim, K. J. Lee, J. Y. Cheon, J. H. Lee, S. H. Joo, and H. R. Moon, "Nanoporous metal oxides with tunable and nanocrystalline frameworks via conversion of metal-organic frameworks," *J. Am. Chem. Soc.,* vol. 135, pp. 8940-8946, 2013.

[29] J. H. Kim, S. H. Kim, and S. Shiratori, "Fabrication of nanoporous and hetero structure thin film via a layer-by-layer self assembly method for a gas sensor," *Sens. Actuator B Chem.,* vol. 102, pp. 241-247, 2004.

[30] T. Waitz, B. Becker, T. Wagner, T. Sauerwald, C. D. Kohl, and M. Tiemann, "Ordered nanoporous SnO_2 gas sensors with high thermal stability," *Sens. Actuator B Chem.,* vol. 150, pp. 788-793, 2010.

[31] C. Lu and Z. Chen, "High-temperature resistive hydrogen sensor based on thin nanoporous rutile TiO_2 film on anodic aluminum oxide," *Sens. Actuator B Chem.,* vol. 140, pp. 109-115, 2009.

[32] N. Taguchi, "A metal oxide gas sensor," 45-38200, 1962.

[33] M. Ahsan, M. Z. Ahmad, T. Tesfamichael, J. Bell, W. Wlodarski, and N. Motta, "Low temperature response of nanostructured tungsten oxide thin films toward hydrogen and ethanol," *Sens. Actuators B Chem.,* vol. 173, pp. 789-796, 2012.

[34] Z. Wang, Z. Li, J. Sun, H. Zhang, W. Wang, W. Zheng, *et al.,* "Improved hydrogen monitoring properties based on p-NiO/n-SnO_2 heterojunction composite nanofibers," *J. Phys. Chem. C,* vol. 114, pp. 6100-6105, 2010.

[35] M. M. Arafat, B. Dinan, S. A. Akbar, and A. S. M. A. Haseeb, "Gas sensors based on one dimensional nanostructured metal-oxides: A review," *Sensors,* vol. 12, pp. 7207-7258, 2012.

[36] H. Gu, Z. Wang, and Y. Hu, "Hydrogen gas sensors based on semiconductor oxide nanostructures," *Sensors,* vol. 12, pp. 5517-5550, 2012.

[37] L. Liu, S. Li, J. Zhuang, L. Wang, J. Zhang, H. Li, *et al.*, "Improved selective acetone sensing properties of Co-doped ZnO nanofibers by electrospinning," *Sens. Actuator B Chem.,* vol. 155, pp. 782-788, 2011.

[38] R. S. Devan, R. A. Patil, J.-H. Lin, and Y.-R. Ma, "One-dimensional metal-oxide nanostructures: recent developments in synthesis, characterization, and applications," *Adv. Funct. Mater.,* vol. 22, pp. 3326-3370, 2012.

[39] C. J. Thompson, G. G. Chase, A. L. Yarin, and D. H. Reneker, "Effects of parameters on nanofiber diameter determined from electrospinning model," *Polymer,* vol. 48, pp. 6913-6922, 2007.

[40] J. T. McCann, D. Li, and Y. Xia, "Electrospinning of nanofibers with core sheath, hollow or porous structures," *J. Mater. Chem.,* vol. 15, pp. 735-738, 2005.

[41] W. Qin, L. Xu, J. Song, R. Xing, and H. Song, "Highly enhanced gas sensing properties of porous SnO_2–CeO_2 composite nanofibers prepared by electrospinning," *Sens. Actuator B Chem.,* vol. 185, pp. 231-237, 2013.

[42] Z. Zhang, X. Li, C. Wang, L. Wei, Y. Liu, and C. Shao, "ZnO hollow nanofibers: fabrication from facile single capillary electrospinning and applications in gas sensors," *J. Phys. Chem. C,* vol. 113, pp. 19397-19403, 2009.

[43] K. Asokan, J. Y. Park, S.-W. Choi, and S. S. Kim, "Nanocomposite ZnO-SnO_2 nanofibers synthesized by electrospinning method," *Nanoscale Res. Lett.,* vol. 5, pp. 747-752, 2010.

[44] M. Vettraino, M. L. Trudeau, and D. M. Antonelli, "Synthesis and electronic properties of reduced mesoporous sodium niobium oxides," *Adv. Mater.,* vol. 12, pp. 337-+, 2000.

[45] D. D. Yao, R. A. Rani, A. P. O'Mullane, K. Kalantar-zadeh, and J. Z. Ou, "High performance electrochromic devices based on anodized nanoporous Nb_2O_5," *J. Phys. Chem. C*, vol. 118, pp. 476-481, 2014.

[46] R. A. Rani, A. S. Zoolfakar, A. P. O'Mullane, M. W. Austin, and K. Kalantar-Zadeh, "Thin films and nanostructures of niobium pentoxide: fundamental properties, synthesis methods and applications," *J. Mater. Chem. A*, vol. 2, pp. 15683-15703, 2014.

[47] J. Choi, J. H. Lim, J. Lee, and K. J. Kim, "Porous niobium oxide films prepared by anodization-annealing-anodization," *Nanotechnology*, vol. 18, 055603. 2007.

[48] H. Masuda, F. Hasegwa, and S. Ono, "Self-ordering of cell arrangement of anodic porous alumina formed in sulfuric acid solution," *J. Electrochem. Soc.*, vol. 144, pp. L127-L130, 1997.

[49] B. Orel, M. Macek, J. Grdadolnik, and A. Meden, "In situ UV-Vis and ex situ IR spectroelectrochemical investigations of amorphous and crystalline electrochromic Nb_2O_5 films in charged/discharged states," *J. Solid State Electr.*, vol. 2, pp. 221-236, 1998.

[50] N. Ozer, D. G. Chen, and C. M. Lampert, "Preparation and properties of spin-coated Nb_2O_5 films by the sol-gel process for electrochromic applications," *Thin Solid Films*, vol. 277, pp. 162-168, 1996.

[51] D. Deniz, D. J. Frankel, and R. J. Lad, "Nanostructured tungsten and tungsten trioxide films prepared by glancing angle deposition," *Thin Solid Films*, vol. 518, pp. 4095-4099, 2010.

[52] T. Yang, Y. Zhang, Y. Cai, and H. Tian, "Effect of processing parameters on anodic nanoporous tungsten oxide film structure and porosity for hydrogen detection," *J. Mater. Res.*, vol. 29, pp. 166-174, 2014.

[53] V. Khatko, G. Gorokh, A. Mozalev, D. Solovei, E. Llobet, X. Vilanova, *et al.*, "Tungsten trioxide sensing layers on highly ordered nanoporous alumina template," *Sens. Actuator B Chem.*, vol. 118, pp. 255-262, 2006.

[54] M. Z. Ahmad, A. Z. Sadek, J. Z. Ou, M. H. Yaacob, K. Latham, and W. Wlodarski, "Facile synthesis of nanostructured WO_3 thin films and their characterization for ethanol sensing," *Mater. Chem. Phys.*, vol. 141, pp. 912-919, 2013.

[55] S. J. Ippolito, S. Kandasamy, K. Kalantar-zadeh, and W. Wlodarski, "Hydrogen sensing characteristics of WO_3 thin film conductometric sensors activated by Pt and Au catalysts," *Sens. Actuators B Chem.*, vol. 108, pp. 154-158, 2005.

[56] J. Zeng, M. Hu, W. Wang, H. Chen, and Y. Qin, "NO_2-sensing properties of porous WO_3 gas sensor based on anodized sputtered tungsten thin film," *Sens. Actuators B Chem.*, vol. 161, pp. 447-452, 2012.

[57] M. H. Yaacob, M. Z. Ahmad, A. Z. Sadek, J. Z. Ou, J. Campbell, K. Kalantar-zadeh, *et al.*, "Optical response of WO_3 nanostructured thin films sputtered on different transparent substrates towards hydrogen of low concentration," *Sens. Actuators B Chem.*, vol. 177, pp. 981-988, 2013.

[58] M. Z. Ahmad, J. H. Kang, A. Z. Sadek, A. Moafi, G. Sberveglieri, and W. Wlodarski, "Synthesis of WO_3 nanorod based thin films for ethanol and H_2 sensing," in *26th European Conference on Solid-State Transducers, Eurosensor 2012*, pp. 358-361.

[59] Y. L. Sandler and M. Gazith, "Surface properties of germanium," *J. Phys. Chem.* , vol. 63, pp. 1095-1102, 1959.

[60] T. Seiyama, A. Kato, K. Fujiishi, and M. Nagatani, "A new detector for gaseous components using semiconductive thin films," *Anal. Chem*, vol. 34, pp. 1502-1503, 1962.

[61] M. M. Y. A. Alsaif, S. Balendhran, M. R. Field, K. Latham, W. Wlodarski, J. Z. Ou, *et al.*, "Two dimensional α-MoO_3 nanoflakes obtained using solvent-assisted grinding and sonication method: Application for H_2 gas sensing," *Sens. Actuator B Chem.*, vol. 192, pp. 196-204, 2014.

[62] P.-C. Chen, G. Shen, and C. Zhou, "Chemical sensors and electronic noses based on 1-D metal oxide nanostructures," *IEEE T. Nanotechnol.*, vol. 7, pp. 668-682, 2008.

[63] A. Z. Sadek, S. Choopun, W. Wlodarski, S. J. Ippolito, and K. Kalantar-zadeh, "Characterization of ZnO nanobelt based gas sensor for H_2, NO_2 and hydrocarbon sensing," *IEEE Sens. J.*, vol. 7, pp. 919-924, 2007.

[64] M. Z. Ahmad, A. Wisitsoraat, A. S. Zoolfakar, R. Ab Kadir, and W. Wlodarski, "Investigation of RF sputtered tungsten trioxide nanorod thin film gas sensors prepared with a glancing angle deposition method toward reductive and oxidative analytes," *Sens. Actuators B Chem.*, vol. 183, pp. 364-371, 2013.

[65] P. Gunawan, L. Mei, J. Teo, J. Ma, J. Highfield, Q. Li, *et al.*, "Ultrahigh sensitivity of Au/1D alpha-Fe_2O_3 to acetone and the sensing mechanism," *Langmuir*, vol. 28, pp. 14090-14099, 2012.

[66] X. Feng, J. Jiang, H. Ding, R. Ding, D. Luo, J. Zhu, *et al.*, "Carbon-assisted synthesis of mesoporous SnO_2 nanomaterial as highly sensitive ethanol gas sensor," *Sens. Actuator B Chem.*, vol. 183, pp. 526-534, 2013.

[67] Y. Tan, C. Li, Y. Wang, J. Tang, and X. Ouyang, "Fast response and high sensitivity gas sensors based on SnO_2 hollow spheres," *Thin Solid Films*, vol. 516, pp. 7840-7843, 2008.

[68] L. Zhang and Y. Yin, "Hierarchically mesoporous SnO_2 nanosheets: hydrothermal synthesis and highly ethanol sensitive properties operated at low temperature," *Sens. Actuator B Chem.*, vol. 185, pp. 594-601, 2013.

[69] Z. Zhang, R. Zou, G. Song, L. Yu, Z. Chen, and J. Hu, "Highly aligned SnO_2 nanorods on graphene sheets for gas sensors," *J. Mater. Chem*, vol. 21, pp. 17360-17365, 2011 2011.

[70] M. Wu, W. Zeng, and Y. Li, "Hydrothermal synthesis of novel SnO_2 nanoflowers and their gas sensing properties," *Mater. Lett.*, vol. 104, pp. 34-36, 2013.

[71] E. Comini, G. Faglia, G. Sberveglieri, Z. W. Pan, and Z. L. Wang, "Stable and highly sensitive gas sensors based on semiconducting oxide nanobelts," *Appl. Phys. Lett.*, vol. 81, pp. 1869-1871, 2002.

[72] T. Suzuki, T. Yamazaki, K. Takahashi, and T. Yokoi, "Effect of platinum distribution on the hydrogen gas sensor properties in tin oxide thin films," *J. Mater. Sci*, vol. 24, pp. 2127-2131, 1989.

[73] E. Comini, G. Faglia, G. Sberveglieri, D. Calestani, L. Zanotti, and M. Zha, "Tin oxide nanobelts electrical and sensing properties," *Sens. Actuator B Chem.*, vol. 111, pp. 2-6, 2005.

[74] L. L. Fields, J. P. Zheng, Y. Cheng, and P. Xiong, "Room temperature low power hydrogen sensor based on a single tin dioxide nanobelt," *Appl. Phys. Lett.*, vol. 88, 2006.

[75] C. Jin, H. Kim, S. Park, H. W. Kim, S. Lee, and C. Lee, "Enhanced ethanol gas sensing properties of SnO_2 nanobelts functionalized with Au," *Ceram. Int.*, vol. 38, pp. 6585-6590, 2012.

[76] L. H. Qian, K. Wang, H. T. Fang, Y. Li, and X. L. Ma, "Au nanoparticles enhance CO oxidation onto SnO_2 nanobelt," *Mater. Chem. Phys.,* vol. 103, pp. 132-136, 2007.

[77] L. H. Qian, K. Wang, Y. Li, H. T. Fang, Q. H. Lu, and X. L. Ma, "CO sensor based on Au-decorated SnO_2 nanobelt," *Mater. Chem. Phys.,* vol. 100, pp. 82-84, 2006.

[78] E. M. El-Maghraby, A. Qurashi, and T. Yamazaki, "Synthesis of SnO_2 nanowires their structural and H_2 gas sensing properties," *Ceram. Int.,* vol. 39, pp. 8475-8480, 2013.

[79] B. Wang, L. F. Zhu, Y. H. Yang, N. S. Xu, and G. W. Yang, "Fabrication of a SnO_2 nanowire gas sensor and sensor performance for hydrogen," *J. Phys. Chem. C,* vol. 112, pp. 6643-6647, 2008.

[80] Y. Shen, T. Yamazaki, Z. Liu, D. Meng, and T. Kikuta, "Hydrogen sensors made of undoped and Pt doped SnO_2 nanowires," *J. Alloy Compd.,* vol. 488, pp. L21-L25, 2009.

[81] Y. Shen, T. Yamazaki, Z. Liu, D. Meng, T. Kikuta, N. Nakatani, *et al.*, "Microstructure and H_2 gas sensing properties of undoped and Pd doped SnO_2 nanowires," *Sens. Actuator B Chem.,* vol. 135, pp. 524-529, 2009.

[82] A. Koeck, A. Tischner, T. Maier, M. Kast, C. Edtmaier, C. Gspan, *et al.*, "Atmospheric pressure fabrication of SnO_2-nanowires for highly sensitive CO and CH_4 detection," *Sens. Actuator B Chem.,* vol. 138, pp. 160-167, 2009.

[83] Y. Wang, H. C. Zeng, and J. Y. Lee, "Highly reversible lithium storage in porous SnO_2 nanotubes with coaxially grown carbon nanotube overlayers," *Adv. Mater.,* vol. 18, pp. 645-+, 2006.

[84] J. Zhang, J. Guo, H. Xu, and B. Cao, "Reactive template fabrication of porous SnO_2 nanotubes and their remarkable gas sensing performance," *ACS Appl. Mater. Interfaces,* vol. 5, pp. 7893-7898, 2013.

[85] W.-S. Kim, B.-S. Lee, D.-H. Kim, H.-C. Kim, W.-R. Yu, and S.-H. Hong, "SnO_2 nanotubes fabricated using electrospinning and atomic layer deposition and their gas sensing performance," *Nanotechnology,* vol. 21, 2010.

[86] Y. Jia, L. He, Z. Guo, X. Chen, F. Meng, T. Luo, *et al.*, "Preparation of porous tin oxide nanotubes using carbon nanotubes as templates and their gas sensing properties," *J. Phys. Chem. C,* vol. 113, pp. 9581-9587, 2009.

[87] N. G. Cho, D. J. Yang, M.-J. Jin, H.-G. Kim, H. L. Tuller, and I.-D. Kim, "Highly sensitive SnO_2 hollow nanofiber based NO_2 gas sensors," *Sens. Actuator B Chem.,* vol. 160, pp. 1468-1472, 2011.

[88] L. Wang, X. Luo, X. Zheng, R. Wang, and T. Zhang, "Direct annealing of electrospun synthesized high-performance porous SnO_2 hollow nanofibers for gas sensors," *RSC Advances,* vol. 3, pp. 9723-9728, 2013.

[89] J. Cao, T. Zhang, F. Li, H. Yang, and S. Liu, "Enhanced ethanol sensing of SnO_2 hollow micro/nanofibers fabricated by coaxial electrospinning," *New J. Chem.,* vol. 37, pp. 2031-2036, 2013.

[90] Y. Zhang, X. He, J. Li, Z. Miao, and F. Huang, "Fabrication and ethanol sensing properties of micro gas sensor based on electrospun SnO_2 nanofibers," *Sens. Actuator B Chem.,* vol. 132, pp. 67-73, 2008.

[91] J.-K. Choi, I.-S. Hwang, S.-J. Kim, J.-S. Park, S.-S. Park, U. Jeong, *et al.*, "Design of selective gas sensors using electrospun Pd-doped SnO_2 hollow nanofibers," *Sens. Actuator B Chem.,* vol. 150, pp. 191-199, 2010.

[92] H. Zhang, Z. Li, L. Liu, X. Xu, Z. Wang, W. Wang, *et al.*, "Enhancement of hydrogen monitoring properties based on Pd-SnO_2 composite nanofibers," *Sens. Actuator B Chem.*, vol. 147, pp. 111-115, 2010.

[93] Z.-M. Cui, A. Mechai, L. Guo, and W.-G. Song, "Palladium nanoparticles on the inner wall of tin oxide hollow nanospheres with enhanced hydrogen sensing properties," *RSC Adv.*, vol. 3, pp. 14979-14982, 2013.

[94] J. M. Lee, J.-e. Park, S. Kim, S. Kim, E. Lee, S.-J. Kim, *et al.*, "Ultrasensitive hydrogen gas sensors based on Pd-decorated tin dioxide nanostructures: room temperature operating sensors," *Int. J. Hydrogen Energ.*, vol. 35, pp. 12568-12573, 2010.

[95] B.-H. Jang, O. Landau, S.-J. Choi, J. Shin, A. Rothschild, and I.-D. Kim, "Selectivity enhancement of SnO_2 nanofiber gas sensors by functionalization with Pt nanocatalysts and manipulation of the operation temperature," *Sens. Actuator B Chem.*, vol. 188, pp. 156-168, 2013.

[96] J. Shin, S.-J. Choi, I. Lee, D.-Y. Youn, C. O. Park, J.-H. Lee, *et al.*, "Thin wall assembled SnO_2 fibers functionalized by catalytic Pt nanoparticles and their superior exhaled breath sensing properties for the diagnosis of diabetes," *Adv. Funct. Mater*, vol. 23, pp. 2357-2367, 2013.

[97] E. Nikan, A. A. Khodadadi, and Y. Mortazavi, "Highly enhanced response and selectivity of electrospun ZnO doped SnO_2 sensors to ethanol and CO in presence of CH_4," *Sens. Actuator B Chem.*, vol. 184, pp. 196-204, 2013.

[98] S.-W. Choi, A. Katoch, J. Zhang, and S. S. Kim, "Electrospun nanofibers of CuO-SnO_2 nanocomposite as semiconductor gas sensors for H_2S Detection," *Sens. Actuator B Chem.*, vol. 176, pp. 585-591, 2013.

[99] L. Liu, C. Guo, S. Li, L. Wang, Q. Dong, and W. Li, "Improved H_2 sensing properties of Co-doped SnO_2 nanofibers," *Sens. Actuator B Chem.,* vol. 150, pp. 806-810, 2010.

[100] H. Du, J. Wang, M. Su, P. Yao, Y. Zheng, and N. Yu, "Formaldehyde gas sensor based on SnO_2/In_2O_3 hetero-nanofibers by a modified double jets electrospinning process," *Sens. Actuator B Chem.,* vol. 166–167, pp. 746-752, 2012.

[101] S. Wei, Y. Zhang, and M. Zhou, "Toluene sensing properties of SnO_2-ZnO hollow nanofibers fabricated from single capillary electrospinning," *Solid State Commun.,* vol. 151, pp. 895-899, Jun 2011.

[102] H. Huang, Y. C. Lee, O. K. Tan, W. Zhou, N. Peng, and Q. Zhang, "High sensitivity SnO_2 single nanorod sensors for the detection of H_2 gas at low temperature," *Nanotechnology,* vol. 20, 2009.

[103] J. Cao, T. Zhang, F. Li, H. Yang, and S. Liu, "Enhanced ethanol sensing of SnO_2 hollow micro/nanofibers fabricated by coaxial electrospinning," *New J. Chem.,* vol. 37, pp. 2031-2036, 2013.

[104] Z. Wang, Z. Li, T. Jiang, X. Xu, and C. Wang, "Ultrasensitive hydrogen sensor based on Pd^0-loaded SnO_2 electrospun nanofibers at room temperature," *ACS Appl. Mater. Interfaces,* vol. 5, pp. 2013-2021, 2013.

[105] S. Tian, X. Ding, D. Zeng, J. Wu, S. Zhang, and C. Xie, "A low temperature gas sensor based on Pd-functionalized mesoporous SnO_2 fibers for detecting trace formaldehyde," *RSC Adv.,* vol. 3, pp. 11823-11831, 2013.

[106] J. Y. Park, K. Asokan, S.-W. Choi, and S. S. Kim, "Growth kinetics of nanograins in SnO_2 fibers and size dependent sensing properties," *Sens. Actuator B Chem.,* vol. 152, pp. 254-260, 2011.

[107] M. Momirlan and T. N. Veziroglu, "Current status of hydrogen energy," *Renew Sust. Energ. Rev.,* vol. 6, pp. 141-179, 2002.

[108] M. Momirlan and T. N. Veziroglu, "The properties of hydrogen as fuel tomorrow in sustainable energy system for a cleaner planet," *Int. J. Hydrogen Energ.,* vol. 30, pp. 795-802, 2005.

[109] K. Hall, "4.14 - Future perspective on hydrogen and fuel cells," in *Comprehensive Renewable Energy,* A. Sayigh, Ed., ed Oxford: Elsevier, 2012, pp. 351-360.

[110] D. Hart, "Hydrogen end uses and economics," in *Encyclopedia of Energy,* C. J. Cleveland, Ed., ed. New York: Elsevier, 2004, pp. 231-239.

[111] S. Dunn, "Hydrogen, history of " in *Encyclopedia of Energy,* C. J. Cleveland, Ed., ed. New York: Elsevier, 2004, pp. 241-252.

[112] R. Ramachandran and R. K. Menon, "An overview of industrial uses of hydrogen," *Int. J. Hydrogen Energ.,* vol. 23, pp. 593-598, 1998.

[113] T. Huebert, L. Boon-Brett, G. Black, and U. Banach, "Hydrogen sensors - A review," *Sens. Actuator B Chem.,* vol. 157, pp. 329-352, 2011.

[114] K. J. Choi and H. W. Jang, "One dimensional oxide nanostructures as gas sensing materials: review and issues," *Sensors,* vol. 10, pp. 4083-4099, 2010.

[115] T. Hyodo, N. Nishida, Y. Shimizu, and M. Egashira, "Preparation and gas sensing properties of thermally stable mesoporous SnO_2," *Sens. Actuator B Chem.,* vol. 83, pp. 209-215, 2002.

[116] Y.-H. Choi and S.-H. Hong, "H_2 sensing properties in highly oriented SnO_2 thin films," *Sens. Actuator B Chem.,* vol. 125, pp. 504-509, 2007.

[117] G. Wen, Y. Zhang, S. Shuang, C. Dong, and M. M. F. Choi, "Application of a biosensor for monitoring of ethanol," *Biosens. Bioelectron.,* vol. 23, pp. 121-129, 2007.

[118] E. Comini, G. Faglia, G. Sberveglieri, Y. X. Li, W. Wlodarski, and M. K. Ghantasala, "Sensitivity enhancement towards ethanol and methanol of TiO_2 films doped with Pt and Nb," *Sens. Actuators B Chem.*, vol. 64, pp. 169-174, 2000.

[119] C. Lamy, A. Lima, V. LeRhun, F. Delime, C. Coutanceau, and J. M. Leger, "Recent advances in the development of direct alcohol fuel cells (DAFC)," *J. Power Sources,* vol. 105, pp. 283-296, 2002.

[120] Y. Lin and S. Tanaka, "Ethanol fermentation from biomass resources: current state and prospects," *Applied Microbiol. Biot.*, vol. 69, pp. 627-642, 2006.

[121] G. Kampf, F. A. Pitten, P. Heeg, and B. Christiansen, "Efficacy of two ethanol-based skin antiseptics on the forehead at shorter application times," *BMC Microbiol.*, vol. 7, p. 85, 2007.

[122] A. S. Zoolfakar, M. Z. Ahmad, R. A. Rani, J. Z. Ou, S. Balendhran, S. Zhuiykov, *et al.*, "Nanostructured copper oxides as ethanol vapour sensors," *Sens. Actuators B Chem.*, vol. 185, pp. 620-627, 2013.

[123] S. J. Ippolito, A. Ponzoni, K. Kalantar-Zadeh, W. Wlodarski, E. Comini, G. Faglia, *et al.*, "Layered WO_3/ZnO/36° $LiTaO_3$ SAW gas sensor sensitive towards ethanol vapour and humidity," *Sens. Actuators B Chem.*, vol. 117, pp. 442-450, 2006.

[124] S. J. Ippolito, A. Ponzoni, K. Kalantar-zadeh, W. Wlodarski, E. Comini, G. Faglia, *et al.*, "Ethanol sensor based on layered WO_3/ZnO/36° $LiTaO_3$ SAW devices," in *Transducers '05, Digest of Technical Papers, Vols 1 and 2*, 2005, pp. 1915-1918.

[125] C. Elosua, I. Vidondo, F. J. Arregui, C. Bariain, A. Luquin, M. Laguna, *et al.*, "Lossy mode resonance optical fiber sensor to detect organic vapors," *Sens. Actuators B Chem.*, vol. 187, pp. 65-71, 2013.

[126] Y. Zhao, Z. C. Feng, and Y. Liang, "SnO_2 gas sensor films deposited by pulsed laser ablation," *Sens. Actuators B Chem.*, vol. 56, pp. 224-227, 1999.

[127] K. Potje-Kamloth, "Semiconductor junction gas sensors," *Chem. Rev.*, vol. 108, pp. 367-399, 2008.

[128] L. Wang, H. Dou, Z. Lou, and T. Zhang, "Encapsuled nanoreactors (Au@SnO_2): a new sensing material for chemical sensors," *Nanoscale,* vol. 5, pp. 2686-2691, 2013.

[129] A. Lajn, H. v. Wenckstern, Z. Zhang, C. Czekalla, G. Biehne, J. Lenzner, *et al.*, "Properties of reactively sputtered Ag, Au, Pd, and Pt Schottky contacts on n-type ZnO," *J. Vac. Sci. Technol. B.*, vol. 27, pp. 1769-1773, 2009.

[130] J. Mizsei, P. Sipilä, and V. Lantto, "Structural studies of sputtered noble metal catalysts on oxide surfaces," *Sens. Actuators B Chem.*, vol. 47, pp. 139-144, 1998.

[131] I. T. Weber, A. Valentini, L. F. D. Probst, E. Longo, and E. R. Leite, "Influence of noble metals on the structural and catalytic properties of Ce-doped SnO_2 systems," *Sens. Actuators B Chem.*, vol. 97, pp. 31-38, 2004.

[132] L. Wang, Z. Lou, R. Wang, T. Fei, and T. Zhang, "Ring-like PdO-NiO with lamellar structure for gas sensor application," *J. Mater. Chem.*, vol. 22, pp. 12453-12456, 2012.

[133] Y. Hu, J. Zhou, P.-H. Yeh, Z. Li, T.-Y. Wei, and Z. L. Wang, "Supersensitive, fast-response nanowire sensors by using Schottky contacts," *Adv. Mater.*, vol. 22, pp. 3327-3332, 2010.

[134] M. Calatayud, A. Markovits, M. Menetrey, B. Mguig, and C. Minot, "Adsorption on perfect and reduced surfaces of metal oxides," *Catal. Today,* vol. 85, pp. 125-143, 2003.

[135] K. Hiehata, A. Sasahara, and H. Onishi, "Local work function analysis of Pt/TiO_2 photocatalyst by a Kelvin probe force microscope," *Nanotechnology,* vol. 18, 2007.

[136] K. D. Schierbaum, U. K. Kirner, J. F. Geiger, and W. Göpel, "Schottky-barrier and conductivity gas sensors based upon Pd/SnO_2 and Pt/TiO_2," *Sens. Actuators B Chem.*, vol. 4, pp. 87-94, 1991.

[137] T.-Y. Wei, P.-H. Yeh, S.-Y. Lu, and Z. Lin-Wang, "Gigantic enhancement in sensitivity using Schottky contacted nanowire nanosensor," *J. Am. Chem. Soc.*, vol. 131, pp. 17690-17695, 2009.

[138] S. Kandasamy, A. Trinchi, W. Wlodarski, E. Comini, and G. Sberveglieri, "Hydrogen and hydrocarbon gas sensing performance of Pt/WO_3/SiC MROSiC devices," *Sens. Actuators B Chem.*, vol. 111, pp. 111-116, 2005.

[139] M. Shafiei, A. Z. Sadek, J. Yu, K. Latham, M. Breedon, D. McCulloch, *et al.*, "A hydrogen gas sensor based on Pt/nanostructured WO_3/SiC Schottky diode," *Sens. Lett.*, vol. 9, pp. 11-15, 2011.

[140] M. Shafiei, J. Yu, M. Breedon, N. Motta, Q. Wu, Z. Hu, *et al.*, "Hydrogen gas sensors based on thermally evaporated nanostructured MoO_3 Schottky diode: A comparative study," in *Proceedings of IEEE Sensors Conference, Limerick*, 2011, pp. 8-11.

[141] M. Shafiei, J. Yu, M. Breedon, A. Moafi, K. Kalantar-zadeh, W. Wlodarski, *et al.*, "Pt/MoO_3 nano-flower/SiC Schottky diode based hydrogen gas sensor," in *9th IEEE Conf. Sens. Kona*, 2010, pp. 354-357.

[142] J. Yu, "Enhancement of electric field properties of Pt/nanoplatelet MoO_3/SiC Schottky diode," *J. Phys. D. Appl. Phys.*, vol. 43, p. 025103, 2010.

[143] J. Yu, S. J. Ippolito, M. Shafiei, D. Dhawan, W. Wlodarski, and K. Kalantar-zadeh, "Reverse biased Pt/nanostructured MoO_3/SiC Schottky diode based hydrogen gas sensors," *Appl. Phys. Lett.*, vol. 94, p. 013504, 2009.

[144] R. A. Rani, A. S. Zoolfakar, J. Z. Ou, R. Ab. Kadir, H. Nili, K. Latham, *et al.*, "Reduced impurity-driven defect states in anodized nanoporous Nb_2O_5: the possibility of improving performance of photoanodes," *Chem. Commun.*, vol. 49, pp. 6349-6351, 2013.

[145] J. Z. Ou, R. A. Rani, M.-H. Ham, M. R. Field, Y. Zhang, H. Zheng, *et al.*, "Elevated temperature anodized Nb_2O_5 : A photoanode material with exceptionally large photoconversion efficiencies," *ACS Nano*, vol. 6, pp. 4045-4053, 2012.

[146] M. K. Siddiki, S. Venkatesan, and Q. Qiao, "Nb_2O_5 as a new electron transport layer for double junction polymer solar cells," *Phys. Chem. Chem. Phys.*, vol. 14, pp. 4682-4686, 2012.

[147] G. Ramírez, S. E. Rodil, S. Muhl, D. Turcio-Ortega, J. J. Olaya, M. Rivera, *et al.*, "Amorphous niobium oxide thin films," *J. Non-Cryst. Solids*, vol. 356, pp. 2714-2721, 2010.

[148] X. Fang, L. Hu, K. Huo, B. Gao, L. Zhao, M. Liao, *et al.*, "New ultraviolet photodetector based on individual Nb_2O_5 nanobelts," *Adv. Funct. Mater.*, vol. 21, pp. 3907-3915, 2011.

[149] K. Yoshimura, T. Miki, S. Iwama, and S. Tanemura, "Characterization of niobium oxide electrochromic thin films prepared by reactive d.c. magnetron sputtering," *Thin Solid Films*, vol. 282, pp. 235-238, 1996.

[150] T. Hyodo, J. Ohoka, Y. Shimizu, and M. Egashira, "Design of anodically oxidized Nb_2O_5 films as a diode-type H_2 sensing material," *Sens. Actuators B Chem.*, vol. 117, pp. 359-366, 2006.

[151] Z. Wang, Y. Hu, W. Wang, X. Zhang, B. Wang, H. Tian, *et al.*, "Fast and highly-sensitive hydrogen sensing of Nb_2O_5 nanowires at room temperature," *Int. J. Hydrogen Energ.*, vol. 37, pp. 4526-4532, 2012.

[152] Y. D. Wang, L. F. Yang, Z. L. Zhou, Y. F. Li, and X. H. Wu, "Effects of calcining temperature on lattice constants and gas-sensing properties of Nb_2O_5," *Mater. Lett.*, vol. 49, pp. 277-281, 2001.

[153] H. G. Moon, H. W. Jang, J.-S. Kim, H.-H. Park, and S.-J. Yoon, "A route to high sensitivity and rapid response Nb_2O_5-based gas sensors: TiO_2 doping, surface embossing, and voltage optimization," *Sens. Actuators B Chem.*, vol. 153, pp. 37-43, 2011.

[154] J. Choi, J. H. Lim, S. Rho, D. Jahng, J. Lee, and K. J. Kim, "Nanoporous niobium oxide for label-free detection of DNA hybridization events," *Talanta*, vol. 74, pp. 1056-1059, 2008.

[155] H. L. Skriver and N. M. Rosengaard, "Surface energy and work function of elemental metals," *Phys. Rev. B*, vol. 46, pp. 7157-7168, 1992.

[156] J. Z. Ou, S. Balendhran, M. R. Field, D. G. McCulloch, A. S. Zoolfakar, R. A. Rani, *et al.*, "The anodized crystalline WO_3 nanoporous network with enhanced electrochromic properties," *Nanoscale*, vol. 4, pp. 5980-5988, 2012.

[157] D. Di Yao, M. R. Field, A. P. O'Mullane, K. Kalantar-zadeh, and J. Z. Ou, "Electrochromic properties of TiO_2 nanotubes coated with electrodeposited MoO_3," *Nanoscale*, vol. 5, pp. 10353-10359, 2013.

[158] J. Z. Ou, M. H. Yaacob, M. Breedon, H. D. Zheng, J. L. Campbell, K. Latham, *et al.*, "In situ Raman spectroscopy of H_2 interaction with WO_3 films," *Phys. Chem. Chem. Phys.*, vol. 13, pp. 7330-7339, 2011.

[159] M. H. Yaacob, J. Yu, K. Latham, K. Kalantar-Zadeh, and W. Wlodarski, "Optical hydrogen sensing properties of nanostructured Pd/MoO_3 films," *Sens. Lett.*, vol. 9, pp. 16-20, 2011.

[160] D. D. Yao, J. Z. Ou, K. Latham, S. Zhuiykov, A. P. O'Mullane, and K. Kalantar-zadeh, "Electrodeposited α- and β-phase MoO_3 films and investigation of their gasochromic properties," *Cryst. Growth Des.*, vol. 12, pp. 1865-1870, 2012.

[161] M. Aegerter, "Sol-gel chromogenic materials and devices," in *Optical and electronic phenomena in sol-gel glasses and modern application*. vol. 85, ed: Springer Berlin Heidelberg, 1996, pp. 149-194.

[162] R. C. Korosec and P. Bukovec, "Sol-gel prepared NiO thin films for electrochromic applications," *Acta Chim. Slov.*, vol. 53, pp. 136-147, 2006.

[163] G. A. Niklasson and C. G. Granqvist, "Electrochromics for smart windows: thin films of tungsten oxide and nickel oxide, and devices based on these," *J. Mater. Chem.*, vol. 17, pp. 127-156, 2007.

[164] H. Moulki, C. Faure, M. Mihelcic, A. S. Vuk, F. Svegl, B. Orel, *et al.*, "Electrochromic performances of nonstoichiometric NiO thin films," *Thin Solid Films*, vol. 553, pp. 63-66, 2014.

[165] R. Romero, E. A. Dalchiele, F. Martin, D. Leinen, and J. R. Ramos-Barrado, "Electrochromic behaviour of Nb_2O_5 thin films with different morphologies obtained by spray pyrolysis," *Sol. Energ. Mat. Sol. C*, vol. 93, pp. 222-229, 2009.

[166] A. V. Rosario and E. C. Pereira, "Optimisation of the electrochromic properties of Nb_2O_5 thin films produced by sol-gel route using factorial design," *Sol. Energ. Mat. Sol. C.*, vol. 71, pp. 41-50, 2002.

[167] A. Verma and P. K. Singh, "Sol-gel derived nanostructured niobium pentoxide thin films for electrochromic applications," *Indian J. Chem. A*, vol. 52, pp. 593-598, 2013.

[168] G. R. Lee and J. A. Crayston, "Electrochromic Nb_2O_5 and Nb_2O_5/silicone composite thin films prepared by sol-gel processing," *J. Mater. Chem.*, vol. 1, pp. 381-386, 1991.

[169] K. Yoshimura, T. Miki, and S. Tanemura, "Electrochromic properties of niobium oxide thin films prepared by DC magnetron sputtering," *J. Electrochem. Soc.*, vol. 144, pp. 2982-2985, 1997.

[170] K. Yoshimura, T. Miki, S. Iwama, and S. Tanemura, "Niobium oxide electrochromic thin-films prepared by reactive DC magnetron sputtering," *Jpn. J. Appl. Phys. 2*, vol. 34, pp. L1293-L1296, 1995.

[171] W. Hu, Z. Liu, D. Tian, S. Zhang, Y. Zhao, and K. Yao, "Morphological evolution of Nb_2O_5 in a solvothermal reaction: From Nb_2O_5 grains to Nb_2O_5 nanorods and hexagonal Nb_2O_5 nanoplatelets," *J. Wuhan Univ. Technol.*, vol. 24, pp. 245-248, 2009.

[172] M. Wei, Z.-m. Qi, M. Ichihara, and H. Zhou, "Synthesis of single-crystal niobium pentoxide nanobelts," *Acta Mater.*, vol. 56, pp. 2488-2494, 2008.

[173] H. Luo, M. Wei, and K. Wei, "Synthesis of Nb_2O_5 nanorods by a soft chemical process," *J. Nanomater.*, p. 758353, 2009.

[174] H. Luo, M. Wei, and K. Wei, "Synthesis of Nb_2O_5 nanosheets and its electrochemical measurements," *Mater. Chem. Phys.*, vol. 120, pp. 6-9, 2010.

[175] Y. Zhao, C. Eley, J. Hu, J. S. Foord, L. Ye, H. He, *et al.*, "Shape-dependent acidity and photocatalytic activity of Nb_2O_5 nanocrystals with an active TT (001) surface," *Angew. Chem. Int. Edit.*, vol. 51, pp. 3846-3849, 2012.

[176] R. A. Rani, A. S. Zoolfakar, J. Subbiah, J. Z. Ou, and K. Kalantar-zadeh, "Highly ordered anodized Nb_2O_5 nanochannels for dye-sensitized solar cells," *Electrochem. Commun.*, vol. 40, pp. 20-23, 2014.

[177] M. M. Rahman, R. A. Rani, A. Z. Sadek, A. S. Zoolfakar, M. R. Field, T. Ramireddy, *et al.*, "A vein-like nanoporous network of Nb_2O_5 with a higher lithium intercalation discharge cut-off voltage," *J. Mater. Chem. A*, vol. 1, pp. 11019-11025, 2013.

[178] J. Z. Ou, R. A. Rani, M.-H. Ham, M. R. Field, Y. Zhang, H. Zheng, *et al.*, "Elevated temperature anodized Nb_2O_5: A photoanode material with exceptionally large photoconversion efficiencies," *ACS Nano*, vol. 6, pp. 4045-4053, 2012.

[179] A. Mozalev, R. M. Vazquez, C. Bittencourt, D. Cossement, F. Gispert-Guirado, E. Llobet, *et al.*, "Formation-structure-properties of niobium-oxide nanocolumn arrays via self-organized anodization of sputter-deposited aluminum-on-niobium layers," *J. Mater. Chem. C*, vol. 2, pp. 4847-4860, 2014.

[180] K. Lee, Y. Yang, M. Yang, and P. Schmuki, "Formation of highly ordered nanochannel Nb oxide by self-organizing anodization," *Chem. Eur. J*, vol. 18, pp. 9521-9524, 2012.

[181] H. Wang, Z. Lu, S. Xu, D. Kong, J. J. Cha, G. Zheng, *et al.*, "Electrochemical tuning of vertically aligned MoS_2 nanofilms and its application in improving hydrogen evolution reaction," *P. Natl. Acad. Sci. USA*, vol. 110, pp. 19701-19706, 2013.

[182] S. K. Deb, "Reminiscences on the discovery of electrochromic phenomena in transition metal oxides," *Sol. Energ. Mat. Sol. C.*, vol. 39, pp. 191-201, 1995.

[183] C. G. Granqvist, "Electrochromic tungsten oxide films: Review of progress 1993–1998," *Sol. Energ. Mat. Sol. C.*, vol. 60, pp. 201-262, 2000.

[184] D. T. Gillaspie, R. C. Tenent, and A. C. Dillon, "Metal-oxide films for electrochromic applications: present technology and future directions," *J. Mater. Chem.*, vol. 20, pp. 9585-9592, 2010.

[185] D. D. Yao, R. A. Rani, A. P. O'Mullane, K. Kalantar-zadeh, and J. Z. Ou, "Enhanced coloration efficiency for electrochromic devices based on anodized Nb_2O_5/electrodeposited MoO_3 binary systems," *J. Phys. Chem. C,* vol. 118, pp. 10867-10873, 2014.

[186] B. Melody, T. Kinard, and P. Lessner, "The non-thickness-limited growth of anodic oxide films on valve metals," *Electrochem. Solid St.,* vol. 1, pp. 126-129, 1998.

[187] N. Truong Nhat, D. Kim, D.-Y. Jeong, M.-W. Kim, and J. U. Kim, "Formation behavior of nanoporous anodic aluminum oxide films in hot glycerol/phosphate electrolyte," *Electrochim. Acta,* vol. 83, pp. 288-293, 2012.

[188] S. Yang, Y. Aoki, and H. Habazaki, "Effect of electrolyte temperature on the formation of self-organized anodic niobium oxide microcones in hot phosphate-glycerol electrolyte," *Appl. Surf. Sci.,* vol. 257, pp. 8190-8195, 2011.

[189] Q. Lu, T. Hashimoto, P. Skeldon, G. E. Thompson, H. Habazaki, and K. Shimizu, "Nanoporous anodic niobium oxide formed in phosphate/glycerol electrolyte," *Electrochem. Solid St.,* vol. 8, pp. B17-B20, 2005.

[190] Y. Oikawa, T. Minami, H. Mayama, K. Tsujii, K. Fushimi, Y. Aoki, *et al.*, "Preparation of self-organized porous anodic niobium oxide microcones and their surface wettability," *Acta Mater.,* vol. 57, pp. 3941-3946, 2009.

[191] S. K. Deb, "Opportunities and challenges in science and technology of WO_3 for electrochromic and related applications," *Sol. Energ. Mat. Sol. C,* vol. 92, pp. 245-258, 2008.

[192] M. Gillet, K. Aguir, C. Lemire, E. Gillet, and K. Schierbaum, "The structure and electrical conductivity of vacuum-annealed WO_3 thin films," *Thin Solid Films,* vol. 467, pp. 239-246, 2004.

[193] H. Watanabe, K. Fujikata, Y. Oaki, and H. Imai, "Band-gap expansion of tungsten oxide quantum dots synthesized in sub-nano porous silica," *Chem. Commun.*, vol. 49, pp. 8477-8479, 2013.

[194] A. Z. Sadek, H. Zheng, M. Breedon, V. Bansal, S. K. Bhargava, K. Latham, *et al.*, "High-temperature anodized WO_3 nanoplatelet films for photosensitive devices," *Langmuir*, vol. 25, pp. 9545-9551, 2009.

[195] B. Cao, J. Chen, X. Tang, and W. Zhou, "Growth of monoclinic WO_3 nanowire array for highly sensitive NO_2 detection," *J. Mater. Chem.*, vol. 19, pp. 2323-2327, 2009.

[196] Z. Gu, T. Zhai, B. Gao, X. Sheng, Y. Wang, H. Fu, *et al.*, "Controllable assembly of WO_3 nanorods/nanowires into hierarchical nanostructures," *J. Phys. Chem. B*, vol. 110, pp. 23829-23836, 2006.

[197] H. G. Choi, Y. H. Jung, and D. K. Kim, "Solvothermal synthesis of tungsten oxide nanorod/nanowire/nanosheet," *J. Am. Ceram. Soc.*, vol. 88, pp. 1684-1686, 2005.

[198] J. Zhang, J.-p. Tu, X.-h. Xia, X.-l. Wang, and C.-d. Gu, "Hydrothermally synthesized WO_3 nanowire arrays with highly improved electrochromic performance," *J. Mater. Chem.*, vol. 21, pp. 5492-5498, 2011.

[199] J. Z. Ou, R. A. Rani, S. Balendhran, A. S. Zoolfakar, M. R. Field, S. Zhuiykov, *et al.*, "Anodic formation of a thick three-dimensional nanoporous WO_3 film and its photocatalytic property," *Electrochem. Commun.*, vol. 27, pp. 128-132, 2013.

[200] J. Z. Ou, M. Z. Ahmad, K. Latham, K. Kalantar-zadeh, G. Sberveglieri, and W. Wlodarski, "Synthesis of the nanostructured WO_3 via anodization at elevated temperature for H_2 sensing applications," *Procedia Engineering*, vol. 25, 2011.

[201] C. S. Rout, K. Ganesh, A. Govindaraj, and C. N. R. Rao, "Sensors for the nitrogen oxides, NO_2, NO and N_2O, based on In_2O_3 and WO_3 nanowires," *Appl. Phys. A-Mater.,* vol. 85, pp. 241-246, 2006.

[202] X.-Y. Xue, B. He, S. Yuan, L.-L. Xing, Z.-H. Chen, and C.-H. Ma, "SnO_2/WO_3 core-shell nanorods and their high reversible capacity as lithium-ion battery anodes," *Nanotechnology,* vol. 22, 2011.

[203] H. Zheng, Y. Tachibana, and K. Kalantar-zadeh, "Dye-sensitized solar cells based on WO_3," *Langmuir,* vol. 26, pp. 19148-19152, 2010.

[204] T. Siciliano, A. Tepore, G. Micocci, A. Serra, D. Manno, and E. Filippo, "WO_3 gas sensors prepared by thermal oxidization of tungsten," *Sens. Actuators B Chem.,* vol. 133, pp. 321-326, 2008.

[205] M. Shafiei, A. Z. Sadek, J. Yu, K. Latham, M. Breedon, D. McCulloch, *et al.*, "A hydrogen gas sensor based on Pt/nanostructured WO_3/SiC Schottky diode," *Sens. Lett,* vol. 9, pp. 11-15, 2011.

[206] Y. Liu, J. Yu, F. X. Cai, W. M. Tang, and P. T. Lai, "A novel hydrogen sensor based on Pt/WO_3/Si MIS Schottky diode," in *Electron Devices and Solid-State Circuits (EDSSC), 2013 IEEE International Conference of*, 2013, pp. 1-2.

[207] M. H. Yaacob, M. Breedon, K. Kalantar-zadeh, and W. Wlodarski, "Absorption spectral response of nanotextured WO_3 thin films with Pt catalyst towards H_2," *Sens. Actuators B Chem.,* vol. 137, pp. 115-120, 2009.

[208] C. W. Walter, C. F. Hertzler, P. Devynck, G. P. Smith, and J. R. Peterson, "Photodetachment of WO_3 : The electron affinity of WO_3," *J. Chem. Phys.,* vol. 95, pp. 824-827, 1991.

[209] D. Haridas, K. Sreenivas, and V. Gupta, "Improved response characteristics of SnO_2 thin film loaded with nanoscale catalysts for LPG detection," *Sens. Actuators B Chem.*, vol. 133, pp. 270-275, 2008.

[210] I. Lundström, S. Shivaraman, C. Svensson, and L. Lundkvist, "A hydrogen−sensitive MOS field−effect transistor," *Appl. Phys. Lett.*, vol. 26, pp. 55-57, 1975.

[211] N. Yamamoto, S. Tonomura, T. Matsuoka, and H. Tsubomura, "A study on a palladium-titanium oxide Schottky diode as a detector for gaseous components," *Surf. Sci.*, vol. 92, pp. 400-406, 1980.

[212] K. I. Lundstrom, M. S. Shivaraman, and C. M. Svensson, "A hydrogen sensitive Pd-gate MOS transistor," *J. Appl. Phys.*, vol. 46, pp. 3876-3881, 1975.

[213] K. Bourenane, A. Keffous, G. Nezzal, A. Bourenane, Y. Boukennous, and A. Boukezzata, "Influence of thickness and porous structure of SiC layers on the electrical properties of Pt/SiC-pSi and Pd/SiC-pSi Schottky diodes for gas sensing purposes," *Sens. Actuators B Chem.*, vol. 129, pp. 612-620, 2008.

[214] Y.-F. Sun, S.-B. Liu, F.-L. Meng, J.-Y. Liu, Z. Jin, L.-T. Kong, *et al.*, "Metal oxide nanostructures and their gas sensing properties: A review," *Sensors*, vol. 12, pp. 2610-2631, Mar 2012.

[215] Y. Shimizu and M. Egashira, "Basic aspects and challenges of semiconductor gas sensors," *MRS Bulletin*, vol. 24, pp. 18-24, 1999.

[216] T. Wagner, S. Haffer, C. Weinberger, D. Klaus, and M. Tiemann, "Mesoporous materials as gas sensors," *Chem. Soc. Rev.*, vol. 42, pp. 4036-4053, 2013.

[217] T. Hyodo, Y. Shimizu, and M. Egashira, "Design of mesoporous oxides as semiconductor gas sensor materials," *Electrochemistry*, vol. 71, pp. 387-393, 2003.

[218] F. Hossein-Babaei, S. Abbaszadeh, and M. S. Esfahani, "Gas sensitive porous silver-rutile high-temperature Schottky diode on thermally oxidized titanium," *IEEE Sens. J.*, vol. 9, pp. 237-243, 2009.

[219] R. A. Kadir, R. A. Rani, A. S. Zoolfakar, J. Z. Ou, M. Shafiei, W. Wlodarski, *et al.*, "Nb_2O_5 Schottky based ethanol vapour sensors: Effect of metallic catalysts," *Sens. Actuators B Chem.*, vol. 202, pp. 74-82, 2014.

[220] A. Salehi, A. Nikfarjam, and D. J. Kalantari, "Pd/porous-GaAs Schottky contact for hydrogen sensing application," *Sens. Actuators B Chem.*, vol. 113, pp. 419-427, 2006.

[221] A. Salehi and D. J. Kalantari, "Characteristics of highly sensitive Au/porous-GaAs Schottky junctions as selective CO and NO gas sensors," *Sens. Actuators B Chem.*, vol. 122, pp. 69-74, 2007.

[222] J. M. Macak, H. Tsuchiya, A. Ghicov, K. Yasuda, R. Hahn, S. Bauer, *et al.*, "TiO_2 nanotubes: Self-organized electrochemical formation, properties and applications," *Curr. Opin. Solid St. M.*, vol. 11, pp. 3-18, 2007.

[223] H. Masuda, F. Hasegwa, and S. Ono, "Self-ordering of cell arrangement of anodic porous alumina formed in sulfuric acid solution," *J. Electrochem. Soc.*, vol. 144, pp. L127-L130, 1997.

[224] H. E. Prakasam, K. Shankar, M. Paulose, O. K. Varghese, and C. A. Grimes, "A new benchmark for TiO_2 nanotube array growth by anodization," *J. Phys. Chem. C*, vol. 111, pp. 7235-7241, 2007.

[225] B. Pandey, P. S. Thapa, D. A. Higgins, and T. Ito, "Formation of self-organized nanoporous anodic oxide from metallic gallium," *Langmuir*, vol. 28, pp. 13705-13711, 2012.

Chapter 2

Electrospun Granular Hollow SnO_2 Nanofibers Hydrogen Gas Sensors Operating at Low Temperatures

2.1 Introduction

In chapter 1, it was highlighted that the specific aim of Chapter 2 was to present the work of PhD candidate on incorporating electrospin coated SnO_2 nanofibers for hydrogen gas sensing. This work is focused on altering the stoichiometry and morphology of the nanofibers in order to meet the objectives of reduced operating temperature and high sensitivity to hydrogen (H_2) gas.

In this chapter, the outcomes investigations regarding H_2 gas sensors based on hollow and filled - well aligned electrospun SnO_2 nanofibers are presented. SnO_2 nanofibers with diameters ranging from 80 to 400 nm are successfully synthesized in which the diameter of the nanofibers can be controlled by adjusting the concentration of polyacrylonitrile in the solution for electrospinning. The presence of the polymer results in the formation of granular walls for the nanofibers which are presented in detail in this chapter. The author presents the correlation between nanofibers morphology, structure, oxygen vacancy contents and the gas sensing performances. From the X-ray photoelectron spectroscopy analysis presented in this chapter, it is revealed that the granular hollow SnO_2 nanofibers, which show the highest responses, contain a significant number of oxygen vacancies, which are favorable for gas sensor operating at low temperatures.

The work presented in this chapter was published as a full article in the *Journal of Physical Chemistry C* [1].

2.2 Experimental

2.2.1 Synthesis of SnO_2 nanofibers

SnO_2 nanofibers were electrospun from solutions containing stannous chloride ($SnCl_2.2H_2O$), polyvinyl pyrrolidone (PVP, molecular weight (M_w) =1,300,000), polyacrylonitrile (PAN, M_w=150,000) and dimethylformamide (DMF). Two precursor solutions were prepared as follows:

Solution A: A 0.02 M of stannous chloride was dissolved in 20 mL DMF mixed and stirred for 6 h. Subsequently, 6 g of PVP was dissolved in the solution and continuously stirred for 12 h using vigorous magnetic stirring.

Solution B: Here, 1 g of PAN was dissolved in 10 mL of DMF and kept at 80 ˚C for 12 h and cooled down to the room temperature for 12 h.

Consequently, 4 mL of solution A was mixed with 1, 2 and 3 mL of solution B which are denoted as PAN 1, PAN 2 and PAN 3, respectively. All these solutions were then magnetically stirred for 3 h at speed of 1000 rpm for PAN 1 and PAN 2, and 1500 rpm for PAN 3, and separately electrospun on quartz substrates attached on rotating electrode under an applied voltage of 20 kV, by using a syringe that was kept at a distance of 15 cm from the quartz substrate. The electrospun were conducted for 40 min for each sample. The apparatus utilized for electrospinning is depicted in Figure 2.1(a). The flow rate of the solutions was kept at 0.4 mL/h during the electrospinning process. The as-electrospun samples were annealed for 4 h at 500 °C in air at a heating ramping up of 5 °C/min. During heat treatment, PAN and PVP were decomposed and the $SnCl_2.2H_2O$ precursor was transformed into SnO_2 nanofibers.

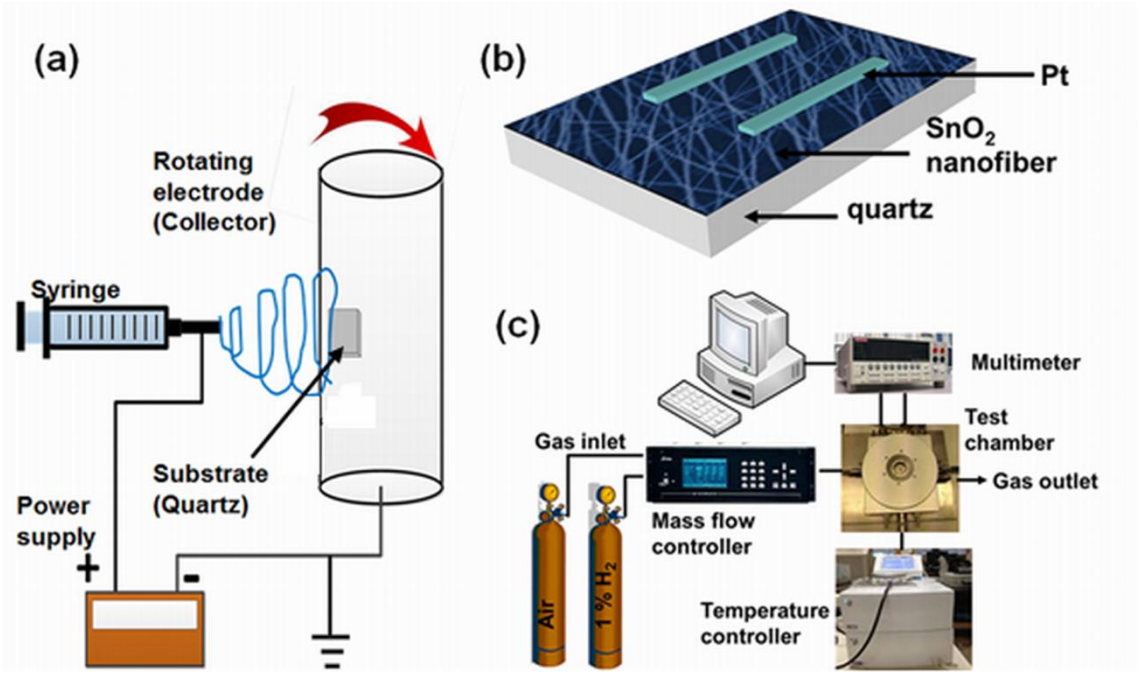

Figure 2.1: Schematic illustration of (a) electrospinning apparatus, (b) three-dimensional configuration of the gas sensor, and (c) gas sensing measurement system.

2.2.2 SnO_2 gas sensor fabrication

For forming the electrodes, Pt layer with the thickness of ~20 nm was deposited on top of the SnO_2 nanofibers using a GATAN PECS^{TM} (Precision Etching Coating System) thin film coater. The distance between Pt electrodes was 0.5 mm and the width of each electrode side was 0.15 mm. The three-dimensional gas sensor configuration is shown in Figure 1(b).

2.2.3 Structural characterization

The surface morphology and structural properties of SnO_2 nanofibers were characterized using scanning electron microscopy (SEM - Zeiss Supra 55VP FEG SEM). Transmission electron microscopy (TEM) images were obtained using a JEOL TEM 2100 and the atomic force microscopy (AFM) images were acquired using Digital

Instruments D3100 Atomic Force Microscope. The crystallographic properties were studied *via* X-ray diffraction (XRD) using a Bruker D8 Discover microdiffractometer fitted with a general area detector diffraction system (GADDS) that accommodated Cu-Kα radiation (λ = 1.54178 Å). To determine the surface properties of the SnO_2 nanofibers, X-ray photoelectron spectroscopy (XPS) was performed using a Thermo Scientific K-α instrument using Al K-α X-ray source (1486.7 eV) with pass energy of 50 eV. Raman characterizations were performed using a HORIBA-XploRA confocal Raman microscope, incorporating a 532 nm 40 mW laser as the excitation source.

2.2.4 Gas sensing measurements

The performance of the gas sensors was assessed in a LINKAM (Scientific Instruments) gas testing chamber. Detail of the measurement set-up can be seen in the schematic diagram as presented in Figure 2.1(c). Electrical connections to the gas sensors were achieved by physically connecting needle probes to the Pt electrodes of the sensors. A Keithley 2001 multimeter was used for measuring the changes of sensor resistance over time and a computer was used for logging data from the multimeter. Initially, the responses of the sensors were measured in the presence of 1% H_2 gas in the ambient air where the temperatures were altered in the range of 100 – 200 °C in order to determine their optimum operating temperature. Finally, full range tests for each sensor were performed at the determined optimum operating temperature. Each sensor was exposed to H_2 gas pulse sequences of 0.06%, 0.12%, 0.25%, 0.50% and 1% H_2 in the ambient air. The H_2 gas concentration was accurately controlled using a computerized mass flow control (MFC) multi-channel gas calibration system. Gas exposure time was 10 min for each pulse of H_2 gas and the chamber was purged with synthetic air for 10 min between pulses to allow the sensors to recover in atmospheric conditions. For all the experiments, the total flow was fixed to be 200 sccm.

2.3 Results and discussion

2.3.1 SnO_2 nanofibers characterizations

The lower magnification SEM image of electrospun SnO_2 nanofibers in Figure 2.2 shows a well aligned texture, which has been demonstrated to be favorable in gas sensing performance due to the enhanced surface-to-volume ratio [2]. Figure 2.3 shows typical SEM images of SnO_2 nanofibers with diameters of the nanofibers ranging from 80 to 400 nm. It has been shown that the morphology and diameter of nanofibers depend on the added polymer concentration in the electrospinning solution [3-5]. In this work, electrospinning PAN 1 and PAN 2 solutions resulted in the formations of hollow tubular nanofibers with average diameters of ~80 and 250 nm, respectively, as shown in Figure 2.3(a, b, d, e). On the other hand, nanofibers electrospun using solution PAN 3 resulted in nanofibers consisting of multiple small hollow channels and a diameter of ~400 nm as presented in Figure 2.3(c, f). As also demonstrated by Choi *et al.*, these granular walls are formed after the annealing process [6]. However, they obtained larger grains in the order of 50 nm. It can be seen from that in this work all electrospun nanofibers are also corrugated, containing smaller grains.

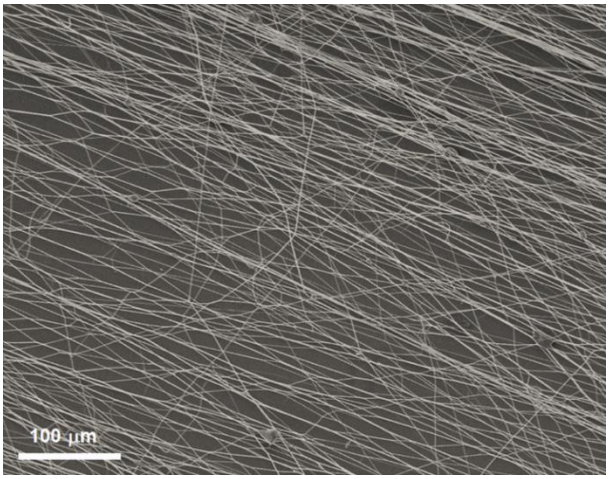

Figure 2.2: Low magnification SEM image of the well-aligned SnO_2 nanofibers (PAN 1). The other samples are not shown for brevity

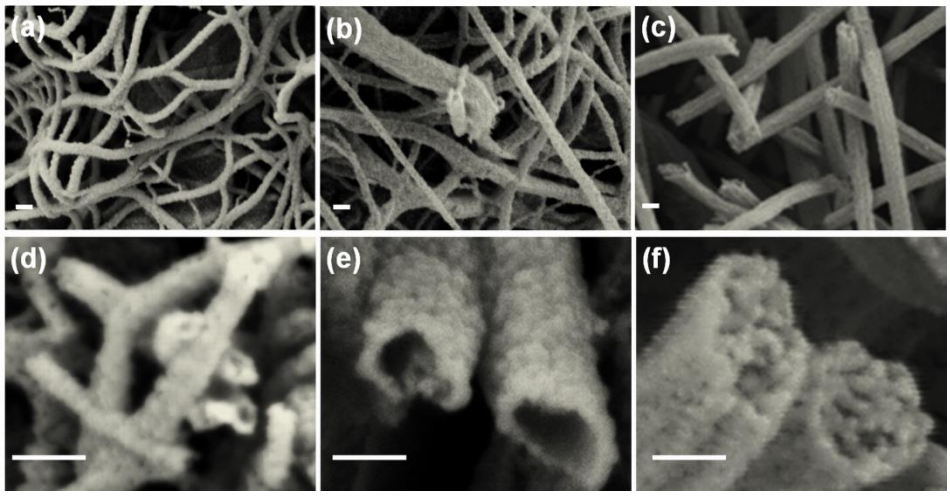

Figure 2.3: SEM images of the SnO_2 nanofibers electrospun using solution of (a) PAN 1, (b) PAN 2 and (c) PAN 3 and (d−f) magnified image of parts a−c, respectively (scale bar = 200 nm).

Further morphology characterization was conducted using TEM as presented in Figure 2.4. The TEM images of hollow (PAN 1) and solid (PAN 3) SnO_2 nanofibers show that both samples have a corrugated surface composed of many aggregated grains. As can be seen the fibers are hollow and made of walls, which are formed from connected nanoparticles in nanofiber that has been established using the PAN 1 solution. In the case of PAN 3, the fiber is larger and filled.

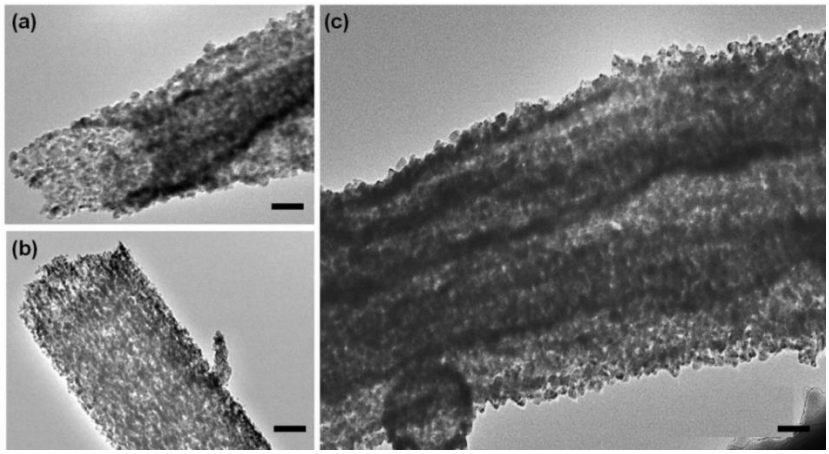

Figure 2.4: TEM images of the SnO_2 nanofibers electrospun using solution of (a, b) PAN 1 (hollow structure) and (c) PAN 3 (solid structure) with the scale bar of 50 nm.

It is obvious that the concentration of PAN has significantly affect the average diameter of the electrospun nanofibers. He *et al.* [4] have established an allometrical relationship between the diameter (d) of the electrospun nanofibers and the solution concentration (C) in form of:

$$d \propto C^{\delta} \tag{2.1}$$

where δ is the scaling exponent which depends on the polymer type. It is suggested that the diameter of electrospun nanofibers increase approximately linearly with the solution concentration. It is also observed that, when solution of PAN 3 (3 mL) was used, filled nanofibers were obtained, while for PAN 1 and PAN 2 solutions, the obtained nanofibers were hollow. It is known that the solution concentration and viscosity are two closely correlated factors in electrospinning. Increase of the solution concentration will increase the solution viscosity [7]. The viscosity and the surface tension of the solution increase the diameter and the amount of mass per cross-section during the fiber formation in the electrospinning process. It is suggested that increase of solution viscosity from PAN 1 to PAN 2 and PAN 3, result in the formation of thicker nanofibers.

Various methods have been investigated in order to obtain hollow and filled nanofibers. For example, Wang *et al.* attained solid and hollow SnO_2 nanofiber by altering the annealing temperature of the electrospun samples [8]. The uses of sacrificial precursor materials such as PVP, PAN and PMMA have shown to result in hollow nanofiber [9-12]. For the work in this chapter, the author used phase separated, mixed polymer composite solution of PAN and PVP. PAN 1 and PAN 2 were magnetically stirred at speed of 1000 rpm, while the stirring speed of PAN 3 was 1500 rpm.

Due to the immiscibility and incompatibility between PVP and PAN as well as the elongations during the electrospinning, phase separation occurs. It is suggested that the PAN domains form the core of the nanofiber, whereas the PVP/$SnCl_2$ forms the shell of the nanofibers [13]. During calcination, PAN and PVP decompose leaving hollow nanofibers while the $SnCl_2$ is oxidized and converted to SnO_2.

The transformation from hollow nanofibers in samples that were formed using PAN 1 and PAN 2 solutions to filled nanofibers using PAN 3 solution can be due to the increase in the stirring speed. At the stirring speed of 1000 rpm, larger PAN droplets are established that can rejoin forming elongated PAN morphologies at the centre of the mixed solution, while injected out of the syringe (schematically illustrated in Figure 2.5 (a)). As a result, the $SnCl_2$ which is mainly in PVP are generally pushed to the side forming hollow nanofibers after the calcination. However, by increasing the stirring speed from 1000 to 1500 rpm, the drop sizes of PAN within the mixed solution becomes smaller. In this case, the PAN and $SnCl_2$ are more randomly dispersed in the PVP solution, and together with PVP, are injected out of the syringe in a much more mixed state (schematically illustrated in Figure 2.5(b)). As such, after the calcination filled SnO_2 nanofibers are obtained.

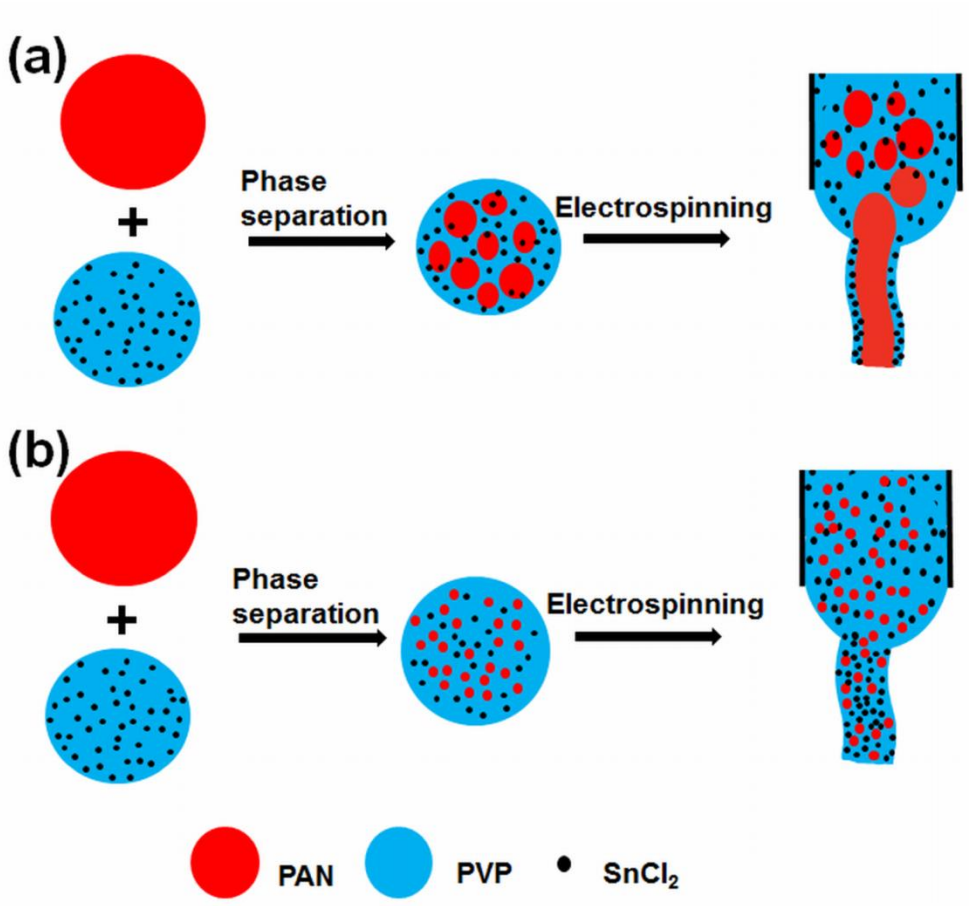

Figure 2.5: The illustrative diagram for the formation mechanism of SnO_2 nanofibers electrospun using solution of (a) PAN 1 and PAN 2 (hollow structure) and (b) PAN 3 (solid structure).

Figure 2.6 shows the XRD patterns of the SnO_2 nanofibers. The diffraction patterns of samples obtained using PAN 1, PAN 2 and PAN 3 solutions were similar, and peaks of the these samples can be perfectly indexed as the tetragonal rutile structure (JCPDS 41-1445), which are consistent with previous reports [14]. XPS analysis was conducted to identify the surface chemical states and the elemental distribution within the SnO_2 nanofibers.

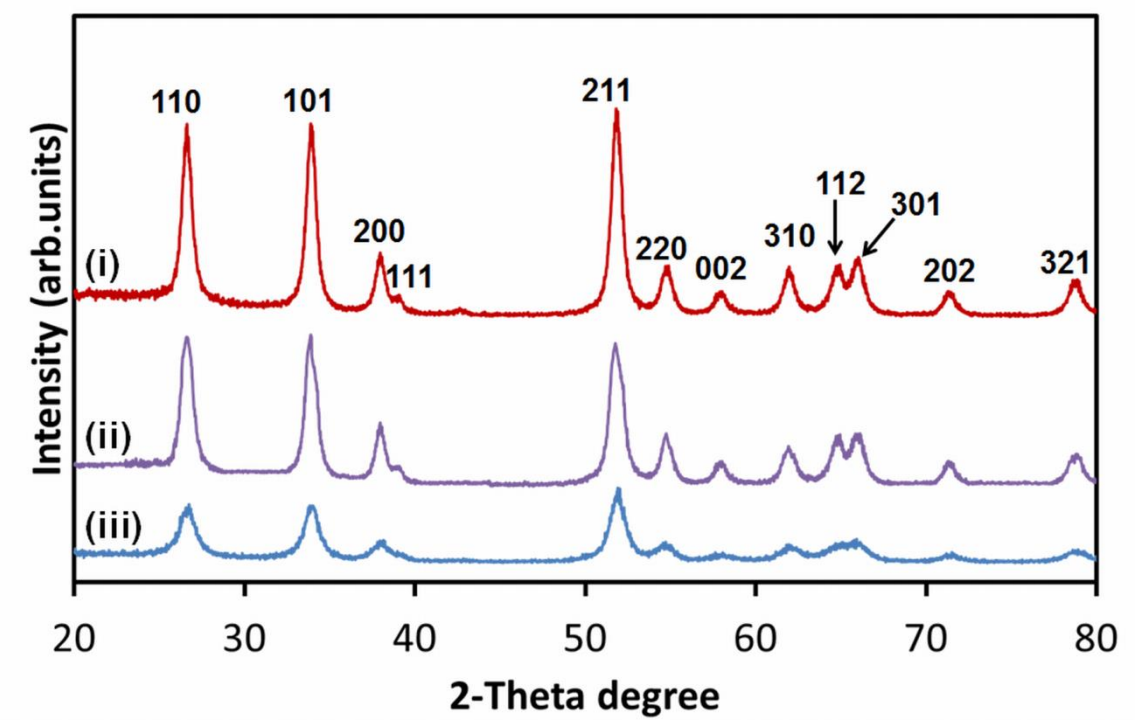

Figure 2.6: XRD patterns of SnO_2 nanofibers electrospun using the solution of (i) PAN 1, (ii) PAN 2, and (iii) PAN 3.

Figure 2.7(a) depicts the XPS full survey spectrum of the samples that were electrospun using PAN 1, PAN 2 and PAN 3 solutions. All clearly indicate the photoelectron peaks of Sn and O. Peaks for $Sn3d_{5/2}$ and $Sn3d_{3/2}$ with a spin-orbit splitting of 8.4 eV is seen in Figure 2.7(b) [15]. This is in agreement with previously reported tin oxide nanostructured films presenting the existence of Sn^{4+} bound to oxygen in the SnO_2 [16, 17]. The peak of $Sn3d_{5/2}$ shows only one symmetric component without a shoulder, indicating the absence of Sn^{2+}. From Figure 2.7(b) it is observed that as the concentration of PAN in the solutions increased, both Sn3d peaks have ~0.4 eV shifts to smaller binding energies, suggesting that the oxygen deficiencies are introduced in the SnO_2 nanofibers.

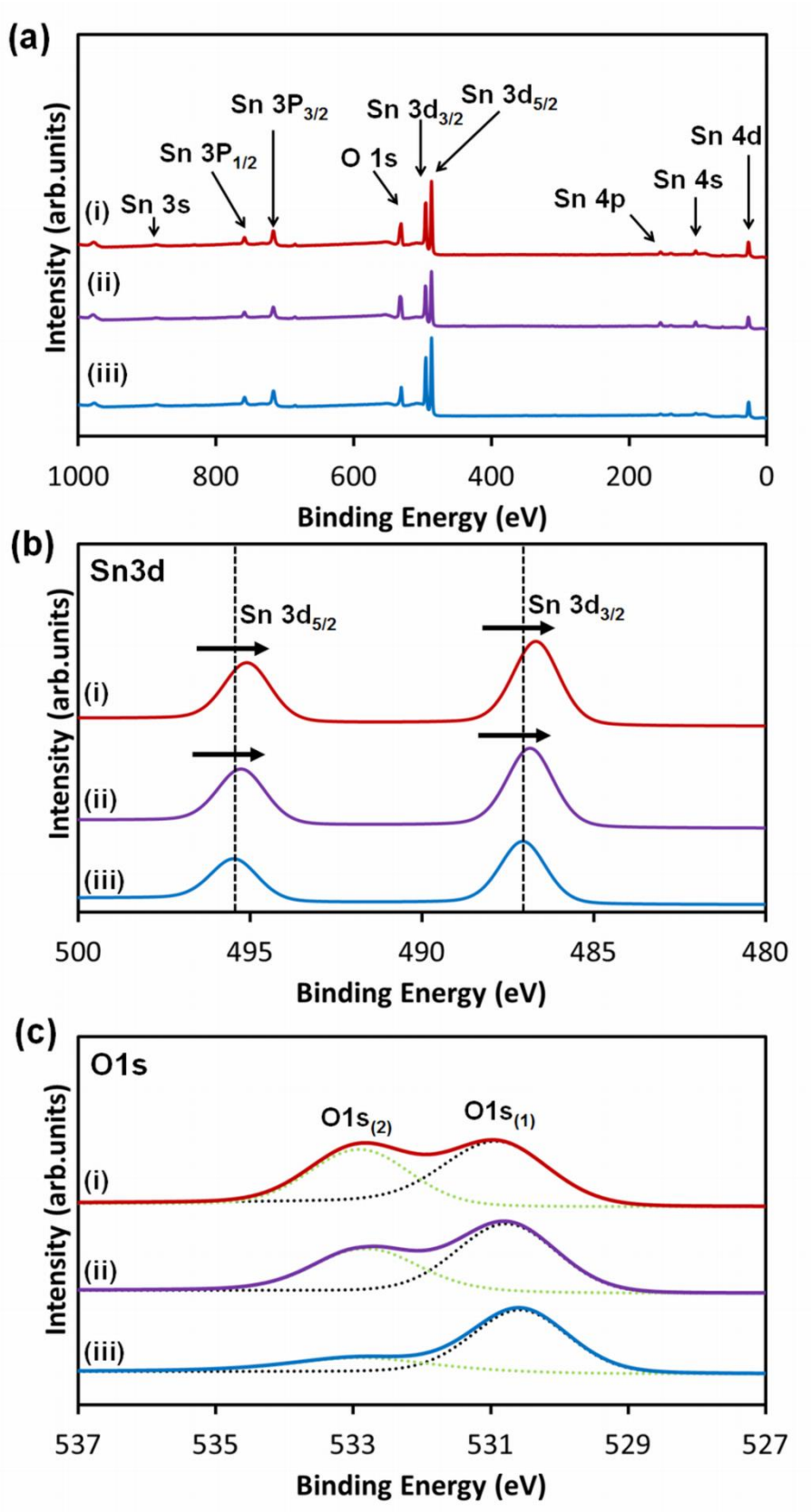

Figure 2.7: XPS spectra of SnO_2 nanofibers (a) survey spectra, (b) Sn3d, and (c) O1s corresponding to sample electrospun using (i) PAN 1 (ii) PAN 2, and (iii) PAN 3.

The broad O1s peaks are resolved by a Lorentzian distribution fitting as shown in Figure 2.7(c), in which two deconvoluted peaks at binding energy of 530.9 ± 0.2 and 532.9 ± 0.2 eV can be identified. The peak at 530.9 ± 0.2 eV is the $O1s_{(1)}$ peak, which is attributed to the coordination of O^{2-} oxygen bounded to tin atoms and denoted as low binding energy component (LBEC) [16, 18]. The other peak at 532.9 ± 0.2 eV ($O1s_{(2)}$ peak) is denoted as the high binding energy component (HBEC) corresponding to either absorbed surface H_2O, or presence of oxygen vacancies and hydroxyl (OH) groups on the surface of the SnO_2. It has been reported that defect electronic states appearing due to SnO_2 annealing at temperatures less than or above 520 °C to result in oxygen vacancies [19]. Yang *et al.* also reported that the H_2O decreased as the annealed temperature increased [20]. In addition, Seo *et al.* reported that the hydroxyl content also decreased as the annealed temperature increased [21]. Considering that the samples have been annealed at high temperature for a very long period, the relatively large contribution of HBEC peak ($O1s_{(2)}$), strongly suggests the presence of oxygen deficiencies in the samples and not absorbed H_2O or hydroxyl group. The relatively large contribution of HBEC peak ($O1s_{(2)}$), strongly suggests the presence of oxygen deficiencies in the samples. It is also observed that the $O1s_{(2)}$ peak develops with the increasing of PAN concentration, where the $O1s_{(2)}$ peak is more pronounced in the samples prepared using PAN 1. Therefore, it is noticed that SnO_2 prepared by PAN 1 has the maximum concentration of oxygen deficiencies. The presence of high oxygen vacancies in the nanofibers is highly beneficial for gas sensing as these oxygen vacancies play an important role as adsorption sites for gaseous species and can greatly enhanced gas sensing performance [22].

For further determination of phase composition of the films, Raman spectra were also obtained, which are presented in Figure 2.8. The SnO_2 peaks are located at 313,

580, 632 and 774 cm^{-1}. The spectra obtained indicate that the film is composed of SnO_2, which is consistent with previous reports [23] and well in agreement with those obtained from XRD and XPS analysis.

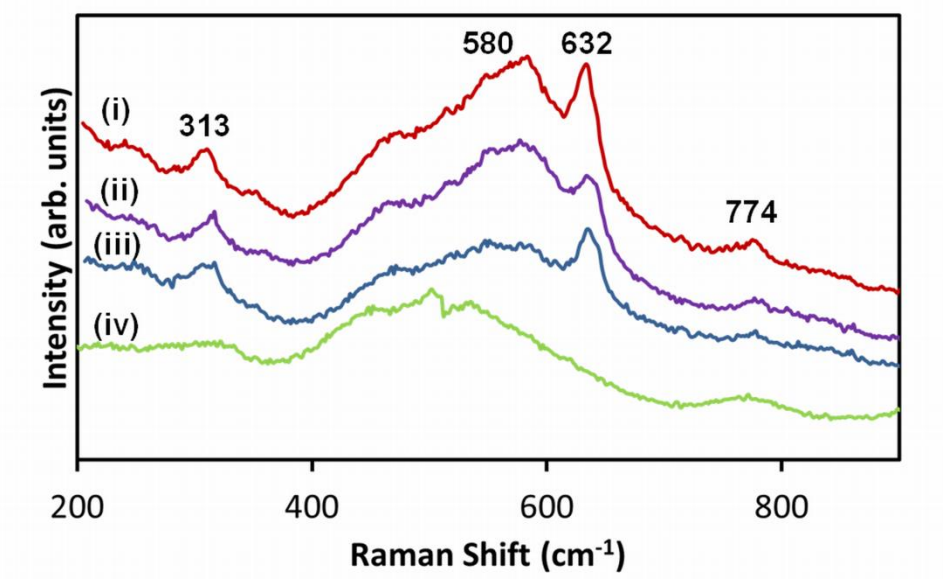

Figure 2.8: Raman spectra of SnO2 nanofibes electrospun using the solution of (i) PAN 1, (ii) PAN 2, (iii) PAN 3, and (iv) substrate (glass) as a reference.

2.3.2 Gas sensing performances

The operating temperature of the sensors plays a vital role in their sensing properties. In order to promote redox reactions of metal oxide sensors, elevated operating temperatures are required to achieve the optimum functionalities [24]. The measurements were initially conducted by obtaining the sensors' responses in the presence of 1% H_2 gas in synthetic air, where the temperatures were altered in the range of 100–200 °C. The optimum operating temperature was determined by comparing the responses. The sensor response (*SR*) is defined as;

$$SR = \left(\frac{R_{air}}{R_{gas}} \right) \tag{2.2}$$

where R_{air} and R_{gas} are the sensor resistances in air and in the target gas, respectively [25].

Figure 2.9(a-c) present the responses towards 1 % of H_2 for the SnO_2 nanofiber sensors electrospun using PAN 1, PAN 2 and PAN 3 solutions, respectively, at different temperatures. From the response curves, it can be seen that the largest response appears at 150 °C, which is the optimum operating temperature of the sensors. By further increasing the temperature to 180 and 200 °C the responses gradually decreased.

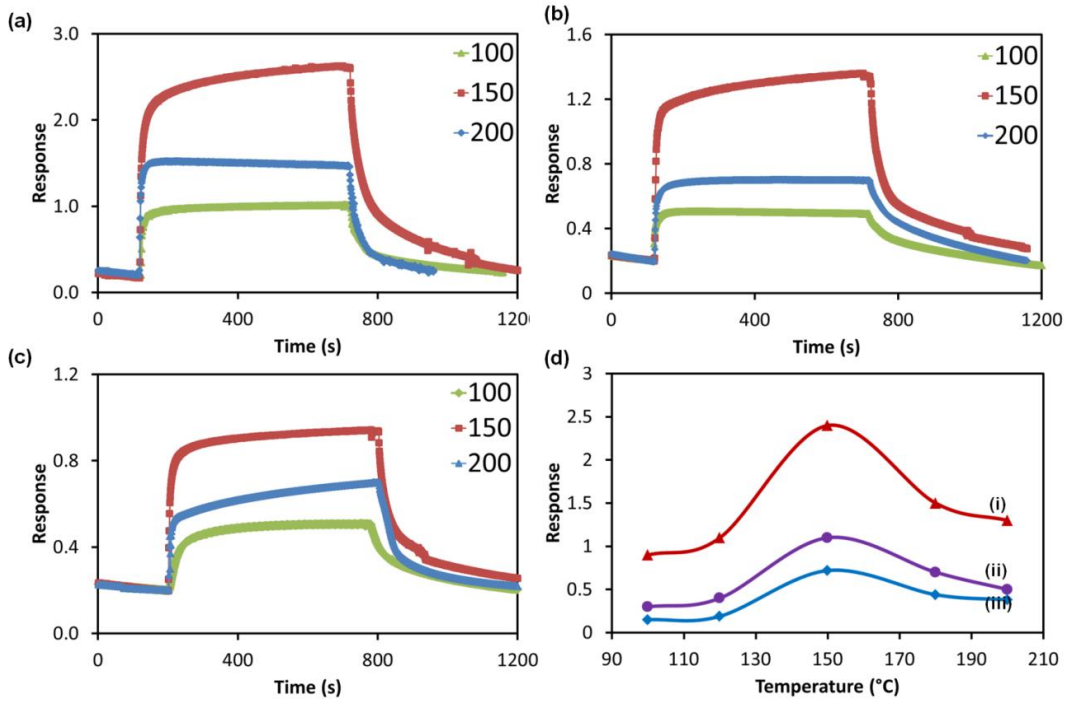

Figure 2.9: Responses to 1% H_2 of the SnO_2 sensor electrospun using (a) PAN 1, (b) PAN 2, and (c) PAN 3, measured in 1.0% H_2 gas at temperatures ranging from 100 to 200 °C and (d) plot of sensor responses as a function of operating temperatures of (i) PAN 1, (ii) PAN 2, and (iii) PAN 3.

The response of the gas sensor is based on changes of the electrical resistance induced by adsorption/desorption of the target gas molecules on its surface. In the air ambient, oxygen molecules are first adsorbed onto SnO_2 surface to form single or

double oxygen ions, depending on the temperature, extracting electrons from the conduction band, as [26]:

$$O_2\,(g) \rightarrow O_2(ads) \tag{2.3}$$

$$O_2\,(ads) + e^- \rightarrow O_2^-\,(ads) \tag{2.4}$$

$$O_2^-\,(ads) + e^- \rightarrow 2O^-(ads) \tag{2.5}$$

$$O^-(ads) + e^- \rightarrow O_2^-\,(ads) \tag{2.6}$$

It has been reported that below 150 °C, oxygen adsorption at the surface is mainly in form of O_2^-, while above 150 °C chemisorbed oxygen transforms into both O_2^- and O^- simultaneously [27, 28]. The accumulated oxygen species which are ionosorbed on the surface result in a decrease in the electron concentration and increase the potential barrier. Consequently, the resistance of the sensor increases. At elevated temperatures, upon an exposure to the H_2 gas, H_2 molecules react with the oxygen ions according to the following reaction producing water molecules [29]:

$$H_2\,(gas) + O_2^- \rightarrow H_2O\,(gas) + e^- \tag{2.7}$$

The electrons are released back to conduction band which results in an increase of the electron concentrations in SnO_2 nanofibers and decreases the depletion width. Thereby, resistance of the sensors decreases. The reactions are reversible at elevated temperatures, wherein after exposure to air again, the baseline recovers quickly to the original value because of the re-adsorption of oxygen. At relatively low temperatures, a small number of O_2 molecules produce adsorbed O_2^- [30]. Consequently, the responses of the sensors are small. At elevated temperatures, the dominant process becomes the adsorption of O_2^-, while a larger number of the surface sites have enough energy to participate in the interactions [27]. This results in an increase of the response. However,

if the temperature increases further, progressively more desorption of the adsorbed oxygen ionic species previously occurs and the response decreases [30]. Thus, the optimal temperature for a gas sensor is at which the aforementioned two factors are in balance. This behavior is in agreement with previously reported results [31].

Figure 2.10(a) presents the dynamic response of the SnO_2 nanofiber gas sensors. It can be observed that, when the sensors were exposed to certain concentration of H_2, the response rapidly increased and reach its equilibrium resistance value. After the exposure to air, all responses decreased to the baseline, indicating a good repeatability and reproducibility of all sensors. As shown in Figure 2.10(b), the response-concentration dependence of SnO_2 nanofiber gas sensors at optimum operating temperature were investigated in the range of of 0.06 to 1% of H_2. The response of all sensors increased gradually by increasing the H_2 concentration, suggesting that the enhancement of the sensor response at higher H_2 concentrations.

Beside sensor response, the response and recovery times are also important factors in evaluating the gas sensing performances. In this work, response time is defined as the time required for the sensor to reach 90% of the stabilized value of its resistance in the presence of the test gas, while the recovery time, defined as the time needed for the sensor to reach 10% of the initial steady state value of its resistance after the gas was removed.

Based on the dynamic performance characterization results, the response and recovery time of the sensors were determined and compared. For SnO_2 nanofibers sensors electrospun using PAN 1, the response times were determined to be 70, 62, 54, 38 and 21 s for the concentration of 0.06, 0.12, 0.25, 0.5 and 1.0 % of H_2, while the recovery times were 401, 389, 365, 355 and 333 s, respectively. Meanwhile, with the same set of H_2 gas concentrations, SnO_2 nanofiber sensors electrospun using PAN 2,

the response times were 74, 81, 82, 42 and 24 s, and recovery times were 424, 353, 326, 384 and 396 s, respectively. The response times of SnO_2 nanofiber sensors electrospun using PAN 3 were obtained to be 91, 103, 66, 46 and 27 s, and the recovery times to be 378, 356, 355, 319 and 459 s, respectively, with the aforementioned concentrations.

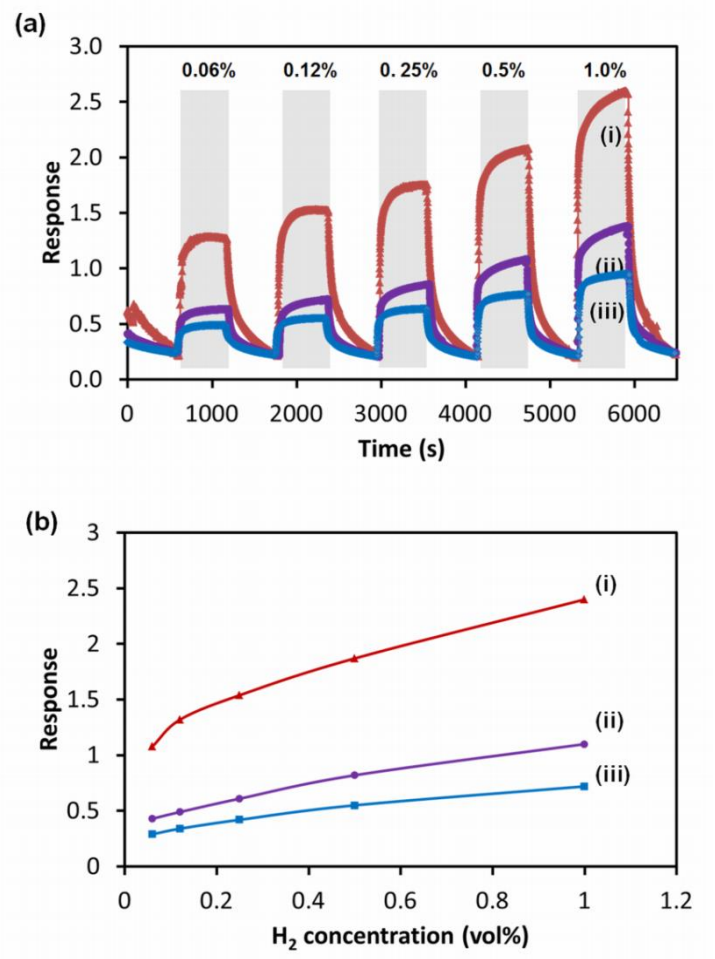

Figure 2.10: (a) Responses and recovery of the SnO_2 nanofiber sensors measured in H_2 gas in the range of 0.16 to 1% at 150 °C and (b) linear plot of sensor responses as a function of H_2 concentration for SnO_2 nanofiber sensors electrospun using (i) PAN 1, (ii) PAN 2, and (iii) PAN 3.

Detailed comparison of sensors response and recovery time is presented in Table 1. Overall, all sensors showed a fairly similar trend in terms of response and recovery times, where the response times are much shorter than the recovery times (approximately five times shorter). The prolonged recovery times might be ascribed to

the low operating temperature of the SnO_2 nanofiber sensors, which can directly suppress the H_2 desorption.

Table 2.1
Response times and recovery times measured at different concentrations of SnO_2 nanofiber sensors electrospun using PAN 1, PAN 2 and PAN 3.

H_2 concentration (%)	Response time (s)			Response time (s)		
	PAN 1	PAN 2	PAN 3	PAN 1	PAN 2	PAN 3
0.06	70	74	91	401	424	378
0.12	62	81	103	389	353	356
0.25	54	82	66	365	326	355
0.5	38	42	46	355	384	319
1	21	24	27	333	396	459

The alignments of nanofibers also have great effects on the gas sensing properties [32]. As compared to randomly oriented nanofibers, aligned nanofibers can avoid entanglement of neighboring fibers, thus reducing the local barrier and further enhance the sensor responses [30]. Furthermore, the alignment of the fibers may provide a distinctive one-dimensional (1D) character of electronic transport along the aligned fibers, which is beneficial for enhancing the sensor's response [32].

It can be clearly seen from the results that the response characteristics are correlated with the fiber diameter, morphology and the concentration of oxygen vacancies. Sensor electrospun using PAN 1 resulted in nanofiber with the smallest diameter and hollow tubular structure, exhibit fast response time as compared to other sensors. It is also observed that the SnO_2 hollow nanofibers (PAN 1 and PAN 2) significantly improve the gas-sensing response to H_2 as compared to multi-channel containing almost solid SnO_2 fibers (PAN 3). This improvement can be ascribed to the enhanced effective surface area of hollow structure because both the inner and outer surfaces of the hollow nanofibers participate in the gas sensing reaction [34]. Therefore,

the SnO_2 hollow nanofibers can react with higher amounts of gas molecules than solid SnO_2 nanofibers, which result in higher response and shorter response and recovery times. Additionally, the sensor electrospun using PAN 1 contains higher number of oxygen vacancies. All these factors have contributed significantly toward enhancement of sensing performance of all sensors to H_2 at lower operating temperatures where the best performance was observed in sensor electrospun using PAN 1.

Oxygen vacancy is consider as one of the most important factors in defining the electronic and chemical properties as well as the adsorption behaviors of metal oxide surfaces [35, 36]. Zhang *et al.* have discussed that abundant electron donor defects, such as oxygen vacancies, enhance metal oxide based sensors' responses and reduce the operating temperature of such sensors [37]. In the presence of ambient air, the abundance of oxygen vacancies in metal oxide sensing elements augments the adsorption of oxygen gas molecules at relatively low temperatures [38]. In addition to oxygen vacancies, the size and morphology of 1D nanostructured-metal oxides also greatly influence their sensing properties [39]. 1D nanostructures with a high surface-to-volume ratio provide more available surface sites for the target molecule absorption and desorption [40]. Another reason for the effectiveness of the 1D structures as sensing elements is that when the cross sectional dimensional of these materials are comparable with the Debye length, the whole bulk of the material can be influenced by the adsorbed molecules.

In order to assess the quality of the developed 1D SnO_2 nanofiber based sensors, their performance are compared with similar hollow SnO_2 based nanostructures, which are reported by other researchers. As presented in the introduction, hollow fibers have been demonstrated by Choi *et al.* for ethanol sensing, which operated at temperatures near 400 °C. Reduced operating temperature to under 200 °C has been reported by

producing hollow nanofibers of binary oxides with metal oxides such as ZnO [10]. Such reports claim that the reduction of the operating temperature would be due to the formation of heterojunctions made of SnO_2 and the other oxide phases, helping the separation of charges. However, both the SEMs presented in such reports as well as the characterization of the materials evidence the existence of the small sized and reduced grains, forming the walls of the nanofibers. These observations are in agreement with the characterizations presented in this chapter that suggest the effect of reduced SnO_2 of small sized grains.

The duration of the electrospinning process is the same for all devices. From the SEM and atomic force microscopy (AFM) images it was also found out that the average number of fibers that are placed on the unit length of the width of the device's surface are the same. According to the observations, there are on average 35 nanofibers cross each 100 μm width of the active area of the device (see Figure 2.2 for the SEM image and Figure 2.11 for the AFM images). So just by comparing the average diameter of the fibers or whether the fiber is hollow or filled the relative surface area can be compared. The cross sectional circumference can be calculated using $4\pi r$ in which r is the inner or outer radius of the fiber. The exposed cross sectional areas of the fibers are 2.89, 5.7812 and 5.024 μm for samples obtained using PAN 1, PAN 2, and PAN 3 solutions, respectively. The sample that used the PAN 1 solution provided the best sensitivity, despite the fact it does not offer the largest surface areas in comparison to other samples. In the PAN 1 case, the enhanced sensitivity can be associated to its wall thickness which is more comparable to the Debye length [41]. It means that the whole thickness of the sample can be efficiently depleted after the exposure to H_2 gas molecules.

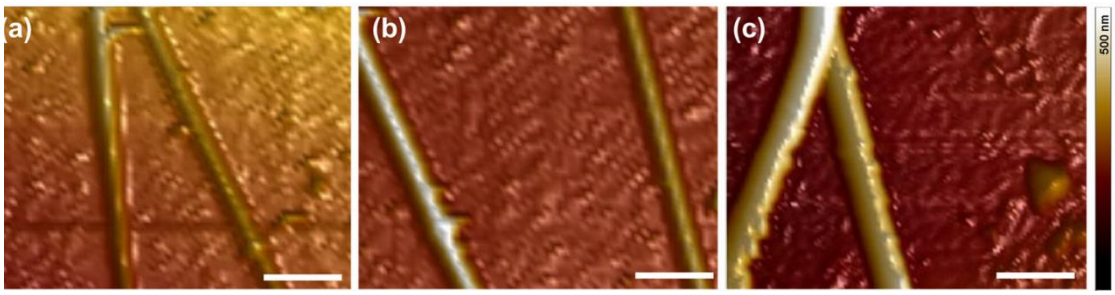

Figure 2.11: AFM images of SnO_2 nanofibers showing an average of 2 fibers crossing the 5 μm width of the active area of the device, electrospun using solutions of (a) PAN 1 (b) PAN 2 and (c) PAN 3 with the scale bar of 1 μm.

The hollow SnO_2 nanofibers showed the optimum operation temperature of 150 °C. The hollow SnO_2 nanofibers with the diameter of 80 – 100 nm (PAN 1), that incorporated corrugated walls of the thicknesses of less than 20 nm (made of same size grains of the same dimension), demonstrated the best responses. As a result, it is suggested that the low operating temperature of the sensors presented in this work is attributed to the small dimensions, small wall thickness and corrugated surface of SnO_2 hollow structure, which enhance the surface area and at the same time, the affinity to H_2. Furthermore, large oxygen vacancies available as adsorption sites of the well-aligned nanofibers, contributed to the augmented sensing performance of the devices.

2.4 Summary

In this chapter, the PhD candidate presented her investigation on the development of H_2 gas sensors based on hollow and filled well-aligned SnO_2 nanofibers with corrugated surfaces prepared *via* electrospinning method with diameters of 80 – 400 nm. The enhancement in the gas sensing properties is attributed to the oxygen vacancies and hollow morphology of SnO_2 nanofibers as well as its corrugated surfaces. The hollow corrugated surface and well-aligned SnO_2 nanofibers provide large accessible surface area for surface reactions. Additionally, this kind of

morphology promotes the oxygen vacancies as shown by the XPS analysis. Significant oxygen vacancies greatly influence the sensing performance at lower operating temperature that result in excellent H_2 gas sensing performance.

In the next chapter, the author will investigate Schottky gas sensors based on Nb_2O_5 nanoporous structures. The focus of the work will be on the studying the effect of different metal catalysts on gas sensors' performances.

References

[1] R. Ab Kadir, Z. Li, A. Z. Sadek, R. A. Rani, A. S. Zoolfakar, M. R. Field, *et al.*, "Electrospun granular hollow SnO_2 nanofibers hydrogen gas sensors operating at low temperatures," *J. Phy. Chem. C*, vol. 118, pp. 3129-3139, 2014.

[2] A. Theron, E. Zussman, and A. L. Yarin, "Electrostatic field assisted alignment of electrospun nanofibres," *Nanotechnology*, vol. 12, pp. 384-390, 2001.

[3] J. M. Deitzel, J. Kleinmeyer, D. Harris, and N. C. Beck Tan, "The effect of processing variables on the morphology of electrospun nanofibers and textiles," *Polymer*, vol. 42, pp. 261-272, 2001.

[4] J.-H. He, Y.-Q. Wan, and J.-Y. Yu, "Effect of concentration on electrospun polyacrylonitrile (PAN) nanofibers," *Fiber Polym.*, vol. 9, pp. 140-142, 2008.

[5] S. Megelski, J. S. Stephens, D. B. Chase, and J. F. Rabolt, "Micro and nanostructured surface morphology on electrospun polymer fibers," *Macromolecules*, vol. 35, pp. 8456-8466, 2002.

[6] J.-K. Choi, I.-S. Hwang, S.-J. Kim, J.-S. Park, S.-S. Park, U. Jeong, *et al.*, "Design of selective gas sensors using electrospun Pd-doped SnO_2 hollow nanofibers," *Sens. Actuator B Chem.*, vol. 150, pp. 191-199, 2010.

[7] C. J. Thompson, G. G. Chase, A. L. Yarin, and D. H. Reneker, "Effects of parameters on nanofiber diameter determined from electrospinning model," *Polymer*, vol. 48, pp. 6913-6922, 2007.

[8] L. Wang, X. Luo, X. Zheng, R. Wang, and T. Zhang, "Direct annealing of electrospun synthesized high-performance porous SnO_2 hollow nanofibers for gas sensors," *RSC Advances*, vol. 3, pp. 9723-9728, 2013.

[9] L. Liu, C. Guo, S. Li, L. Wang, Q. Dong, and W. Li, "Improved H_2 sensing properties of Co doped SnO_2 nanofibers," *Sens. Actuator B Chem.*, vol. 150, pp. 806-810, 2010.

[10] S. Wei, Y. Zhang, and M. Zhou, "Toluene sensing properties of SnO_2-ZnO hollow nanofibers fabricated from single capillary electrospinning," *Solid State Commun.*, vol. 151, pp. 895-899, 2011.

[11] W.-S. Kim, B.-S. Lee, D.-H. Kim, H.-C. Kim, W.-R. Yu, and S.-H. Hong, "SnO_2 nanotubes fabricated using electrospinning and atomic layer deposition and their gas sensing performance," *Nanotechnology*, vol. 21, 2010.

[12] N. G. Cho, D. J. Yang, M.-J. Jin, H.-G. Kim, H. L. Tuller, and I.-D. Kim, "Highly sensitive SnO_2 hollow nanofiber based NO_2 gas sensors," *Sens. Actuator B Chem.*, vol. 160, pp. 1468-1472, 2011.

[13] Z. Zhang, X. Li, C. Wang, L. Wei, Y. Liu, and C. Shao, "ZnO hollow nanofibers: fabrication from facile single capillary electrospinning and applications in gas sensors," *J. Phys. Chem. C*, vol. 113, pp. 19397-19403, 2009.

[14] L. Xiao, J. Li, Q. Li, and L. Zhang, "One pot template free synthesis, formation mechanism, and lithium ions storage property of hollow SnO_2 microspheres," *J. Solid State Chem.*, vol. 14, pp. 931-936, 2010.

[15] J. G. Partridge, M. R. Field, J. L. Peng, A. Z. Sadek, K. Kalantar-zadeh, J. Du Plessis, *et al.*, "Nanostructured SnO_2 films prepared from evaporated Sn and their application as gas sensors," *Nanotechnology*, vol. 19, 2008.

[16] L. Zhang, S. Ge, Y. Zuo, B. Zhang, and L. Xi, "Influence of oxygen flow rate on the morphology and magnetism of SnO_2 nanostructures," *J. Phys. Chem. C*, vol. 114, pp. 7541-7547, 2010.

[17] L. Yan, J. S. Pan, and C. K. Ong, "XPS studies of room temperature magnetic CO doped SnO_2 deposited on Si," *Mat. Sci. Eng. B-Solid,* vol. 128, pp. 34-36, 2006.

[18] G. Tyuliev and S. Angelov, "The nature of excess oxygen in $CO_3O_{4+\epsilon}$," *Appl. Surf. Sci,* vol. 32, pp. 381-391, 1988.

[19] D.F. Cox, T.B. Fryberger, S. Semancik, "Oxygen vacancies and defect electronic states on the SnO_2 (110)-1)*x* surface," *Phys. Rev. B,* 38, 1988.

[20] D.J. Yang, I. Kamienchick, D.Y. Youn, A. Rothschild, I.D. Kim, "Ultrasensitive and highly selective gas sensors based on electrospun SnO_2 nanofibers modified by Pd loading," *Adv. Funct. Mater,* vol. 20, pp. 4258-4264, 2010.

[21] J.-S. Seo, J.-H. Jeon, Y. H. Hwang, H. Park, M. Ryu, S.-H. K. Park and B.-S. Bae, "Solution-processed flexible fluorine-doped indium zinc oxide thin-film transistors fabricated on plastic film at low temperature," *Sci. Rep.*, 3, 2085, 2013.

[22] M. Ahsan, M. Z. Ahmad, T. Tesfamichael, J. Bell, W. Wlodarski, and N. Motta, "Low temperature response of nanostructured tungsten oxide thin films toward hydrogen and ethanol," *Sens. Actuator B Chem.,* vol. 173, pp. 789-796, 2012.

[23] S. H. Sun, G. W. Meng, G. X. Zhang, T. Gao, B. Y. Geng, L. D. Zhang, *et al.*, "Raman scattering study of rutile SnO_2 nanobelts synthesized by thermal evaporation of Sn powders," *Chem. Phys. Lett.,* vol. 376, pp. 103-107, 2003.

[24] C. Yu, Q. Hao, S. Saha, L. Shi, X. Y. Kong, and Z. L. Wang, "Integration of metal oxide nanobelts with microsystems for nerve agent detection," *Appl. Phys. Lett,* vol. 86, p. 063101, 2005.

[25] A. Gurlo and R. Riedel, "In situ and operando spectroscopy for assessing mechanisms of gas sensing," *Angew. Chem. Int. Edit.*, vol. 46, pp. 3826-3848, 2007.

[26] O. V. Safonova, G. Delabouglise, B. Chenevier, A. M. Gaskov, and M. Labeau, "CO and NO_2 Gas Sensitivity of nanocrystalline tin dioxide thin films doped with Pd, Ru and Rh," *Mat. Sci. Eng. C-Bio S.*, vol. 21, pp. 105-111, 2002.

[27] S. C. Chang, "Oxygen chemisorption on tin oxide: correlation between electrical conductivity and EPR measurements," *J. Vac. Sci. Technol.*, vol. 17, pp. 366-369, 1980.

[28] N. Barsan and U. Weimar, "Conduction model of metal oxide gas sensors," *J. Electroceram.*, vol. 7, pp. 143-167, 2001.

[29] H. Zhang, Z. Li, L. Liu, X. Xu, Z. Wang, W. Wang, *et al.*, "Enhancement of hydrogen monitoring properties based on Pd-SnO_2 composite nanofibers," *Sens. Actuator B Chem.*, vol. 147, pp. 111-115, 2010.

[30] D. Manno, G. Micocci, R. Rella, A. Serra, A. Taurino, and A. Tepore, "Titanium oxide thin films for NH_3 monitoring: structural and physical characterizations," *J. Appl. Phys.*, vol. 82, pp. 54-59, 1997.

[31] J. Cao, T. Zhang, F. Li, H. Yang, and S. Liu, "Enhanced ethanol sensing of SnO_2 hollow micro/nanofibers fabricated by coaxial electrospinning," *New J. Chem.*, vol. 37, pp. 2031-2036, 2013.

[32] S.-H. Choi, G. Ankonina, D.-Y. Youn, S.-G. Oh, J.-M. Hong, A. Rothschild, *et al.*, "Hollow ZnO nanofibers fabricated using electrospun polymer templates and their electronic transport properties," *ACS Nano*, vol. 3, pp. 2623-2631, 2009.

[33] Y. Zhao, X.-L. He, J.-P. Li, J. Jia, and X.-G. Gao, "Enhanced gas sensing properties of aligned porous SnO_2 nanofibers," *Chinese Phys. Lett.*, vol. 29, 2012.

[34] F. Gyger, M. Huebner, C. Feldmann, N. Barsan, and U. Weimar, "Nanoscale SnO_2 hollow spheres and their application as a gas sensing material," *Chem. Mater.*, vol. 22, pp. 4821-4827, 2010.

[35] M. W. Ahn, K. S. Park, J. H. Heo, J. G. Park, D. W. Kim, K. J. Choi, *et al.*, "Gas sensing properties of defect-controlled ZnO-nanowire gas sensor," *Appl. Phys. Lett.*, vol. 93, 2008.

[36] R. Schaub, E. Wahlström, A. Rønnau, E. Lægsgaard, I. Stensgaard, and F. Besenbacher, "Oxygen-mediated diffusion of oxygen vacancies on the TiO_2 (110) surface," *Science*, vol. 299, pp. 377-379, 2003.

[37] L. Zhang and Y. Yin, "Hierarchically mesoporous SnO_2 nanosheets: hydrothermal synthesis and highly ethanol sensitive properties operated at low temperature," *Sens. Actuator B Chem.*, vol. 185, pp. 594-601, 2013.

[38] M. Batzill, "Surface Science studies of gas sensing materials: SnO_2," *Sensors*, vol. 6, pp. 1345-1366, 2006.

[39] Y. J. Chen, X. Y. Xue, Y. G. Wang, and T. H. Wang, "Synthesis and ethanol sensing characteristics of single crystalline SnO_2 nanorods," *Appl. Phys. Lett.*, vol. 87, pp. 233503-3, 2005.

[40] Y. Ma, Y. Qu, and W. Zhou, "Surface engineering of one dimensional tin oxide nanostructures for chemical sensors," *Microchim. Acta*, vol. 180, pp. 1181-1200, 2013.

[41] P.-C. Chen, G. Shen, and C. Zhou, "Chemical sensors and electronic noses based on 1-D metal oxide nanostructures," *IEEE T. Nanotechnol.*, vol. 7, pp. 668-682, 2008.

Chapter 3

Nb_2O_5 Schottky Based Ethanol Vapour Sensors: Effect of Metallic Catalysts

3.1 Introduction

In this Chapter, the PhD candidate presents her work on the development of the Schottky gas sensor based on anodized Nb_2O_5 for ethanol sensing.

The aim of work presented in this chapter is to compare the performance of the highly porous Nb_2O_5 Schottky based sensors formed using different catalytic metals for ethanol vapour sensing. The fabricated sensors consist of a fairly ordered nano-vein like porous Nb_2O_5 prepared *via* an elevated temperature anodization method. Subsequently, Pt, Pd and Au were sputtered as both Schottky contacts and catalysts for the comparative studies. These metals are chosen as they have large work functions in comparison to the electron affinity of the anodized Nb_2O_5. It is demonstrated that the device based on Pd/Nb_2O_5 Schottky contact has the highest sensitivity amongst the developed sensors, which will be discussed in this chapter. The sensing behaviors were studied in terms of the Schottky barrier height variations and properties of the metal catalysts.

The outcome of the chapter contributed to one of the PhD candidate's journal papers entitled "Nb_2O_5 Schottky Based Ethanol Vapour Sensors: Effect of Metallic Catalysts" that was published in the journal of *Sensors and Actuators B: Chemical* [1].

3.2 Experimental

3.2.1 Fabrication of nanoporous Nb_2O_5

The Schottky diode based sensor devices were fabricated using niobium foil (99.9% purity, Sigma Aldrich) of 0.25 mm thickness. The foil was cut into pieces of 1.0 cm × 1.0 cm, which were cleaned with acetone, followed by isopropanol and rinsed with deionized water then dried in a stream of high purity nitrogen gas. Nb_2O_5 film synthesized *via* an anodization process that was conducted at 50 °C in the electrolyte of NH_4F/ethylene glycol, containing a small amount of water using a process that was based on the previous work [2]. Films were then annealed at 440 °C for 30 min at the ramp up/down of 2 °C min^{-1} for crystallization. The final stage of the fabrication was the formation of the Schottky contacts. For this study, Pt, Pd and Au layers with the thickness of ~20 nm each were deposited on the annealed Nb_2O_5 film using a GATAN PECS^{TM} sputter coating system. A shadow mask with a 2.5 mm diameter hole was utilized to obtain a circular pad of catalytic contact. Sensor with Pt, Pd and Au contacts will be addressed as Pt–Nb_2O_5, Pd–Nb_2O_5 and Au–Nb_2O_5, respectively, throughout this paper.

3.2.2 Structural characterization

The morphologies of Nb_2O_5 films were studied using scanning electron microscopy (SEM-FEI Nova NanoSEM), while the crystallographic properties of the films were studied *via* X-ray diffraction (XRD) analysis using a Bruker D8 DISCOVER microdiffractometer fitted with a general area detector diffraction system (GADDS) that accommodates Cu-Kα radiation (l = 1.54178 Å). Analysis of the X-ray photoelectron spectrometry (XPS) was conducted using Thermo Scientific K-alpha X-ray Photoelectron.

3.2.3 Measurement setup

The gas sensing measurements devices were conducted in a LINKAM (Scientific Instruments) customized gas testing chamber. A computerized mass flow control (MFC) multi-channel gas calibration system was used, which allowed the sensors to be exposed to ethanol with different concentrations by diluting it using 99.99 % dry synthetic air. This is carried out by adjusting the flow rates of each gas channel, producing a specified concentration of the analyte vapour species flowing at a total constant flow rate of 200 sccm to the LINKAM chamber. Electrical connections to the Schottky gas sensors were achieved by physically connecting the probes to the metal pads (top electrode) and Nb (bottom electrode) as schematically shown in Figure 3.1.

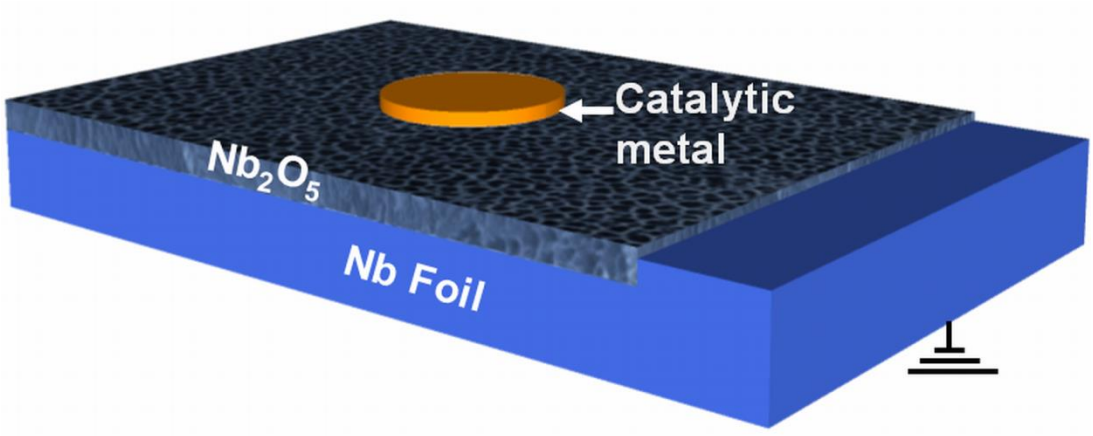

Figure 3.1: Three-dimensional schematic of the Schottky-based Nb_2O_5 ethanol vapour sensor.

The current–voltage (I–V) measurements were carried out using Keithley 2606 current source meter as they were sequentially heated from room temperature to 270 °C and exposed to a mixture of ethanol vapour and air. The sensors were mounted on heaters, which controlled their operational temperatures. The measurements started with the Pd–Nb_2O_5 sensor, and it was observed that the largest voltage shift occurred at 180 °C. Due to this observation and for comparison purposes, the dynamic measurements of other sensors were also obtained at 180 °C. The dynamic responses were measured as a change in the voltage magnitude utilizing an Agilent 34410A digital multimeter to record the voltage alterations under the exposure to ethanol vapour with different concentrations in air.

3.3 Results and discussion

3.3.1 Morphology and structural properties

The SEM images of the cross-sectional and top views of nanoporous Nb_2O_5 after the annodization and annealing processes are presented in Figure 3.2. The thickness of the film in this figure is ~1 μm. From Figure 3.2(b) it is observed that Nb_2O_5 films are made of fairly organized pores, with inner diameters ranging from 30 to 50 nm. Figure 3.2(c) shows the higher magnification cross-sectional images of the nanoporous Nb_2O_5 film. It is observed that the film is made of highly packed vein-like nanostructured networks.

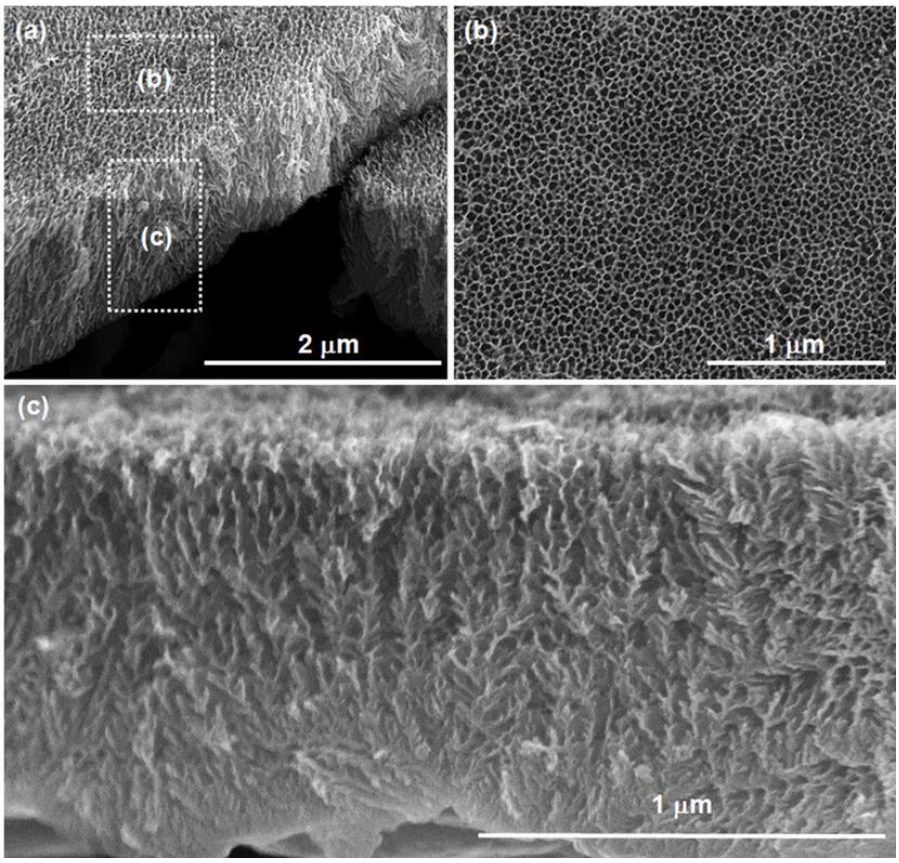

Figure 3.2: SEM images of a Nb_2O_5 nanoporous film after the annealing process: (a) cross-sectional view of the whole nanoporous structure, (b) top view of the nanoporous structure and (c) a higher magnification SEM image of cross-sectional view of the nanoporous structure.

The XPS analysis was carried out in order to investigate the elemental composition of the sensing films. As depicted in Figure 3.3(a-d), XPS survey spectra of the sensors show the presence of Nb, O, Pt, Pd and Au elements with very little carbon as a contaminant. Inset of Figure 3.3(a), shows the high-resolution spectrum for the Nb region that exhibits the $Nb3d_{3/2}$ peaks at 210.08 eV and $Nb3d_{5/2}$ at 207.28 eV. It is observed that the peaks obtained were in agreement with previous reports [3], indicating that the film consists of stoichiometry Nb_2O_5. The inset of Figure 3.3(b) shows the high resolution XPS spectrum focusing on the Pt signature of Pt–Nb_2O_5 film. The peaks can be resolved into Pt4f peak with binding energies of 71.5 ± 0.2 eV for

$Pt4f_{7/2}$ and 74.4 ± 0.2 eV for Pt $4f_{5/2}$, respectively. These binding energies correspond to the Pt metallic state [4]. As can be seen in the inset of Figure 3.3(c), two intense peaks centred at 341.3 ± 2 for $Pd3d_{3/2}$ and 335.4 ± 2 for $Pd3d_{5/2}$ are attributed to Pd the metallic state [5, 6]. Inset of Figure 3.3(d) shows an XPS spectrum of Au related area of the Au–Nb_2O_5 film. The Au $4f_{7/2}$ peak appears at a binding energy of 83.98 eV ± 2 and the Au $4f_{5/2}$ peak appears at a binding energy of 87.71 eV± 2 indicating the metallic Au.

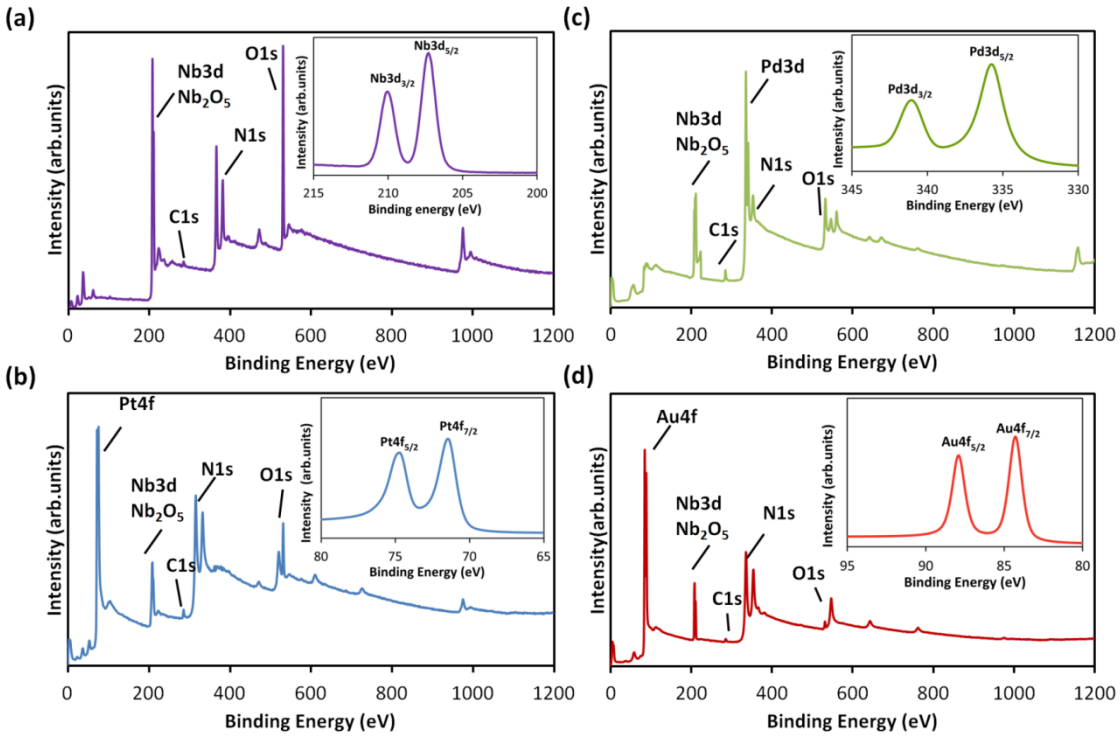

Figure 3.3: (a) XPS survey spectra of Nb_2O_5 (inset: XPS spectrum of Nb3d) (b) Pt–Nb_2O_5 (inset: XPS spectrum of Pt 4f peaks) (c) Pd–Nb_2O_5 (inset: XPS spectrum of Pd 3d peaks and (d) Au–Nb_2O_5 (inset: XPS spectrum of Au 4f peaks) films.

Figure 3.4 shows the XRD patterns of Pt–Nb_2O_5, Pd–Nb_2O_5 and Au–Nb_2O_5 films. All of them display the Nb_2O_5 peaks which can be indexed to the orthorhombic phase of Nb_2O_5 (ICCD-27-1003) depicted by the peaks of 22.6°, 28.3°, 36.6°, 42.4°, 46.2°, 49.7°, 55.1°, 58.3° and 63.1° [7].

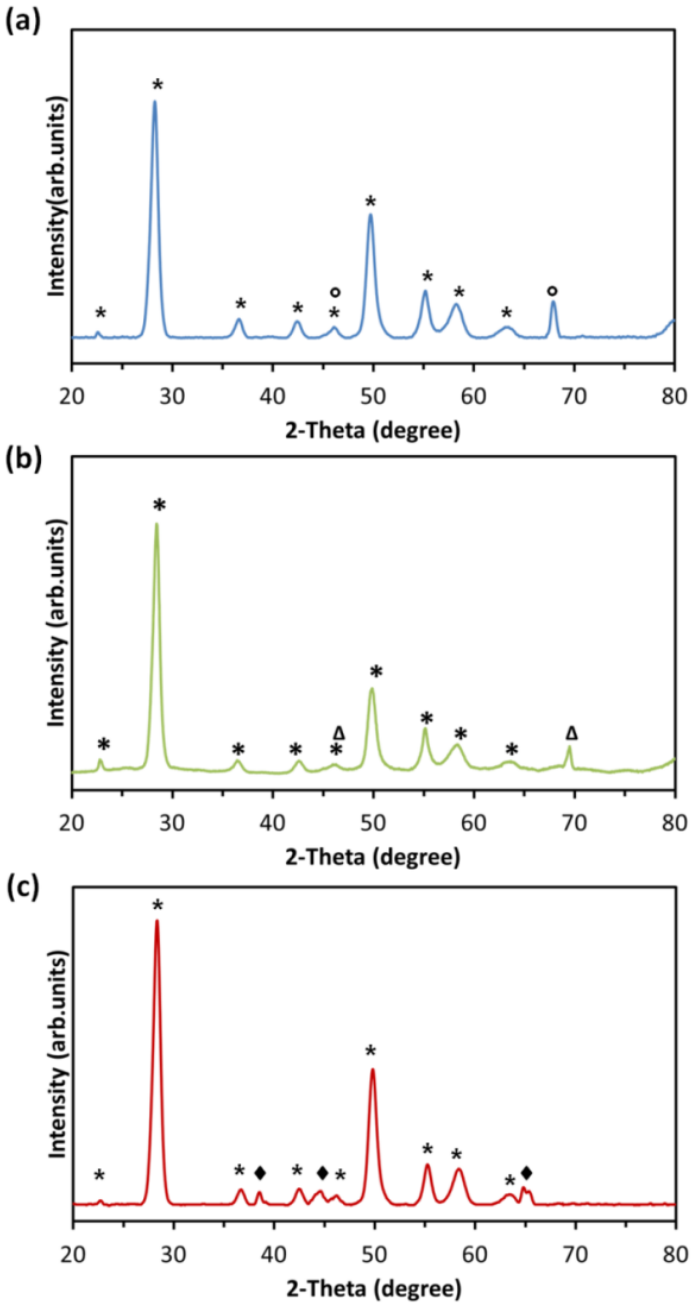

Figure 3.4: XRD patterns of the (a) Pt–Nb_2O_5, (b) Pd–Nb_2O_5 and (d) Au–Nb_2O_5 samples. Orthorhombic Nb_2O_5 (ICDD 27-1003) are indicated by asterisk (*), while Pt, Pd and Au peaks are indicated by ◦, Δ and ♦, respectively.

Figure 3.4(a) shows the XRD pattern of Pt–Nb_2O_5 where the Pt peaks can be observed at 46.55° and 67.85° [8]. Figure 3.4(b) indicates the presence of Pd at peaks of 46.62° and 68.10°, respectively, for the Pd–Nb_2O_5 sample [9]. Figure 3.4(c) reveals the presence of three peaks located at angles of 38.2°, 44.3° and 64.6°, which correspond to Au [10].

3.3.2 Effect of metal catalyst on ethanol sensing

When the metal is brought into an intimate contact with the Nb_2O_5 semiconducting film, an electron barrier is established at the interface. In equilibrium and in the absence of any gas molecules, if the metal work function is larger than Nb_2O_5 electron affinity, a Schottky contact is formed with a built in voltage that depends on the barrier height. For Pt, Pd and Au with relatively large work functions, this barrier height is much more pronounced, which gives rise to a Schottky behaviour for the contact. Nb_2O_5 conduction band edge is ~3.5 eV with reference to vacuum. For the band gap of 3.5 eV, and when Nb_2O_5 is not doped, the Fermi level falls is at ~5.25 eV. This means that Au makes a near ideal ohmic contact with intrinsic Nb_2O_5. In reality, the anodized Nb_2O_5 is *n*-doped [2], which results in the electron affinity shifts closer to the conduction band edge value. This means that it is likely that even the contact with Au is Schottky. Figure 3.5 demonstrates the I–V curves at room temperature for Pt–Nb_2O_5, Pd–Nb_2O_5 and Au–Nb_2O_5 devices. The contact with Au is the closest to ohmic behaviour, while the Pt metal establishes a Schottky contact with the largest barrier height.

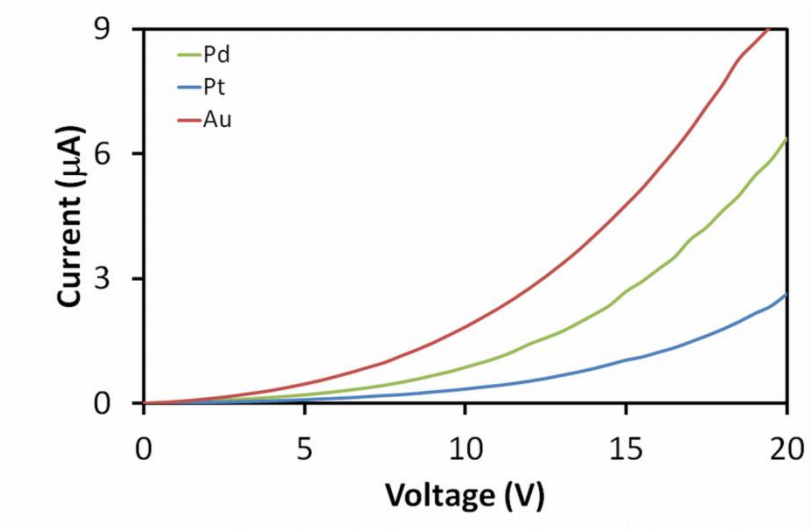

Figure 3.5: Forward-biased I–V characteristics of (i) Au–Nb_2O_5, (ii) Pd–Nb_2O_5 and (iii) Pt–Nb_2O_5 in air at room temperature.

As a reference, the I–V curves of the Pd–Nb_2O_5 device was obtained at different operational temperatures ranging from room temperature (23 °C) to 210 °C and then exposed to 1% ethanol in ambient air for 10 mins. The current was set to 2 μA as at this value the voltage changes were within the accepted range of the multimeter's operation. Figure 3.6 shows the I–V characteristics of this device before and after the exposure to ethanol vapour. It is observed that the highest voltage change occurred at the temperature of 180 °C. Based on this result, as explained in the experimental section and for direct comparison, the measurements of other sensors were also conducted at 180 °C.

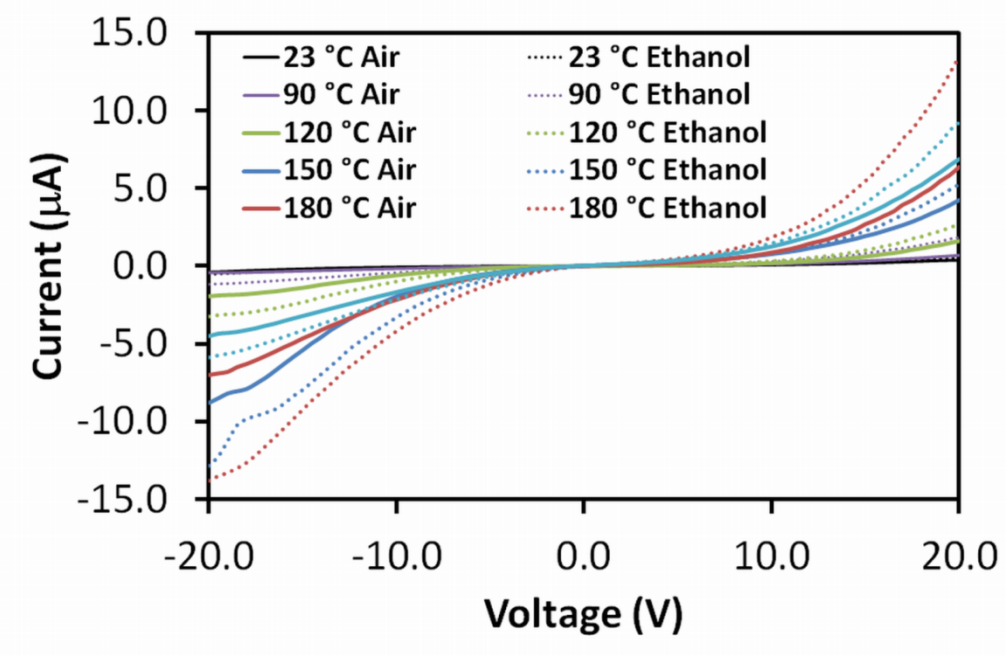

Figure 3.6: I–V characteristics of Pd–Nb_2O_5 in air and 1% ethanol at elevated temperatures.

Figure 3.7(a) and (b) show the I–V characteristics of the sensors and dynamic response of the sensors after the exposure to 1% ethanol concentration, respectively. From Figure 3.7(a-i), it is observed that the sensor with Pt contact gives the lowest forward current value at all voltages in comparison to Pd and Au contacts (Figure 3.7(a-ii,iii)). This is owing to the high Schottky barrier height (SBH) for Pt–Nb_2O_5 device. The current is mainly governed by the SBH. The high work function of the Pt contact metal leads to a high SBH and consequently a small number of free charge carriers' injection. The presented results are in agreement with the work presented by Schmitz *et al.* who observed that Pt on GaN resulted in the largest SBH as compared to Pd and Au [11].

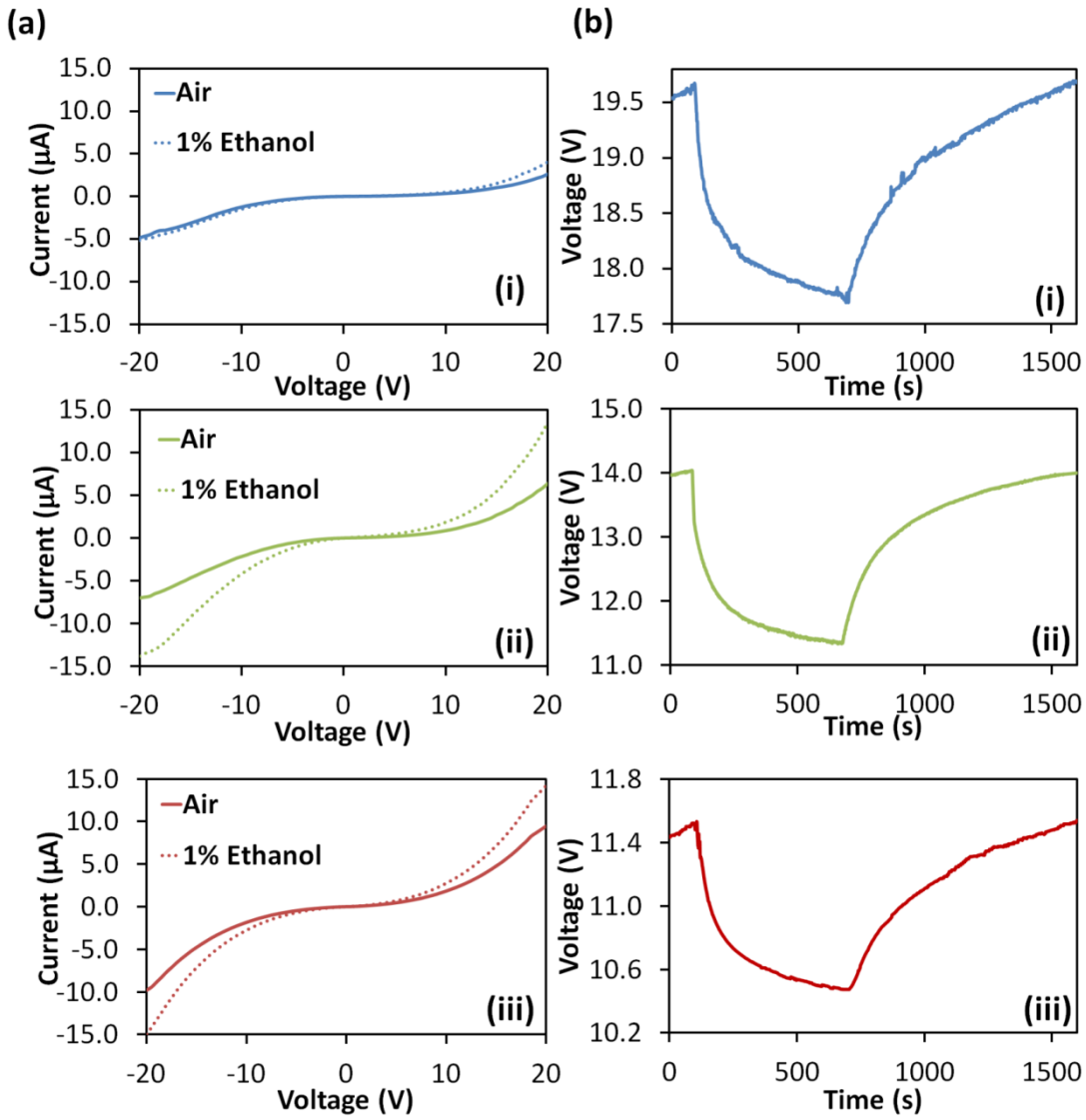

Figure 3.7: (a) I–V characteristics of sensors in air and 1% ethanol (b) dynamic response to 1% ethanol biased at 2A of: (i) Pt–Nb_2O_5, (ii) Pd–Nb_2O_5 and (iii) Au–Nb_2O_5 Schottky gas sensors at 180 °C.

The responses of the sensors biased at 2 μA, while being exposed to 1% ethanol vapour, are shown in Figure 3.7(b). It is observed that Pd–Nb_2O_5 showed the largest voltage shift followed by Pt–Nb_2O_5 and Au–Nb_2O_5. The Pd–Nb_2O_5 sensor exhibited voltage shift of 2.64 V (at the baseline of 14.0 V result in the response relative change of 19.3%), while Pt–Nb_2O_5 and Au–Nb_2O_5 sensors exhibited voltage shifts of 1.87 V

(baseline of 19.9 V and the relative change of 10.1%) and 1.07 V (baseline of 11.5 V and the relative change of 8.7%), respectively.

Further measurements were conducted in the range of room temperature to 270 °C for Pt–Nb_2O_5 and Au–Nb_2O_5 sensors in order to determine their optimum operating temperatures. It is found that the optimum operating temperature of Pt–Nb_2O_5 was 200 °C, while it was 240 °C for Au–Nb_2O_5. Figure 3.8 shows the I–V characteristics and dynamic responses of the Pt–Nb_2O_5 and Au–Nb_2O_5 sensors to 1 % of ethanol vapour at their respective optimum operating temperatures. According to the presented results, the voltage shift of Pt–Nb_2O_5 and Au–Nb_2O_5 is smaller as compared to Pd–Nb_2O_5 sensor. As such, it can be concluded that Pd–Nb_2O_5 sensor exhibits the lowest operating temperature with the highest voltage shift.

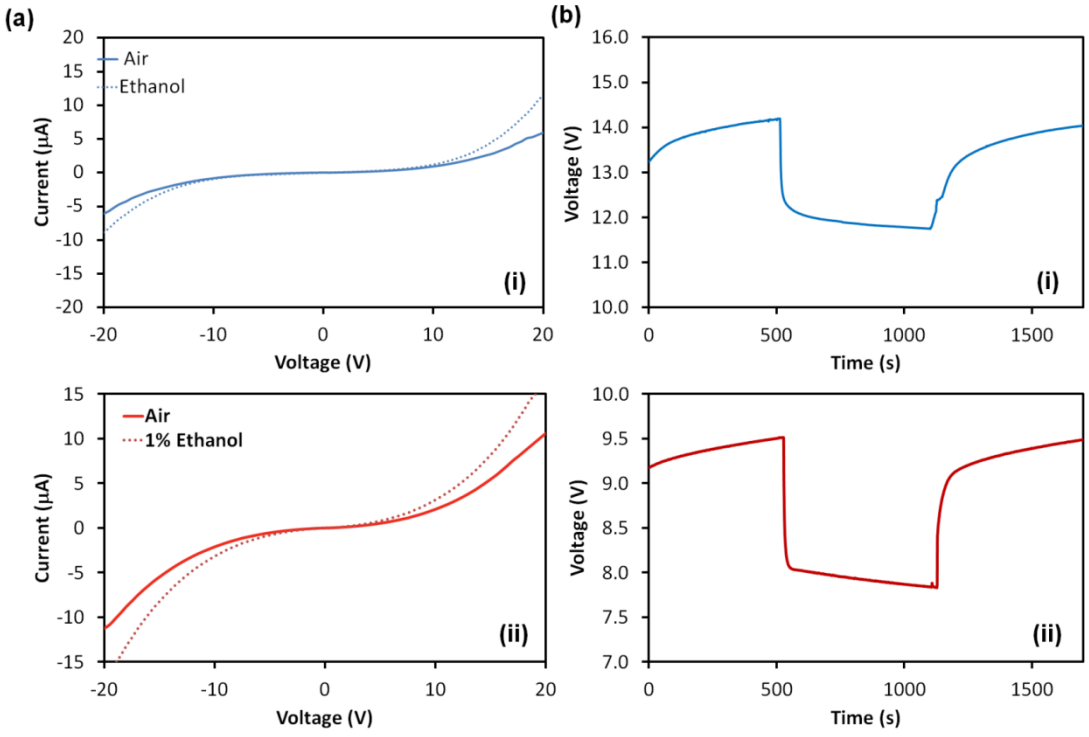

Figure 3.8: (a) I–V characteristics of sensor in air and 1% ethanol (b) dynamic responses to 1% ethanol biased at 2 μA of: (i) Pt–Nb_2O_5 at 200 °C and (ii) Au–Nb_2O_5 at 240 °C.

The voltage shift of each sensor is attributed to the reduction of SBH, which can be calculated using the equations that are presented as follows. According to thermionic emission theory for Schottky diodes, the dependence of forward current on the applied voltage is given by the expression [12]:

$$I = I_s\left\{\exp\left(\frac{qV}{kT}\right)-1\right\} \tag{3.1}$$

where q is the charge of one electron, V is the applied voltage, T is the absolute temperature in Kelvin, k is the Boltzmann's constant and I_s is the saturation current as defined by:

$$I_s = AA^{**}T^2\exp\left(-\frac{q\Phi_B}{kT}\right) \tag{3.2}$$

in which A is the diode area, A^{**} is the Richardson constant and Φ_B is the zero bias Schottky barrier height in eV. The SBH can be extracted from equation (3.2) as:

$$\Phi_B = \frac{kT}{q}\ln\left(\frac{AA^{**}T^2}{I_s}\right) \tag{3.3}$$

Here, I_s can be obtained by the extrapolation of the current density at the zero voltage. Finally, the change in Schottky barrier height can be determined from the following equation:

$$\Delta\Phi_B = \left(\Phi_{BEth} - \Phi_{BAir}\right) \tag{3.4}$$

where Φ_{BAir} and Φ_{BEth} are the SBHs in air and ethanol containing ambiences. Using equations (3.1) to (3.4) the SBH differences of the sensors with Pt, Pd and Au metallic catalysts towards 1% ethanol exposure were calculated and presented in Table 3.1. As can be seen, the Pd contact gives the largest change in the barrier height, while Au based device resulted in the smallest change.

Table 3.1
SBH change under different vapour/ gases

Sensor	Metal	Metal work function	SBH change, $\Delta\Phi_B$ (eV), under different gas or vapour		
			C_2H_5OH	H_2	CH_4
Au–Nb_2O_5	Au	5.4	~ 0.017	~ 0.020	~ 0.008
Pd–Nb_2O_5	Pd	5.6	~ 0.234	~ 0.391	~ 0.203
Pt–Nb_2O_5	Pt	5.7	~ 0.015	~ 0.273	~ 0.007

It has been reported that at a temperature range of ~55 to ~200 °C, ethanol molecules start to dissociate into ethoxides on Pd, Pt and Au as [13-18]:

$$C_2H_5OH\ (g) \rightarrow CH_3CH_2O\ (a) + H\ (a) \qquad (3.5)$$

in which (g) and (a) stand for the gaseous and adsorbed species, respectively. Ethoxides may be further oxidized to acetaldehyde:

$$C_2H_5O\ (a) \rightarrow CH_3CHO\ (g) + H\ (a) \qquad (3.6)$$

It is suggested that the H atoms are further broken down to H^+ and an electron charge (e^-) on the catalytic metal layer. The accumulated absorbed H^+ ions further spills through the catalytic metal and intercalate with Nb_2O_5 to form $H_xNb_2O_5$ [19]. As the system is maintained at an elevated temperature, it is also possible that $H_xNb_2O_5$ breaks down into reduced niobium oxide and produces H_2O [2]. The process can be described as:

$$2H_xNb_2O_5 \rightarrow xH_2O + 2Nb_2O_{(5-x/2)} \qquad (3.7)$$

The released electrons and the formation of $H_xNb_2O_5$ or $Nb_2O_{(5-x/2)}$ reduce the length of depletion region in the semiconductor and cause an effective reduction in the metal-semiconductor barrier height, which allows more free charge carriers to flow. Exposing the device back to air (oxygen environment with no ethanol molecules)

allows the surface of the reduced film to revert back to the original fully oxidized state as follows:

$$Nb_2O_{(5-x/2)} + (x/4)O_2 \rightarrow Nb_2O_5 \qquad (3.8)$$

This means that the original SBH values are regained and the sensors' outputs return to their original baselines.

The changes of SBH of Schottky-based gas sensors with a catalytic metal of larger work function than the electron affinity of the semiconductor is schematically shown in Figure 3.9. The original SBH is determined by the work-function of catalytic metal and the electron affinity of Nb_2O_5. When the metal is brought to an intimate contact with Nb_2O_5, electrons diffuse from the metal to Nb_2O_5 in order to achieve a constant Fermi level throughout the system, forming a thermal equilibrium. This results in the upward band bending within Nb_2O_5 at the interface with metal. Consequently, further electrons in the metal see a barrier (SBH) against their migration into the semiconductor. Upon the exposure to ethanol and its interaction with Nb_2O_5 near the contact area, the SBH is reduced. When the sensor is exposed to air, oxygen molecules are adsorbed at the metal-Nb_2O_5 interface, result in the SBH to increase.

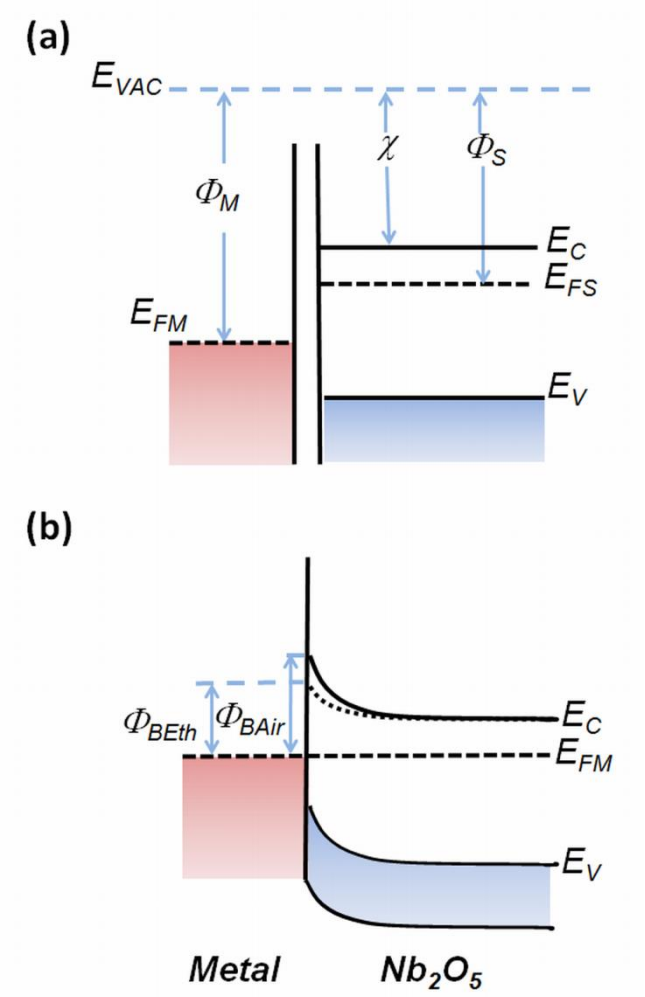

Figure 3.9: Energy band diagram illustrations of a metal and Nb_2O_5 contact for $\Phi_M > \chi$ (a) is before establishing the contact and (b) their corresponding band bending after establishing a contact and exposure to ethanol vapour. χ is the electron affinity of Nb_2O_5, E_{FM} and E_{FS} are the Fermi levels of metal and Nb_2O_5, respectively, E_{VAC} is the reference vacuum level, E_V and E_C are the valence and conduction band and the Φ_{BAir} and Φ_{BEth} are the SBHs in air and ethanol.

A plot of measured voltage shifts of the sensors equipped with different catalysts, under different ethanol concentrations (ranging from 0.06 to 1 %) is shown in Figure 3.10. At a low concentration (0.06 and 0.12%), the Pt–Nb_2O_5 shows a higher voltage shift as compared to Pd–Nb_2O_5 and Au–Nb_2O_5. From the plots, it is clearly seen that the Pd–Nb_2O_5 device exhibited the largest sensitivity towards ethanol at

ethanol concentrations above 0.25%. It has been suggested that the change in barrier height induced by hydrogen adsorption is proportional to the hydrogen coverage of the surface [20]. It has also been reported that Pt is effective to increase the response of the adsorption at low concentrations of hydrogen [21]. Ethanol and hydrogen breakdowns onto a catalytic metal on a metal oxide semiconductor have a certain similarity as they both produce H atoms in the process. Due to this, the author concluded that they show a reasonably similar catalytic behaviour towards ethanol. These explain why the barrier height changes of the Pd−Nb_2O_5 sensor were higher than that of the Pt−Nb_2O_5 sensor at high concentrations of ethanol vapour.

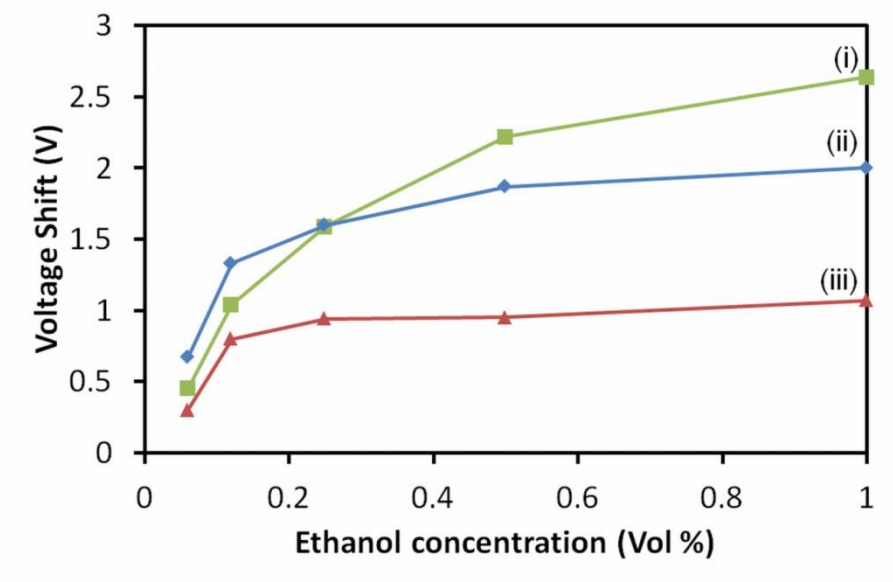

Figure 3.10: Barrier height changes of the sensors at different ethanol concentrations obtained at 180 °C (i) Pd–Nb_2O_5 (ii) Pt–Nb_2O_5 and (iii) Au–Nb_2O_5.

The response times were measured as time taken needs to reach 90% of its maximum response and on the other hand the recovery time was defined as time that sensor needs to recover to its 90% of its baseline and are presented in Table 3.2. Generally, it is observed that Pd–Nb_2O_5 exhibit faster response as compared to Pt–Nb_2O_5 and Au–Nb_2O_5. Response and recovery times for all sensors display a strong

dependence on the ethanol concentration. An increase in ethanol concentration provides more ethanol atoms to be adsorbed on the oxide surface per unit time, thereby favouring the fast electron kinetics. In addition, the increase of ethanol concentration can increase the probability of collision between the atoms and then increase the reaction ratio [29]. On the other hand, the recovery times for all sensors were longer due to the slow desorption kinetics of the ethanol vapour from the interface. As can be seen, the device with the Pd catalytic metal had the shortest response, while the response for the Au–Nb_2O_5 was the slowest.

Table 3.2
Response and recovery time of Nb_2O_5 Schottky gas sensors with different types of metal catalysts

Ethanol concentration (vol %)	Pd		Pt		Au	
	Response time (s)	Recovery time (s)	Response time (s)	Recovery time (s)	Response time (s)	Recovery time (s)
0.06	38	98	57	232	58	227
0.12	34	166	42	283	46	324
0.25	28	152	30	351	25	267
0.5	23	154	16	256	25	259
1.0	17	240	25	273	15	288

For the Pt and Au samples the recovery times at different concentrations are very close. However, for the Pd sample the recovery time is much smaller at low concentrations than that of the higher concentrations. As Pd is more active, it reacts three times faster than Pt with hydrogen containing gas species [22]. Such faster interaction is likely to translate into shorter responses at lower concentrations of ethanol gas for the Pd-Nb_2O_5 based sensor. Obviously as the gas molecules interaction with Pt

and Au are not as fast, there is a minimal difference in the recovery times between the low and high ethanol concentrations for Pt–and Au–Nb_2O_5 based sensors.

As mentioned earlier, ethanol and hydrogen gas molecules breaking downs onto a catalytic metal show certain similarities. It is then logical to compare the observations with previous reports comparing the behaviors of Pt, Pd and Au on metal oxide semiconductors in response to hydrogen. Armgath *et al.* have reported that the hydrogen solubility in Pd is about three orders higher than the hydrogen solubility in Pt [22]. Due to this, it is suggested that similarly the response of ethanol on the Pd device should be larger than that of the Pt device, which describes why the Pd–Nb_2O_5 sensor response is almost twice as large as Pt–Nb_2O_5 device. It is believed that the relatively small shift of the Au–Nb_2O_5 sensor as compared to the Pd–Nb_2O_5 and Pt–Nb_2O_5 is mainly due to the mechanism of the hydrogen adsorption onto Au. It has been reported that the H–Au interaction is weaker than the H–Pt interaction [23]. On Au, a higher hydrogen pressure is required to reach the same fractional coverage as on Pt. Moreover on Au, the activation energy for the dissociation of hydrogen is higher than on Pt. These results are also in agreement with those reported by Yamamoto *et al*. They reported that their TiO_2 Schottky diode based gas sensors sensitivity to hydrogen decreased in the order of Pd > Pt > Au [24]. Additionally, Penza *et al.* have investigated the effect of catalyst on WO_3 sensors and concluded that devices with the Pd catalyst provided the highest sensitivity towards hydrogen as compared to Pt and Au [25].

In order to investigate the selectivity of the sensors, further experiments were conducted. All sensors were exposed to other gases including hydrogen and methane of the same concentration (1% vol). Figure 3.11 shows the dynamic responses, while Figure 3.12 shows the voltage shifts of each sensor under exposure of 1 % target gases

at 180 °C. It is found that all the voltage shifts under hydrogen gas exposure is slightly higher than that of to ethanol vapour.

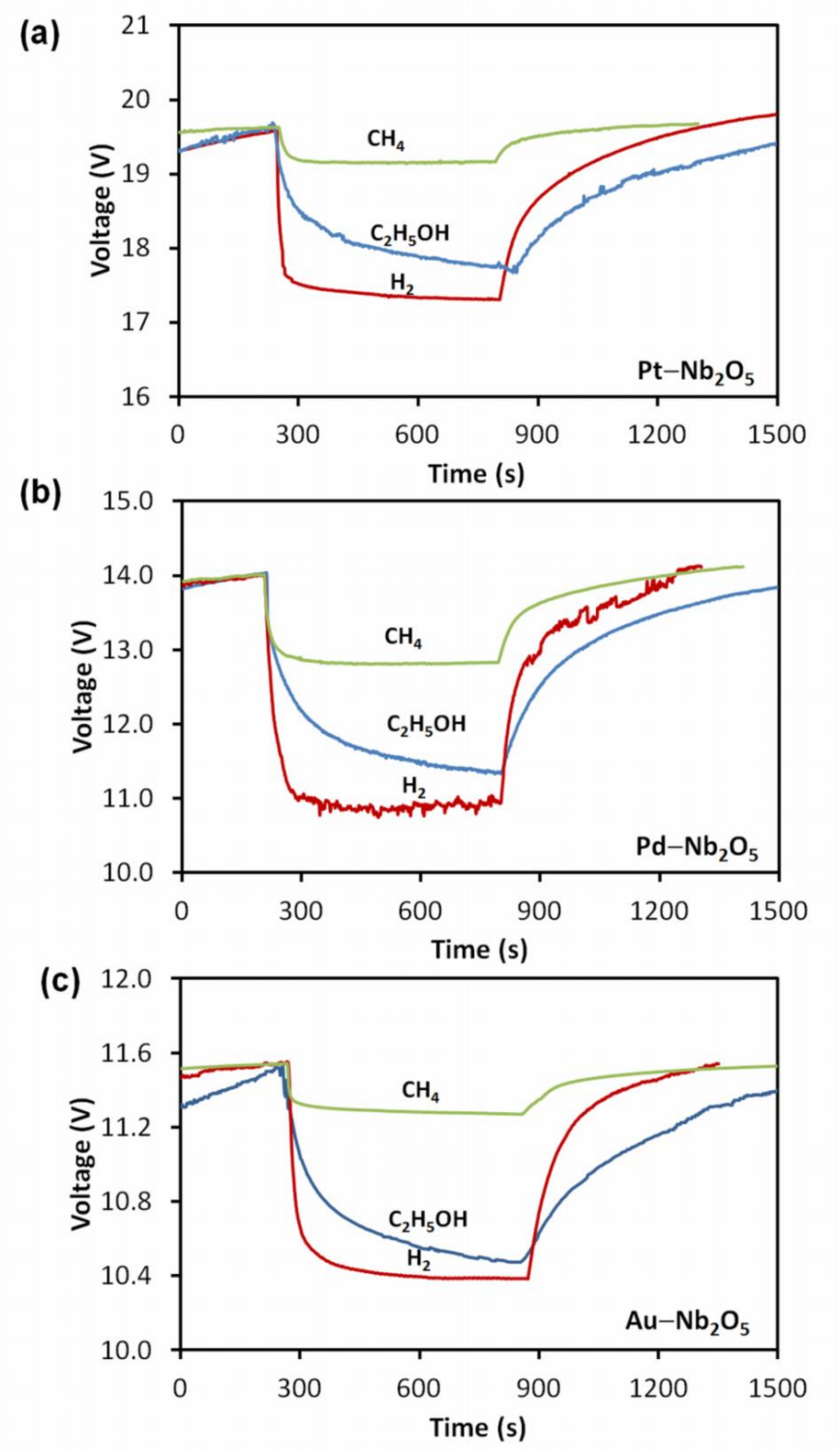

Figure 3.11: Dynamic response to 1% of different vapour/gases at 180 °C of (a) Pt–Nb_2O_5, (b) Pd–Nb_2O_5 and Au–Nb_2O_5 gas sensor.

However, the exposures to methane gas resulted in a relatively smaller voltage shifts. Thus, the sensors exhibited a stronger selectivity to ethanol and hydrogen and were less sensitive to methane gas. The Schottky barrier height change of the three sensors under different target vapour/gases is as shown previously in Table 3.1.

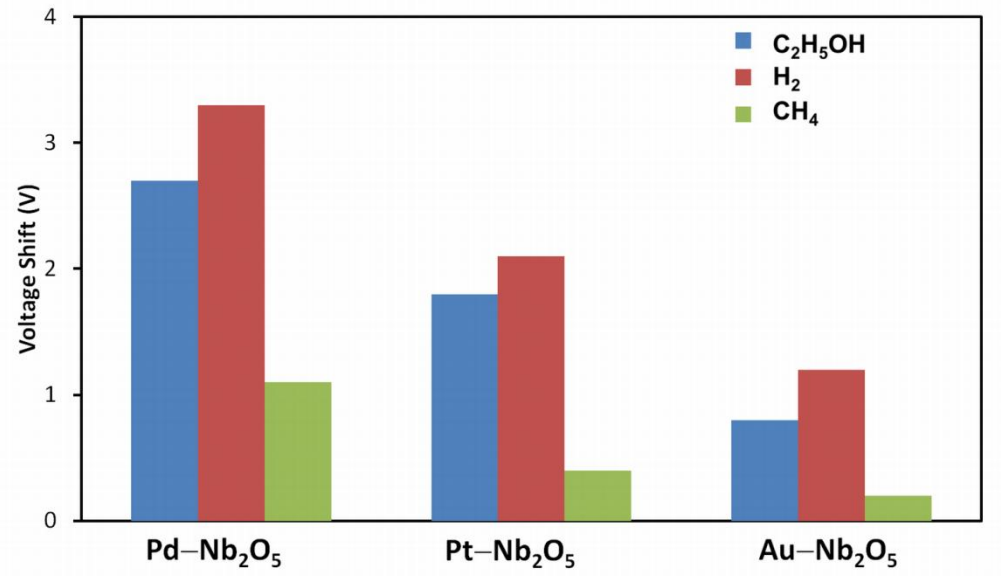

Figure 3.12: Voltage shift of all sensors at concentrations of 1% exposure to different vapour/gases.

In order to study the effect of water vapour on the response properties of ethanol, the PhD candidate conducts additional experiments with Pd–Nb_2O_5. The humidity effect of the sensors were studied by exposing them to the ethanol vapour and 100 % humidity and tested at a temperature of 90 °C. The presence of water vapour when exposed to the reduced $Nb_2O_{(5-\ x/2)}$ either physically cover the surface area, hindering it from further interactions with ethanol or forms a slightly intercalate niobium oxide. In either situation the sensitive layer is less sub-stoichiometry, resulting in a smaller barrier height change.

Exposing the device back to the oxygen rich environment with no ethanol molecules allows the surface of the film to revert back to original fully oxidized state.

However, when the surface exposed to humidity at a low temperature, less adsorption of oxygen species occurs (likely due to the H_2O coverage) [26]. Due to this, the recovery time would increase. As can be seen in Figure 3.13, it is observed that the sensor does not recover to its baseline after each response-recovery cycles, equal to those of the initial measurements, as they required longer time to recover.

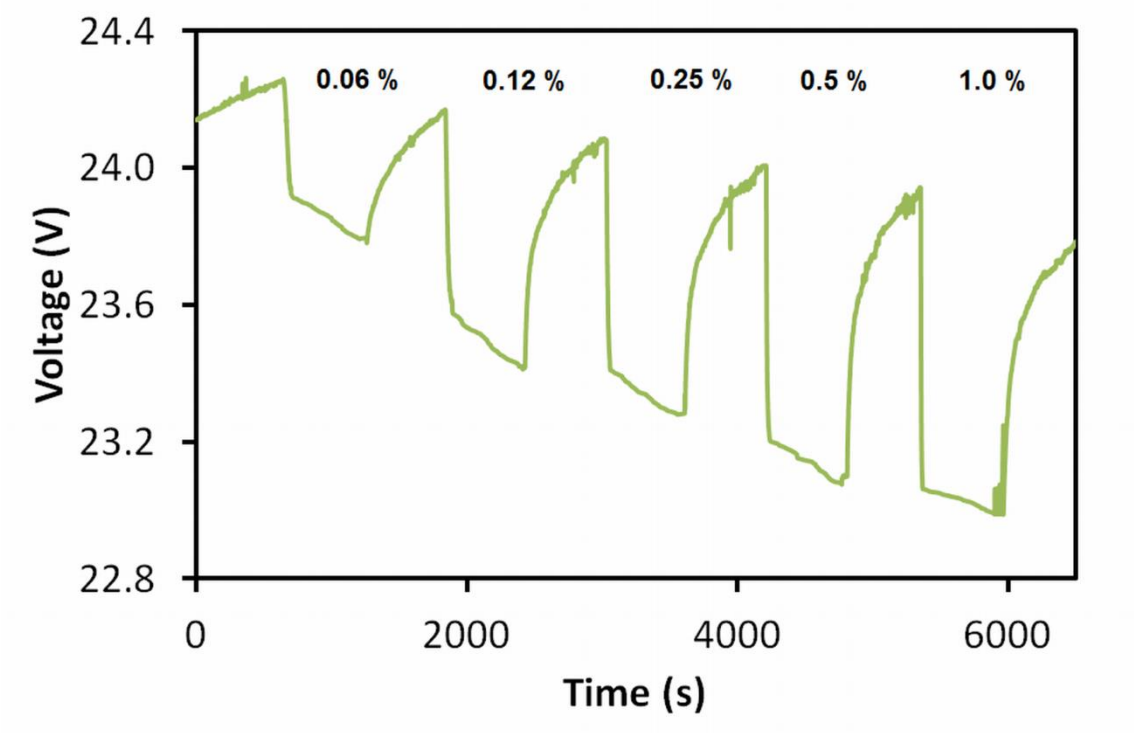

Figure 3.13: Dynamic response of Pd–Nb_2O_5 gas sensor at different ethanol concentrations and 100 % humidity.

3.4 Summary

In this chapter, the PhD candidate presented the outcomes of her investigation on the development of Schottky diode based devices made of metal catalysts and porous Nb_2O_5 towards ethanol sensing. The effects of Pd, Pt and Au metal catalysts on the barrier height of the contacts and sensing properies of the devices were comprehensively studied. Based on the presented results, the author concluded that

sensor with the Pd catalyst offered the best performance. They provided the highest sensitivity. Additionally, short reponse and recovery were achieved with Pd catalyst as well. The better performance of the Pd–Nb_2O_5 gas sensor was attributed to the properties of Pd catalyst, allowing more efficient breakdown of ethanol molecules and better solubility of the H atoms, which resulted in the highest Schottky barrier change. The presented investigation provide an in-depth vision regarding the performance of various catalytic metals in forming Schottky contacts with Nb_2O_5 and their performance as ethanol vapour sensors.

In the next chapter, the author will present her investigations regarding the development of optical gas sensor based on nanoporous Nb_2O_5 fabricated on FTO. The author will discuss in detail the fabrication process, film characterizations and the gas sensing performances.

References

[1] R. A. Kadir, R. A. Rani, A. S. Zoolfakar, J. Z. Ou, M. Shafiei, W. Wlodarski, *et al.*, "Nb_2O_5 Schottky based ethanol vapour sensors: Effect of metallic catalysts," *Sens. Actuators B Chem.*, vol. 202, pp. 74-82, 2014.

[2] R. A. Rani, A. S. Zoolfakar, J. Z. Ou, M. R. Field, M. Austin, and K. Kalantar-zadeh, "Nanoporous Nb_2O_5 hydrogen gas sensor," *Sens. Actuators B Chem.*, vol. 176, pp. 149-156, 2013.

[3] S. Ge, H. Jia, H. Zhao, Z. Zheng, and L. Zhang, "First observation of visible light photocatalytic activity of carbon modified Nb_2O_5 nanostructures," *J. Mater. Chem.*, vol. 20, pp. 3052-3058, 2010.

[4] H. Yamaura, Y. Abe, K. Ino, S. Ezawa, K. Sagata, K. Ikushima, *et al.*, "Carbon oxidation reaction over Pt/spherical alumina beads catalysts prepared by sputtering method," *Top. Catal.*, vol. 53, pp. 648-653, 2010.

[5] C. Varenne, A. Ndiaye, J. Brunet, G. Monier, L. Spinelle, A. Pauly, *et al.*, "Comparison of InP Schottky diodes based on Au or Pd sensing electrodes for NO_2 and O_3 sensing," *Solid State Electron.*, vol. 72, pp. 29-37, 2012.

[6] Y. H. Ng, M. Wang, H. Han, and C. L. L. Chai, "Organic polymer composites as robust, non-covalent supports of metal salts," *Chem. Commun.*, pp. 5530-5532, 2009.

[7] J. Z. Ou, R. A. Rani, M.-H. Ham, M. R. Field, Y. Zhang, H. Zheng, *et al.*, "Elevated temperature anodized Nb_2O_5 : A photoanode material with exceptionally large photoconversion efficiencies," *ACS Nano*, vol. 6, pp. 4045-4053, 2012.

[8] N. Thi Giang Huong, P. Thi Van Anh, P. Thi Xuan, L. Thi Xuan Binh, T. Van Man, and N. Thi Phuong Thoa, "Nano-Pt/C electrocatalysts: synthesis and activity for alcohol oxidation," *Adv. Nat. Sci. Nanosci. Nanotechnol.*, vol. 4, p. 035008, 2013.

[9] X. Liang, C.-j. Liu, and P. Kuai, "Selective oxidation of glucose to gluconic acid over argon plasma reduced Pd/Al_2O_3," *Green Chem.,* vol. 10, pp. 1318-1322, 2008.

[10] A. F. Lee, C. J. Baddeley, C. Hardacre, R. M. Ormerod, R. M. Lambert, G. Schmid, *et al.*, "Structural and catalytic properties of novel Au/Pd bimetallic colloid particles - EXAFS, XRD, and acetylene coupling," *J. Phys. Chem-Us,* vol. 99, pp. 6096-6102, 1995.

[11] A. C. Schmitz, A. T. Ping, M. A. Khan, Q. Chen, J. W. Yang, and I. Adesida, "Schottky barrier properties of various metals on *n*-type GaN," *Semicond. Sci. Tech.,* vol. 11, pp. 1464-1467, 1996.

[12] S.M Sze and K. K. Ng, *Physics of Semiconductor Device*: John Wiley & Sons, Inc Publication, 2006.

[13] B. A. Sexton, K. D. Rendulic, and A. E. Huges, "Decomposition pathways of C_1-C_4 alcohols adsorbed on platinum (111)," *Surf. Sci.,* vol. 121, pp. 181-198, 1982.

[14] A. Gazsi, A. Koós, T. Bánsági, and F. Solymosi, "Adsorption and decomposition of ethanol on supported Au catalysts," *Catal. Today,* vol. 160, pp. 70-78, 2011.

[15] P. Y. Sheng, G. A. Bowmaker, and H. Idriss, "The reactions of ethanol over Au/CeO_2," *Appl. Catal. A-Gen.,* vol. 261, pp. 171-181, 2004.

[16] A. Yee, S. J. Morrison, and H. Idriss, "The reactions of ethanol over M/CeO_2 catalysts - Evidence of carbon-carbon bond dissociation at low temperatures over Rh/CeO_2," *Catal. Today,* vol. 63, pp. 327-335, 2000.

[17] J. L. Davis and M. A. Barteau, "Decarbonylation and decomposition pathways of alcohols on Pd(111)," *Surf. Sci.,* vol. 187, pp. 387-406, 1987.

[18] H. Idriss, "Ethanol reactions over the surfaces of noble metal/cerium oxide catalysts," *Platinum Met. Rev.*, vol. 48, pp. 105-115, 2004.

[19] D. D. Yao, R. Abdul Rani, A. P. O'Mullane, K. Kalantar-zadeh, and J. Z. Ou, "High performance electrochromic devices based on anodized nanoporous Nb_2O_5," *J. Phys. Chem. C*, 2013.

[20] C. C. Cheng, Y. Y. Tsai, K. W. Lin, H. I. Chen, W. H. Hsu, H. M. Chuang, *et al.*, "Hydrogen sensing characteristics of Pd- and Pt-$Al_{0.3}Ga_{0.7}As$ metal-semiconductor (MS) Schottky diodes," *Semicond. Sci. Tech.*, vol. 19, pp. 778-782, 2004.

[21] S. Joo, I. Muto, and N. Hara, "Hydrogen gas sensor using Pt- and Pd-added anodic TiO_2 nanotube films," *J. Electrochem. Soc.*, vol. 157, pp. J221-J226, 2010.

[22] M. Armgarth, D. Soderberg, and I. Lundstrom, "Palladium and platinum gate metal-oxide-semiconductor capacitors in hydrogen and oxygen mixtures," *Appl. Phys. Lett.*, vol. 41, pp. 654-655, 1982.

[23] E. Bus and J. A. van Bokhoven, "Hydrogen chemisorption on supported platinum, gold, and platinum-gold-alloy catalysts," *Phys. Chem. Chem. Phys.*, vol. 9, pp. 2894-2902, 2007.

[24] N. Yamamoto, S. Tonomura, T. Matsuoka, and H. Tsubomura, "A study on a palladium-titanium oxide Schottky diode as a detector for gaseous components," *Surf. Sci.*, vol. 92, pp. 400-406, 1980.

[25] M. Penza, C. Martucci, and G. Cassano, "NO_x gas sensing characteristics of WO_3 thin films activated by noble metals (Pd, Pt, Au) layers," *Sens. Actuators B Chem.*, vol. 50, pp. 52-59, 1998.

[26] C. Wang, L. Yin, L. Zhang, D. Xiang, and R. Gao, "Metal oxide gas sensors: sensitivity and influencing factors," *Sensors*, vol. 10, pp. 2088-2106, 2010.

Chapter 4

Anodized Nb_2O_5: An Optically Responsive System to Hydrogen Gas Molecules

4.1 Introduction

In the previous chapter, the PhD candidate reported the investigation of nanoporous Nb_2O_5 as Schottky-based gas sensors. In this chapter, the author presents the outcome of her research regarding the development of optical gas sensors based on nanoporous Nb_2O_5.

Nanoporous Nb_2O_5 has been shown previously to be a viable electrochromic material with strong intercalation characteristics [1-3]. Despite showing such promising properties, its' potential for optical gas sensing applications, which involve the production of ionic species such as H^+, has yet to be explored. Nanoporous Nb_2O_5 coated with a thin layer of Pt can accommodate a large amount of H^+ ions in a process that results in an energy bandgap change of the material that induces an optical response. In this chapter, the PhD candidate presents her investigations on optical hydrogen gas (H_2) sensor made of highly ordered nanoporous Nb_2O_5 with a large surface to volume ratio prepared *via* a high temperature anodization method. The large active surface area of the film provides enhanced pathways for efficient hydrogen adsorption and dissociation which is facilitated by a thin layer of Pt catalyst. The processes of hydrogen sensing which causes large optical modulations are fully investigated in terms of response magnitudes and dynamics. The hydrogen gas

modulation and sensing properties of Nb_2O_5 can be potentially used for future optical gas sensing systems.

The outcome of this chapter was mostly contributed to one of the PhD candidate's journal papers entitled "Optical Gas Sensing Properties of Nanoporous Nb_2O_5 Films." which has been published in the *ACS Applied Materials & Interfaces* [4].

4.2 Experimental

4.2.1 Synthesis of Nb_2O_5

The Nb films used in this work were prepared by a RF magnetron sputtering system. Fluorine-doped tin oxide (15 Ω sq^{-1}, Dyesol) glass substrates measuring 15 mm × 10 mm were used. Nb films were deposited by means of a RF magnetron sputtering using a circular metallic Nb target of 2 inches in diameter with a purity of 99.95% placed at a distance of 65 mm from the substrate stage. The base pressure of the sputtering chamber was 1.0×10^{-5} Torr and the sputtering pressure was set to 2×10^{-2} Torr in the presence of pure argon (100%). A constant 120 W RF power was used with the substrate temperature fixed at 300 °C for 20 minutes of sputtering. The sputtering process utilizing the aforementioned parameters resulted in Nb metal films with thicknesses of ~350 nm. The sputtered Nb films were anodized in an electrolyte consist of 50 mL glycerol (99% purity) mixed with 6.3 g of K_2HPO_4 (98% purity) (both from Sigma–Aldrich) that was kept at a constant temperature of 180 °C during the anodization process. The anodization was carried out with a conventional two electrode configuration, where the anode was the sample and the cathode was a platinum foil. The anodization duration of 3 mins at a voltage of 5 V resulted in nanoporous Nb_2O_5 of ~500 nm thickness. The films were then washed using deionized water and dried in a

nitrogen stream. The samples were then annealed in a standard laboratory furnace at 500 °C for 1 h in air with a ramp-up and ramp-down rate of 2°C min^{-1} which resulted in transparent crystalline Nb_2O_5 films. A Pt catalytic layer of ~ 1 nm thickness was sputtered onto the film surface to facilitate and enhance the breakdown of hydrogen gas molecules. In previous report, the as-synthesized compact Nb_2O_5 nanoporous films with a thickness of 500 nm demonstrated the optimum coloration efficiency in electrochromic applications [1]. As such, the author chose this thickness for her optical gas sensing investigations.

4.2.2 Structural characterization

The scanning electron microscope (SEM) images of the Nb_2O_5 films were taken with a FEI Nova NanoSEM, while the chemical properties of the films were examined by X-ray photoemission spectroscopy (XPS) using a Thermo K-alpha X-ray source (1486.7 eV) with an energy of 50 eV. The crystalline structure of the Nb_2O_5 films were determined by X-ray diffraction (XRD), characterized by a D8 Advance Bruker AXS with General Area Detector Diffraction System (GADDS) attachment fitted with a 50 μm spot size collimator, incorporating a High Star 2 dimensional detector and CuKα radiation (λ = 0.1542 nm) operating at 40 kV and 40 mA. Raman spectra were measured using an Ocean Optic QE 6500 spectrometer, equipped with a 532 nm 40 mW laser as the excitation source.

4.2.3 Gas sensing measurements

The absorption spectra of the Nb_2O_5 nanoporous films were examined using a testing setup as shown in Figure 4.1(a). The custom-made chamber (Figure 4.1(b)) consisted of an aluminum box with ports for a gas inlet and outlet, ports for light to pass through

and electrical connectors for a heating plate. The optical signal was provided using a deuterium-halogen single beam light source (Micropack DH-200) and measured by a spectrophotometer (Ocean Optics HR 4000). A custom built sample holder was utilized to mount the substrate during testing. The operating temperature of the sensors was regulated using a localized heater which was connected to a dc voltage supply. The hydrogen gas was pulsed into the inlets of the aluminium box where the concentration was accurately controlled using a computerized mass flow control (MFC) multi-channel gas calibration system. Exposure time was 10 min for each pulse of hydrogen gas and the chamber was purged with synthetic air for 10 min between pulses to allow the sensors to recover under atmospheric conditions. The analysis was performed using Spectrasuite software package.

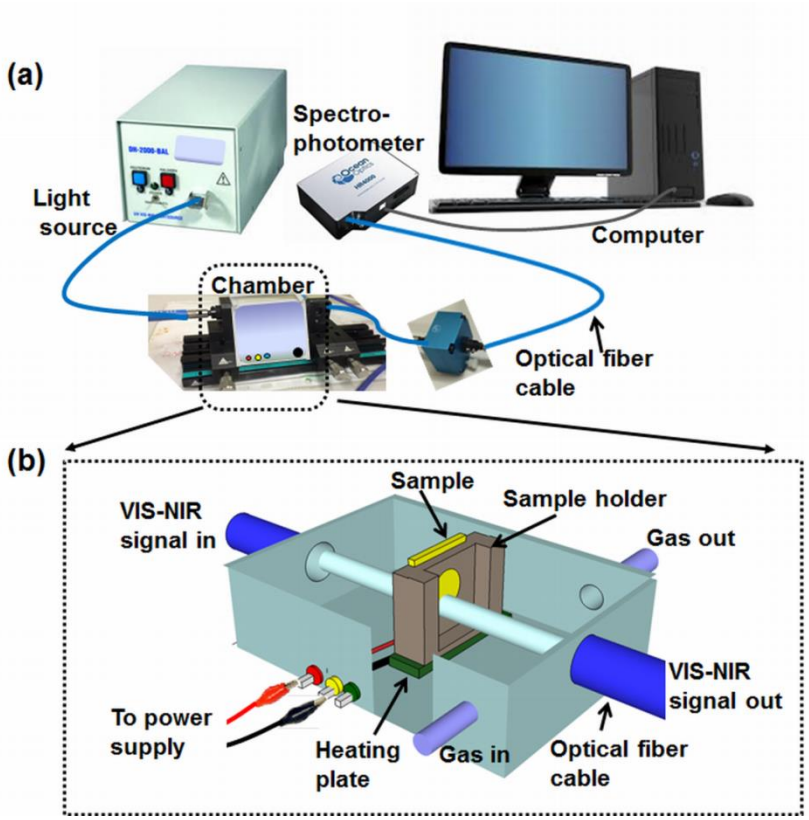

Figure 4.1: The schematic diagrams of (a) the gas sensing measurement set-up and (b) three-dimensional diagram of the optical gas testing chamber.

4.3 Results and discussion

4.3.1 Morphology and structural properties

The surface and cross-sectional SEM images of Nb_2O_5 films are presented in Figure 4.2. From the top-view SEM image of the Nb_2O_5 layer in Figure 4.2(a), it can be clearly seen that, apart from the large pores with an average dimension of 35 nm, smaller pores with a size from 10 to 15 nm were also formed throughout the films, thus making all of the pores connected into a three-dimensional (3D) porous nanostructure. From the cross sectional images as depicted in Figure 4.2(b), it was observed that the anodized thin films were composed of arrays of continuous and highly packed nanoporous networks that are ordered in the vertical direction. This nanoporous structure offer great prospects for optical gas sensing, as the significantly increased surface area should in principle allow faster and more efficient diffusion of target gases.

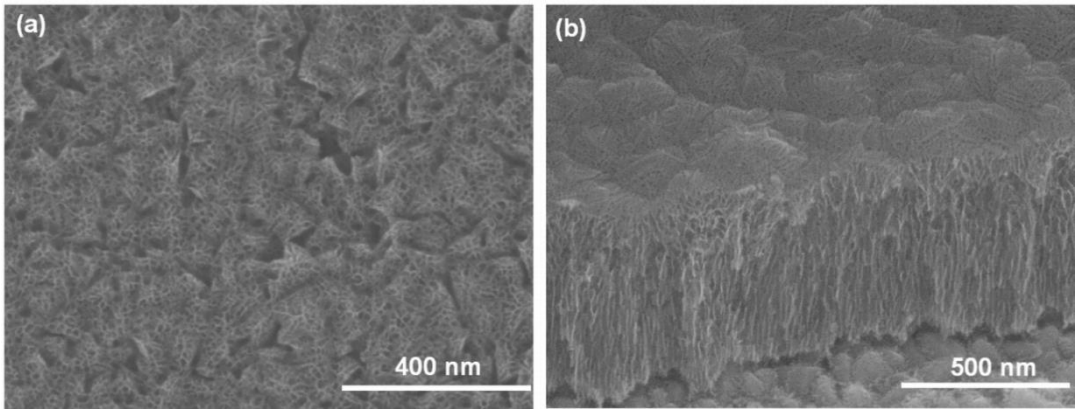

Figure 4.2: SEM images of (a) top view and (b) cross sectional view of anodized Nb_2O_5

An XPS was carried out to determine the composition of the annealed Nb_2O_5 nanoporous films. Figure 4.3(a) shows the survey spectrum of the films indicating the existing of Nb, O, N and C. The existence of minute peaks for N and C in the survey spectrum was attributed to atmospheric contamination. As shown in Figure 4.3(b), the

high resolution spectra exhibits peaks approximately at 210.1 and 207.3 eV, which were accredited to the $Nb3d_{3/2}$ and $Nb3d_{5/2}$ energy levels, respectively. The measured peaks were consistent with a previous report, representing the full stoichiometry of Nb_2O_5 films [1].

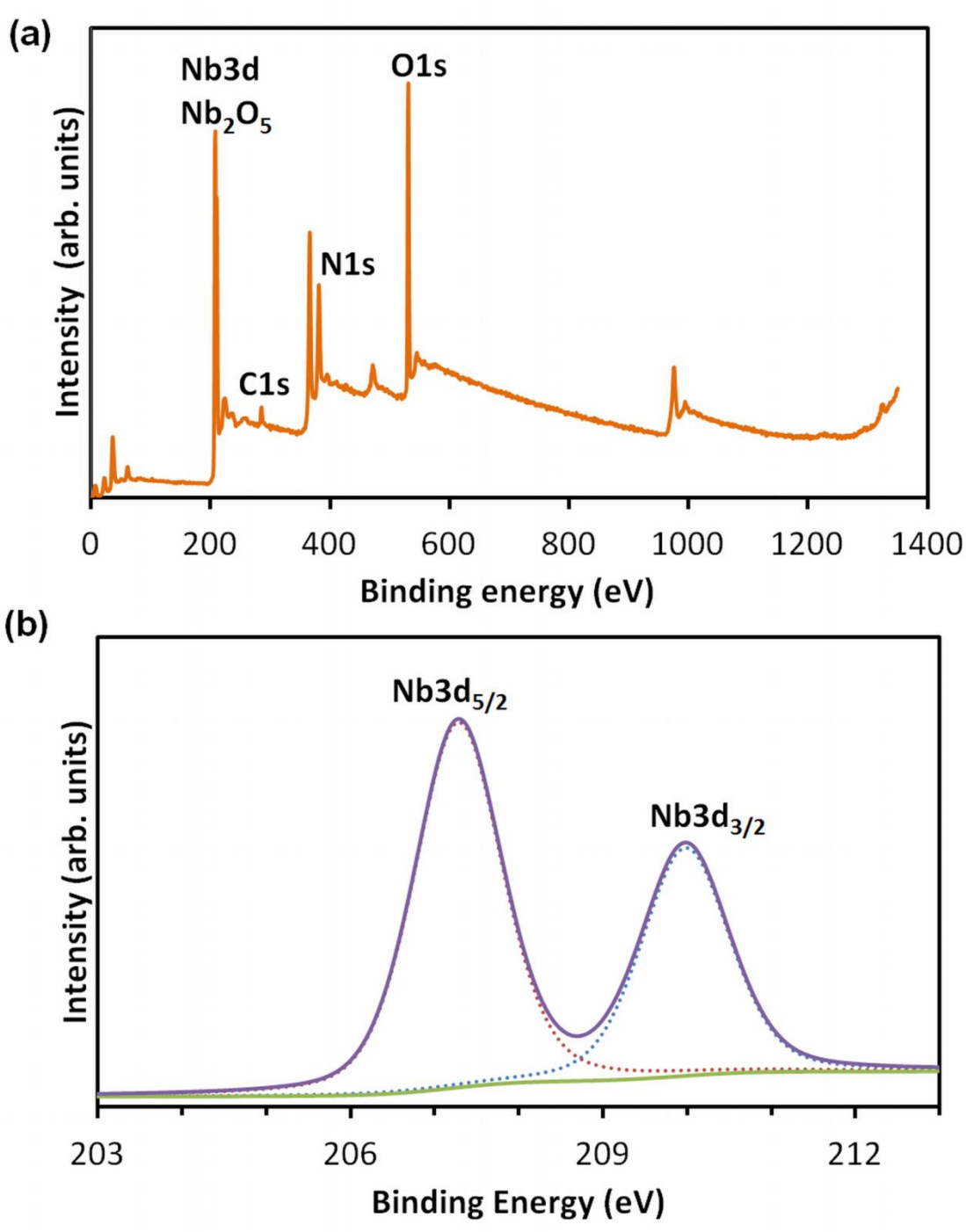

Figure 4.3: (a) The XPS survey scan of nanoporous Nb_2O_5 film and (b) XPS spectrum of Nb3d peaks of the nanoporous Nb_2O_5 film.

XRD measurements were carried out to examine the crystalline structures of the as-anodized and annealed Nb_2O_5. The XRD patterns of the as-anodized sample (Figure 4.4-i) display only Nb peaks together with FTO peaks indicating amorphous nature of the films. The annealed films were crystalline and formed the orthorhombic phase of Nb_2O_5 (ICDD27-1003) after 1 hour of annealing at a temperature of 500 °C as indicated by peaks appearing at 22.6, 28.5, 37.0, 45.0, 46.3, and 55.5 ° 2-theta (Figure 4.4-ii) [5].

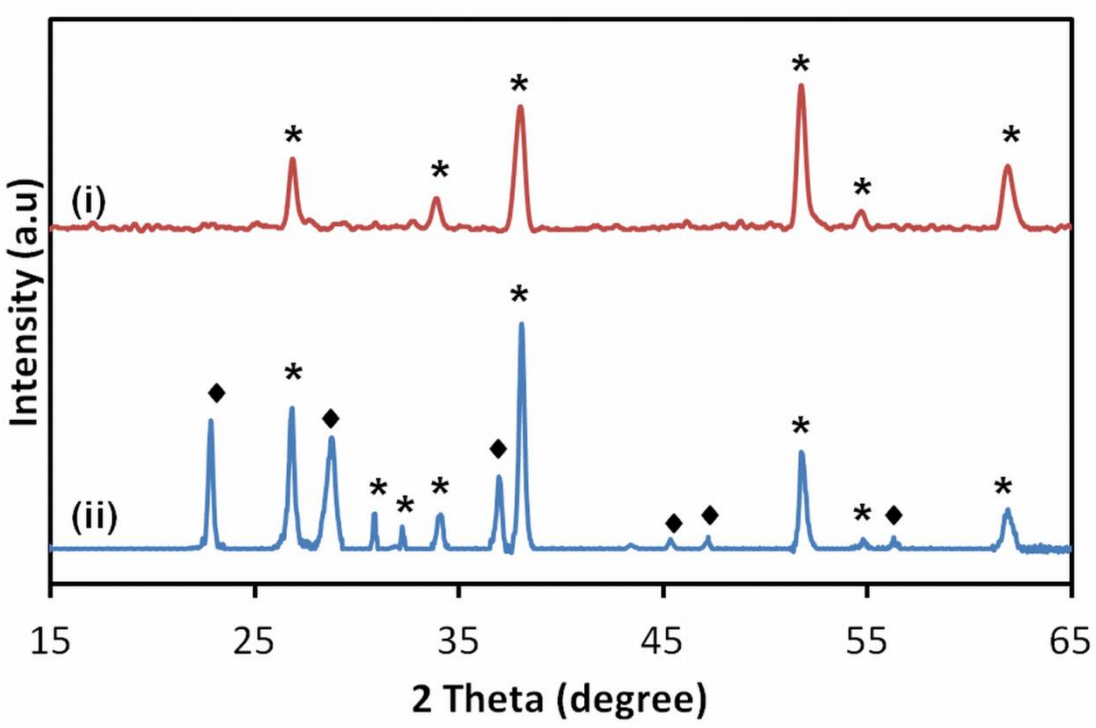

Figure 4.4: (a) The XRD pattern of nanoporous Nb_2O_5 film (i) as anodized and (ii) after annealing in air for 1 hour at 500 °C, orthorhombic phase (ICDD 27-1003) is denoted by ♦, while FTO is denoted by *.

The results were further verified by the Raman spectra presented in Figure 4.5. The broad peaks at 250 cm^{-1} and 650 cm^{-1} were observed in the spectrum of nanoporous films signifying the characteristics of amorphous niobium oxide. After annealing, the Raman peaks for the nanoporous Nb_2O_5 were clearly visible by peaks located at 303 and 460 cm^{-1}. These peak positions are consistent with previous reports

which correspond to the orthorhombic phase of crystalline Nb_2O_5 [6]. The XRD peaks, as well as XPS and Raman analysis confirmed the orthorhombic phase structure of the Nb_2O_5 nanoporous film.

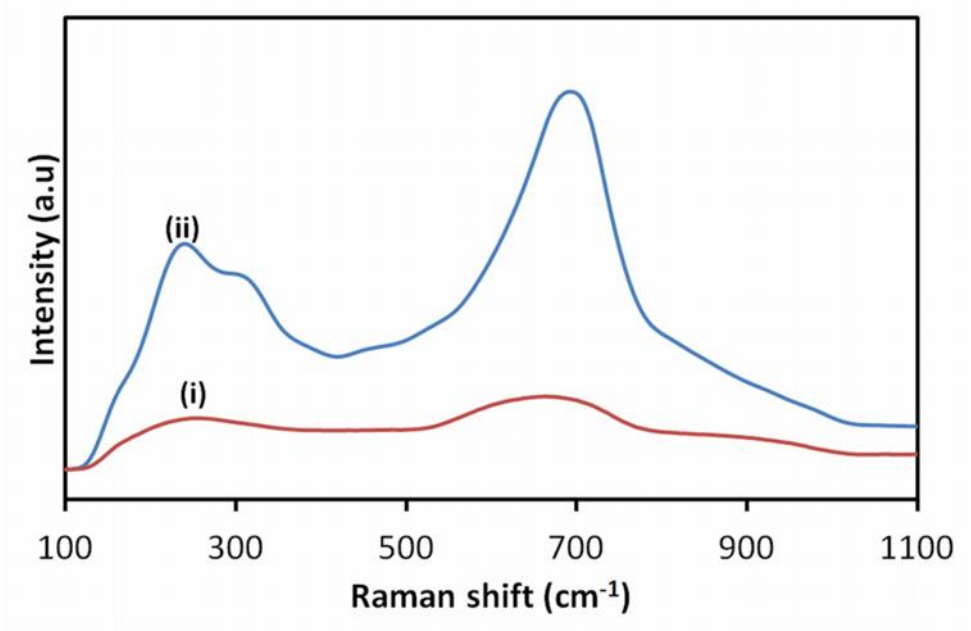

Figure 4.5: Raman spectra of (i) as-anodized and (ii) annealed Nb_2O_5 films.

4.3.2 Gas sensing performances

The optical responses of the Pt/ Nb_2O_5 nanoporous films were first investigated under different operating temperatures. The measurements were conducted at temperatures of 22, 40, 60, 80 and 100 °C by exposing it alternately to synthetic air and 1 % hydrogen gas balanced in air. Temperatures above 100 °C could not be implemented as the test chamber could not withstand such elevated temperatures. It was found that the Pt/ Nb_2O_5 nanoporous films did not show any distinguishable gas response at room temperature as shown in Figure 4.6(a). It is suggested that at low temperature, there is insufficient energy for hydrogen dissociation to happen. It has been reported that higher energy is required to initiate the intercalation process of Nb_2O_5 nanoporous structure due the fact that Nb_2O_5 has a wider band gap and higher conduction band edge as compared to other eminent electrochromic materials [1].

The introduction of 1 % hydrogen gas to the Pt/ Nb_2O_5 nanoporous films at 100 °C resulted in a change of the absorption spectrum over a wide wavelength range from 350 to 900 nm (Figure 4.6(b)). It has been reported that 100 °C was the optimum temperature for an absorbance response as at such temperatures, the adsorption rate of H^+ ions increases due to sufficient energy being available to dissociate molecular hydrogen while at the same time the formation of water vapor on the surface is limited which would decrease the surface area available for the gas adsorption response [7].

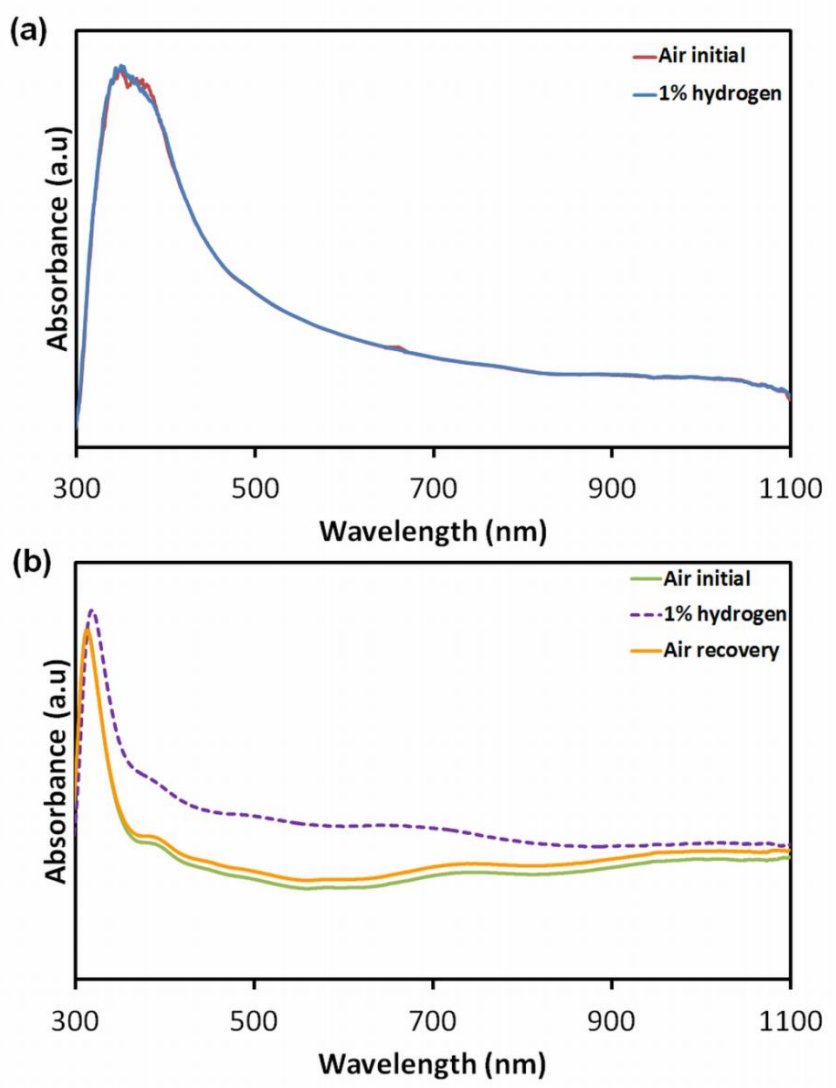

Figure 4.6: Absorbance versus optical wavelength spectra for Pt/Nb_2O_5 nanoporous films exposed to 1 % hydrogen at (a) room temperature and (b) 100 °C.

The optical absorption properties of Nb_2O_5 were tuned by the intercalation of H^+ ions that resulted from the dissociation of hydrogen gas molecules in the presence of the Pt catalyst. These reactions alter the electronic band structure of the Nb_2O_5 nanoporous films [1] which consequently changes the optical absorbance of the films. The detailed mechanism of optical hydrogen gas sensing using nanoporous Nb_2O_5 is discussed in details as follows.

Hydrogen gas dissociates on the Pt catalyst forming hydrogen ions (H^+) and electrons (e^-) [8]:

$$H_2(g) \rightarrow 2H^+ + 2e^- \quad (4.1)$$

The generated hydrogen ions and electrons are simultaneously intercalated into the Nb_2O_5 nanoporous films. Furthermore, water molecules (H_2O) are formed *via* the reduction of Nb_2O_5 to $Nb_2O_{5-x/2}$ as described by the following reactions [1, 5]:

$$Nb_2O_5 + xH^+ + xe^- \leftrightharpoons H_xNb_2O_5 \quad (4.2)$$

$$2H_xNb_2O_5 \leftrightharpoons xH_2O + Nb_2O_{5-x/2} \quad (4.3)$$

The intercalated H^+ ions are embedded into the crystal structure of Nb_2O_5 and the released electrons are transferred to the lowest-lying unoccupied energy levels of Nb_2O_5. Thus, the stoichiometry of the nanoporous film is changed and its electronic band structure is altered, which results in an increase of the Nb_2O_5 film absorbance. Purging the hydrogen gas source from the system by exposing the films to air (oxygen rich environment) the adsorbed oxygen species restores the stoichiometry of the Nb_2O_5 nanoporous films and hence reduce the level of absorbance to the original state as [5]:

$$Nb_2O_{5-x/2} + (x/4)O_2 \leftrightharpoons Nb_2O_5 \quad (4.4)$$

This indicates the reversibility of the chemical reactions, and thereby justifies the use of this material in a repeatable manner and its use in gas sensor.

As mentioned before, the intercalation of H^+ ions reduces the bandgap of Nb_2O_5. The bandgap energies were calculated from the UV-Vis absorption spectra shown in

Figure 6(b) using the Tauc equation [9]. It was found that the bandgap of the anodized Nb_2O_5 film under ambient air exposure was 3.26 eV. The bandgap reduced to 2.99 eV in the presence of 1% hydrogen due to the intercalation of H^+ ions into the Nb_2O_5 film as described by equation (4.2).

Figure 4.7 shows the dynamic response of the Pt/ Nb_2O_5 films towards a 1% hydrogen gas concentration at different operating temperatures from 60 to 100 °C. The measurements were carried out at a single wavelength of 600 nm which was the wavelength where the maximum absorption was recorded in the visible region in Figure 6(b). As discussed before, no response was observed at room temperature, but the response magnitude increased with an increase of operating temperature starting from 60 °C and the maximum absorption change was observed at 100 °C. This might be due to the slow kinetics of hydrogen dissociation over this temperature range. Consequently, this would suppress the injection of both e^- and H^+ into the Nb_2O_5 lattice. However, as the temperature increases, the response increased slightly due to the favorable hydrogen adsorption and dissociation on the catalyst surface.

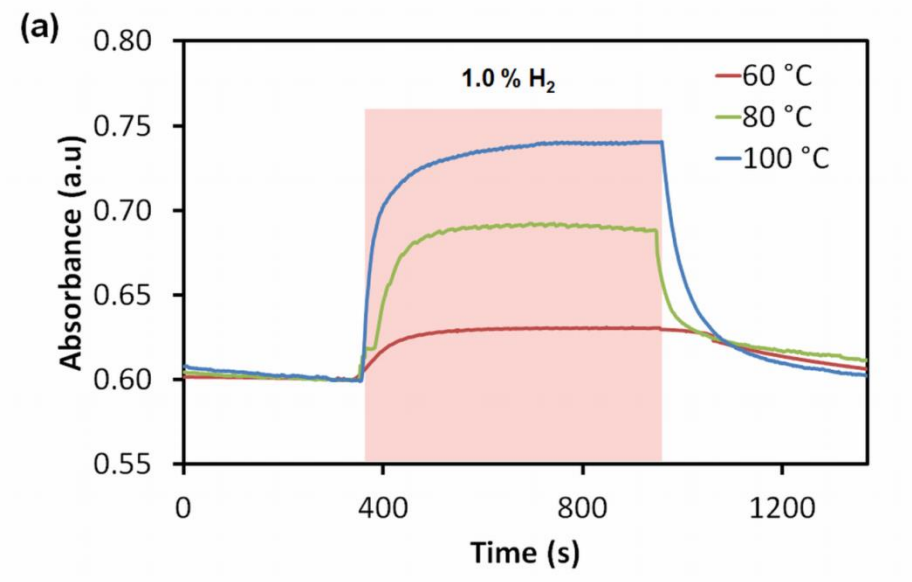

Figure 4.7: The dynamic response of nanoporous Nb_2O_5 optical gas sensors at different temperatures at wavelength of 600 nm under 1% hydrogen exposure.

Figure 4.8(a) shows the dynamic responses of the Pt/ Nb_2O_5 nanoporous films towards hydrogen concentration range of 0.06 to 1.0 %, measured at a single wavelength of 600 nm at 100 °C. It was found that the absorption change increases linearly with increasing hydrogen concentration as observed from the plot shown in Figure 4.8(b). With hydrogen concentrations of 0.06, 0.12, 0.25, 0.5, and 1.0%, absorption changes of 0.03, 0.04, 0.05, 0.08 and 0.12 were recorded. When the gas supply was repeatedly switched from air to hydrogen gas, the baseline remained stable.

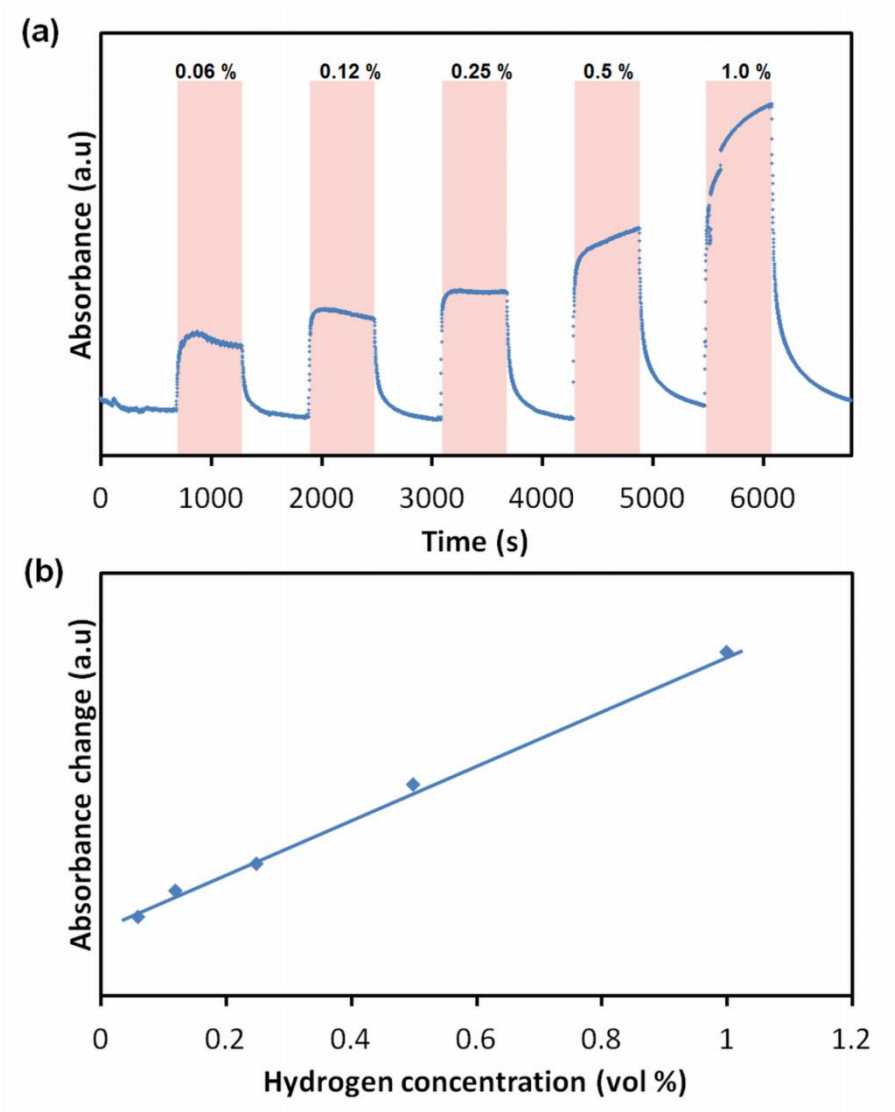

Figure 4.8: (a) Dynamic performance and (b) absorbance change of Pt/Nb_2O_5 nanoporous films based sensor after exposure to different concentration of hydrogen at 100 °C at the wavelength of 600 nm.

The performances of the optical sensors under different hydrogen concentrations were further evaluated in terms of response and recovery time. The response time is defined as the time required for the variation in absorbance to reach 90% of the equilibrium absorbance peak value after a test gas was injected, and the recovery time as the time necessary for the sensor to return to 10% above the equilibrium absorbance peak value in air after releasing the test gas [10]. Figure 4.9 shows the plot of response and recovery times under different concentrations of hydrogen exposure. It was found that, as the concentration of hydrogen increased, the response time decreased. However the sensor required a longer time to recover as the hydrogen concentration increased.

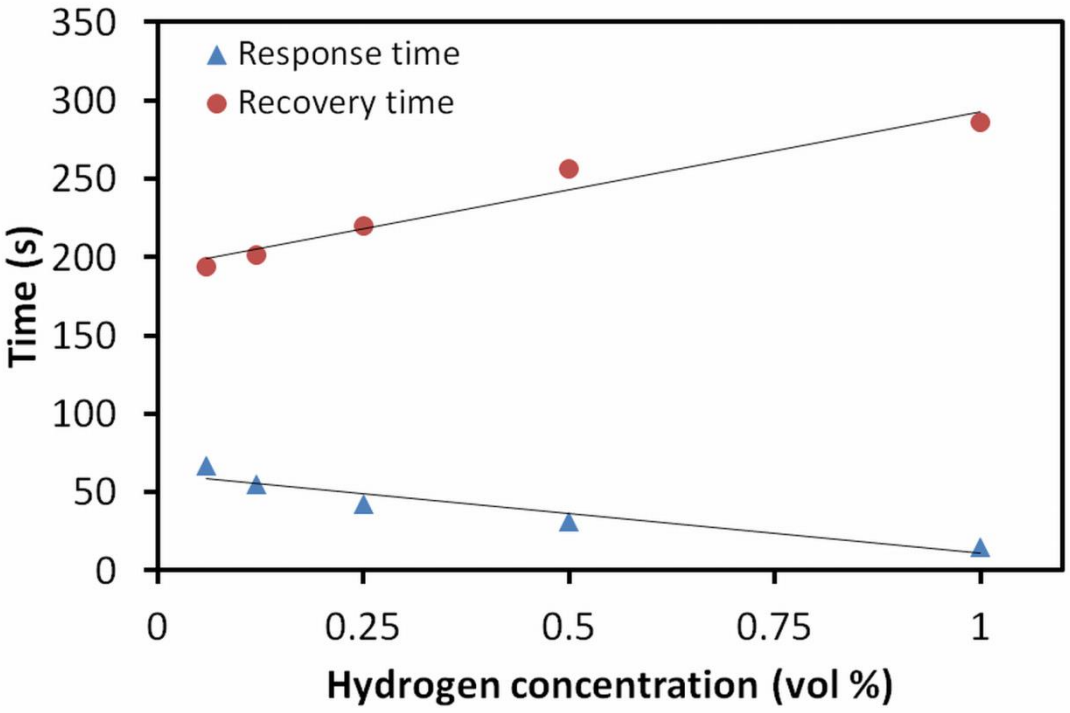

Figure 4.9: Plot of response and recovery times under various hydrogen concentrations

In general, the response time of the sensors is much shorter than the recovery time. Hydrogen concentrations of 0.06, 0.12, 0.25, 0.5 and 1.0 %, result in response times of 62, 52, 45, 32 and 12 s while recovery times were 190, 212, 225, 259 and 275 s respectively. It can be concluded that the Pt/ Nb_2O_5 sensor performances exhibited a

strong dependence on the hydrogen gas concentration. With the increased hydrogen gas concentration, the adsorption of H^+ ions is high; thereby favoring fast electron injections and H^+ intercalations into the Nb_2O_5 films and therefore enhanced response times. However, it is suggested that the increase in hydrogen concentration also results in large changes in the film stoichiometry, and therefore restoring the film to its initial state will take longer.

4.4 Summary

In this chapter, the PhD candidate presented her investigations regarding the development of nanoporous Nb_2O_5 films for optical hydrogen gas sensing. These nanoporous films were obtained using a high temperature anodization technique in a glycerol based electrolyte at 180 ºC that resulted in highly ordered Nb_2O_5 nanostructures. In the gas sensing experiments, the dissociated H^+ ions from the hydrogen gas molecules, facilitated by the presence of a thin Pt layer, changed the optical absorption properties of the Nb_2O_5 film in the visible region. The intercalation of H^+ into the nanoporous films altered the electronic band structure, thereby exhibiting an absorption change which contributed to the sensor response. The optical absorbance measurements upon exposure to hydrogen gas were conducted over a range of temperatures starting from room temperature to 100 °C. The nanoporous films of ~500 nm thickness with a high active surface area demonstrated excellent absorbance changes at 100 °C with a response factor of 12.1 % at 1% hydrogen in ambient air as well as a rapid response and recovery. The presented work is the first report of an optical hydrogen gas sensor based on Nb_2O_5 and future investigations can reveal its applications for sensing other gas species.

In the next chapter, the PhD candidate will present her research on nanoporous WO_3 based systems, as the final section of this PhD dissertation. The author will

present her investigations on the development of highly ordered nanoporous WO_3 Schottky-based gas sensors for sensing ethanol vapour and hydrogen gas.

References

[1] D. D. Yao, R. A. Rani, A. P. O'Mullane, K. Kalantar-zadeh, and J. Z. Ou, "High performance electrochromic devices based on anodized nanoporous Nb_2O_5," *J. Phys. Chem. C,* vol. 118, pp. 476-481, 2014.

[2] D. D. Yao, R. A. Rani, A. P. O'Mullane, K. Kalantar-zadeh, and J. Z. Ou, "Enhanced coloration efficiency for electrochromic devices based on anodized Nb_2O_5/electrodeposited MoO_3 binary systems," *J. Phys. Chem. C,* vol. 118, pp. 10867-10873, 2014.

[3] M. A. Aegerter, "Sol-gel niobium pentoxide: A promising material for electrochromic coatings, batteries, nanocrystalline solar cells and catalysis," *Sol. Energ. Mat. Sol. C,* vol. 68, pp. 401-422, 2001.

[4] R. Ab Kadir, R. A. Rani, M. M. Y. A. Alsaif, J. Z. Ou, W. Wlodarski, A. P. O'Mullane, *et al.*, "Optical gas sensing properties of nanoporous Nb_2O_5 films," *ACS Appl. Mater. Interfaces,* 2015.

[5] R. A. Rani, A. S. Zoolfakar, J. Z. Ou, M. R. Field, M. Austin, and K. Kalantar-zadeh, "Nanoporous Nb_2O_5 hydrogen gas sensor," *Sens. Actuators B Chem.,* vol. 176, pp. 149-156, 2013.

[6] R. Brayner and F. Bozon-Verduraz, "Niobium pentoxide prepared by soft chemical routes: morphology, structure, defects and quantum size effect," *Phys. Chem. Chem. Phys.*, vol. 5, pp. 1457-1466, 2003.

[7] M. H. Yaacob, M. Z. Ahmad, A. Z. Sadek, J. Z. Ou, J. Campbell, K. Kalantar-zadeh, *et al.*, "Optical response of WO_3 nanostructured thin films sputtered on different transparent substrates towards hydrogen of low concentration," *Sens. Actuators B Chem.*, vol. 177, pp. 981-988, 2013.

[8] T. Hübert, L. Boon-Brett, G. Black, and U. Banach, "Hydrogen sensors – A review," *Sens. Actuators B Chem.*, vol. 157, pp. 329-352, 2011.

[9] D. Di Yao, M. R. Field, A. P. O'Mullane, K. Kalantar-zadeh, and J. Z. Ou, "Electrochromic properties of TiO_2 nanotubes coated with electrodeposited MoO_3," *Nanoscale*, vol. 5, pp. 10353-10359, 2013.

[10] M. M. Y. A. Alsaif, M. R. Field, B. J. Murdoch, T. Daeneke, K. Latham, A. F. Chrimes, *et al.*, "Substoichiometric two-dimensional molybdenum oxide flakes: a plasmonic gas sensing platform," *Nanoscale*, 2014.

Chapter 5

Anodized Nanoporous WO_3 Schottky Contact Structure for Hydrogen and Ethanol Sensing

5.1 Introduction

In this chapter, the PhD candidate presents her work on the development of nanoporous tungsten trioxide (WO_3) Schottky-based gas sensors.

The nanoporous WO_3 films were prepared by anodic oxidation of tungsten foil in ethylene glycol mixed with ammonium fluoride and a small amount of water. Anodization resulted in highly ordered WO_3 films with a large surface to volume ratio. Utilizing these nanoporous structures, Schottky diode-based gas sensors were developed by depositing a platinum catalytic contact and tested towards hydrogen gas and ethanol vapour. Analysis of the current–voltage characteristics and dynamic responses of the sensors indicated that these devices exhibited a larger voltage shift in the presence of hydrogen gas compared to ethanol vapour at an optimum operating temperature of 200 °C. The gas sensing mechanism was discussed, by associating the response to the intercalating H^+ species that are generated as the result of the hydrogen and ethanol molecules breakdowns onto Pt/WO_3 contact and their spill over into nanoporous WO_3.

The work presented in this chapter was submitted to the *Journal of Materials Chemistry A* and is currently under review.

5.2 Experimental

5.2.1 Synthesis of WO_3

W foil (99.9% purity) used in this work purchased from Sigma Aldrich and was cut into pieces of 1.0 cm × 1.5 cm. After the clean-up, the cut samples were anodized in an electrolyte of 50 mL ethylene glycol (98% anhydrous) mixed with 10% (wt) NH_4F (98% purity) (both from Sigma-Aldrich) and a small amount of DI water. The anodization was carried out with a conventional anode–cathode configuration at a room temperature [1], where the anode was the W foil piece and the cathode was a platinum foil. The anodization at the voltage of 10 V for durations of 15 minutes resulted in WO_3 films comprising of 500 nm thick nanoporous structures. Upon the completion of anodization, samples were washed using DI water and dried in a nitrogen stream. The as-anodized samples were than annealed by a standard laboratory horizontal furnace at 500 °C for 1 h in air with a ramp-up and ramp-down rate of 2°C min^{-1} which resulted in crystalline WO_3 films.

For establishing the gas sensors, Pt catalytic contact with the thickness of ~15 nm was deposited on top of the WO_3 nanoporous using a GATAN PECS^{TM} (Precision Etching Coating System) thin film coater. The non-anodized side of W substrates were used as the ohmic contact (Figure 5.1(a)).

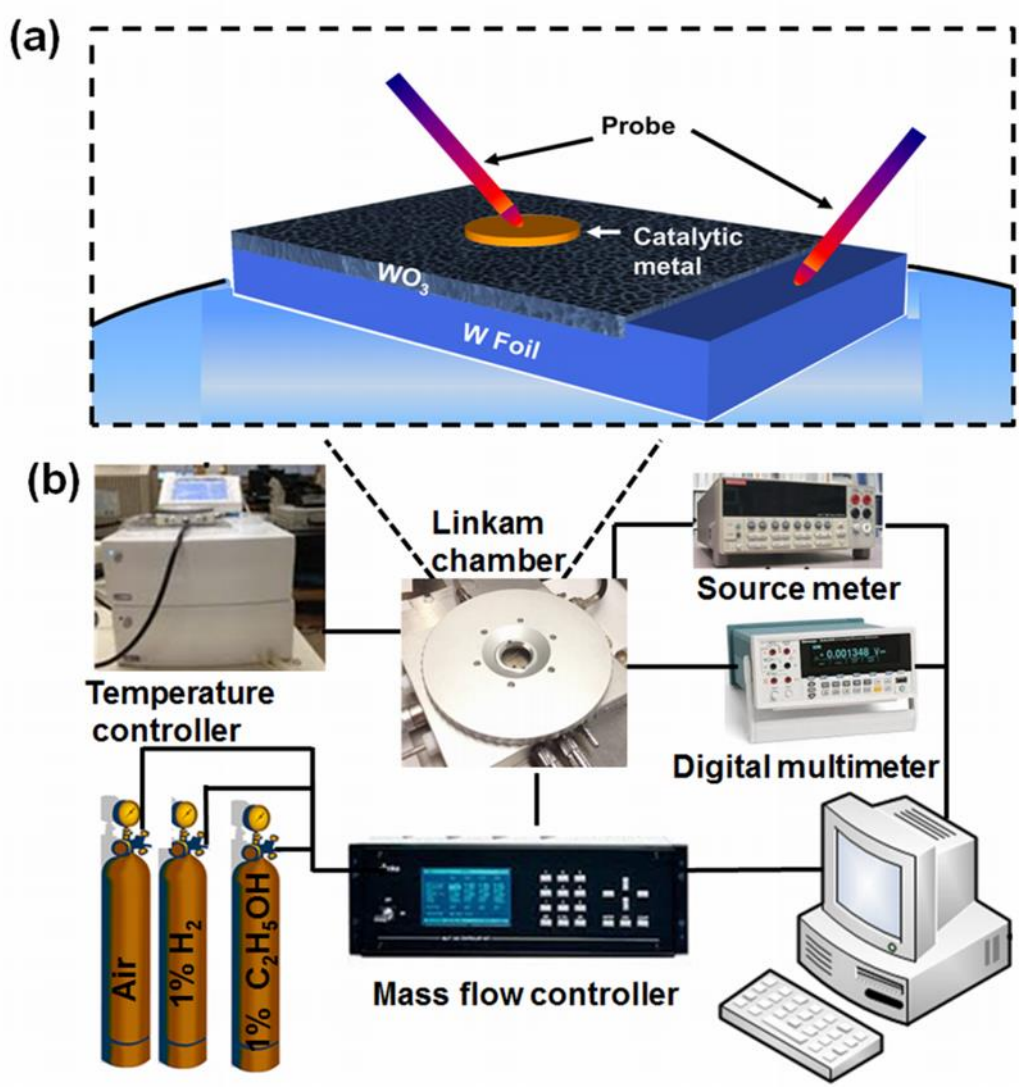

Figure 5.1: The schematic diagrams of (a) three-dimensional Schottky-based WO_3 sensor and (b) the gas sensing measurement set-up.

5.2.2 Structural characterization

The films morphologies and structures were assessed using a scanning electron microscope (SEM - FEI Nova NanoSEM), while the chemical properties of the films were investigated by X-ray photoemission spectroscopy (XPS) using Thermo K-alpha X-ray source (1486.7 eV) with pass energy of 50 eV. The crystallinity of the WO_3 films were characterized by a D8 Advance Bruker AXS X-ray diffractor with General Area Detector Diffraction System (GADDS) attachment fitted with a 50 μm spot size

collimator, incorporating a High Star 2 dimensional detector and CuKα radiation (λ = 0.1542 nm) operating at 40 kV and 40 mA. The Raman spectroscopies were performed using a 532 nm laser at 0.9 mW power with a PerkinElmer Raman Station 400F.

5.2.3 Gas sensing measurement

During the measurements, the sensors were placed in a gas testing chamber connected to the T95 controller (both from Linkam Scientific Instruments), which was capable of controlling the temperature of the device *via* an external micro heater beneath the sensors. The operating system was accessed through Linksys 32 Software Package enabling the users to quickly enter experimental parameters such as temperature and heating rate. A thermocouple is connected to the stage for measuring the sensor surface temperatures online. Detail of the measurement set-up can be seen in the schematic diagram as presented in Figure 5.1(b). The electrical contact was formed by connecting the needle probes to the Pt electrodes of the sensors. I–V characteristics were measured using a Keithley 2600 current source meter. The gas sensor was supplied with a constant bias current (100 μA) in order to measure the dynamic response of the device when it was periodically exposed to ambient air and the analyte gas (hydrogen/ethanol) with the pulse sequence of 0.06%, 0.12%, 0.25%, 0.50% and 1%. The voltage change was recorded utilizing an Agilent 34410A digital multimeter. The concentration was accurately controlled using a computerized mass flow controller (MFC) multi-channel gas calibration system by changing the synthetic air to analyte gas ratio while maintaining a total constant flow rate of 200 sccm (mL/min).

5.3 Results and discussion

5.3.1 Morphology and structural properties

The SEM images of the as anodized and annealed WO_3 films are presented in Figure 5.2. From the top-view SEM image of the WO_3 layer of Figure 5.2(b, c), it is evident that a highly ordered self-organized three-dimensional (3D) nanoporous layer is formed on the entire surface. This porous layer consists of a very regular structure with pores encapsulated by interconnected walls. The pores have average dimensions in the order of 10 to 30 nm and a pore wall thickness ranging from 10 to 20 nm.

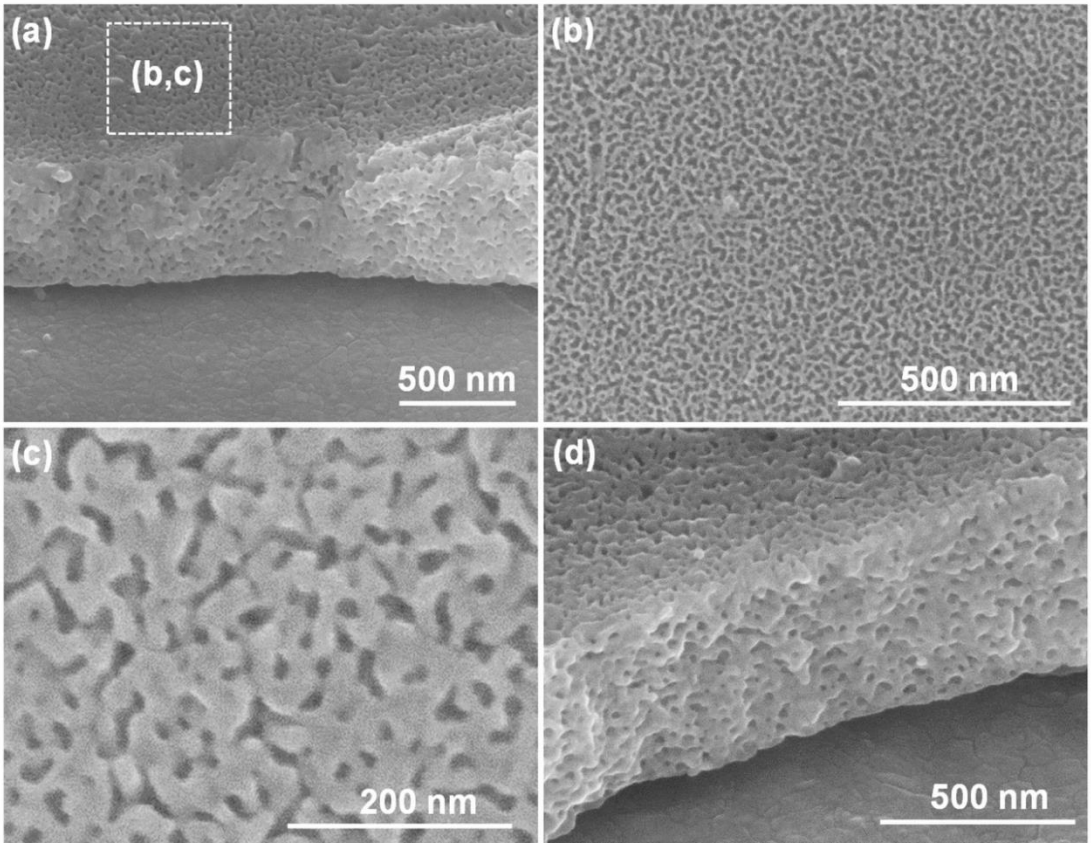

Figure 5.2: SEM images of anodize WO_3 (a) cross sectional view (b) top view (c) a magnified image of the interface in (b) and (d) a magnified image of cross sectional view.

The magnified cross sectional image of WO_3 obtained after anodization at voltage of 10 V for 15 minutes and room temperature presented in Figure 5.2(d) reveals a porous film with the thickness of ~500 nm. The thickness of 500 nm was chosen as Rozina *et al*. have demonstrated that sensing properties can enhance as the thickness of oxide films decreases for anodized oxide films [2]. Thickness below that 500 nm could not be implemented as the short circuit occurred while forming the Schottky contacts.

In order to examine the composition of the porous WO_3 layers, XPS analysis was carried out. Figure 5.3(a) shows the XPS spectra obtained from wide survey scan presenting peaks of W, oxygen (O), nitrogen (N) and carbon (C). Presence of carbon and nitrogen on the surface is attributed to atmospheric contamination. Figure 5.3(b) shows the high resolution core level W 4f spectra of WO_3 films. The binding energies of 35.4 and 37.9 correspond to W $4f_{7/2}$ and W $4f_{5/2}$, respectively, [3] indicating a stoichiometry WO_3 film.

Figure 5.4(a) shows the X-ray diffraction (XRD) patterns of WO_3 films and after annealing. According to the XRD patterns in Figure 4a, the as-anodized nanoporous WO3 film appears to be amorphous (ICDD 04-0806) as only the tungsten peaks exist [4, 5]. The strongest diffraction peaks appear at 23.2, 24.1, 29.5, 33.9, 42.0, 49.5 and 55.5° for the annealed sample. The peaks clearly show the crystalline signature of orthorhombic phase (ICDD 20-1324) WO_3, which is consistent with previous reports [4, 5].

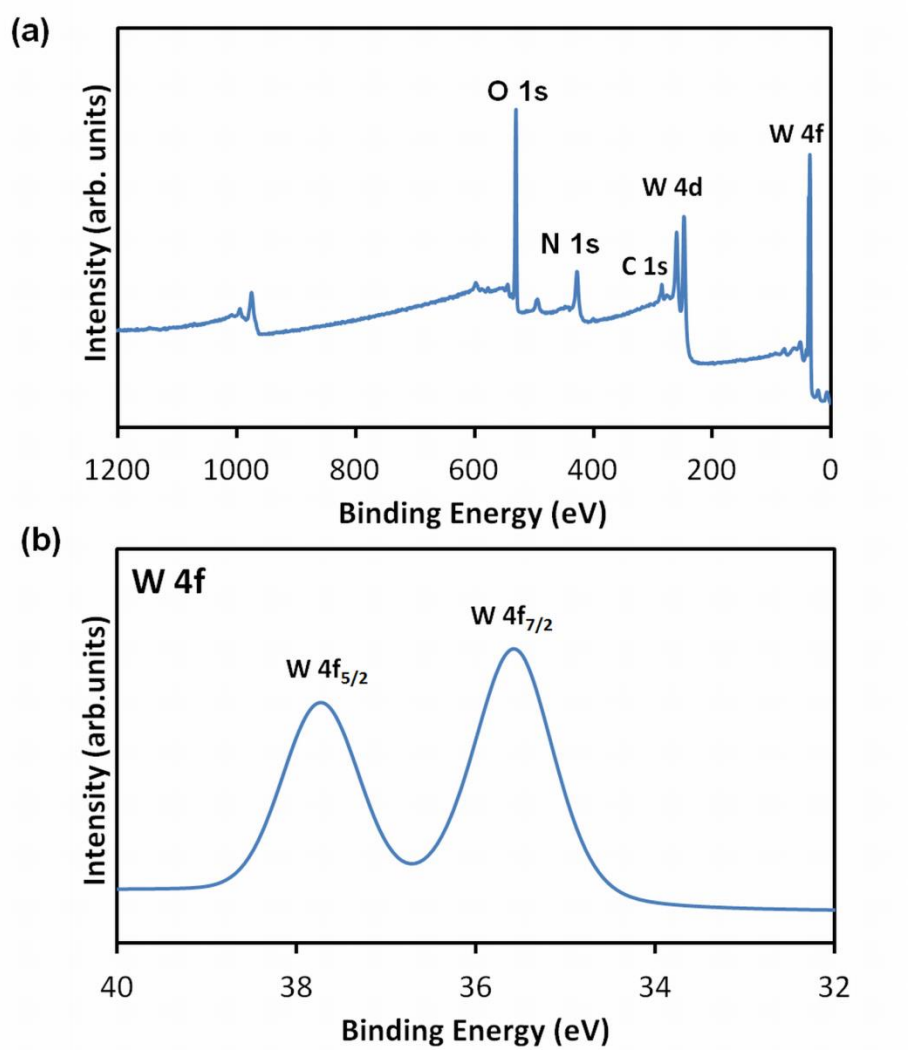

Figure 5.3: (a) The XPS survey scan of nanoporous WO_3 film and (b) XPS spectrum of W 4f peaks of the nanoporous WO_3 film.

This result was further verified by the Raman spectra presented in Figure 5.4(b). The as-anodized WO_3 film exhibited two weak and broad Raman bands centered at 770 and 960 cm^{-1}, respectively. After annealing, new peaks appearing at 807 and 710 cm^{-1} as well as at 134 and 271 cm^{-1}, indicating the O–WO_3 orthorhombic phase of the films [4, 5]. This pattern can be assigned to either monoclinic or orthorhombic phase, as it has been reported that monoclinic phase of WO_3 has a very similar Raman pattern to that of the orthorhombic phase [5]. However, the orthorhombic phase is more likely as it was confirmed by the XRD analysis.

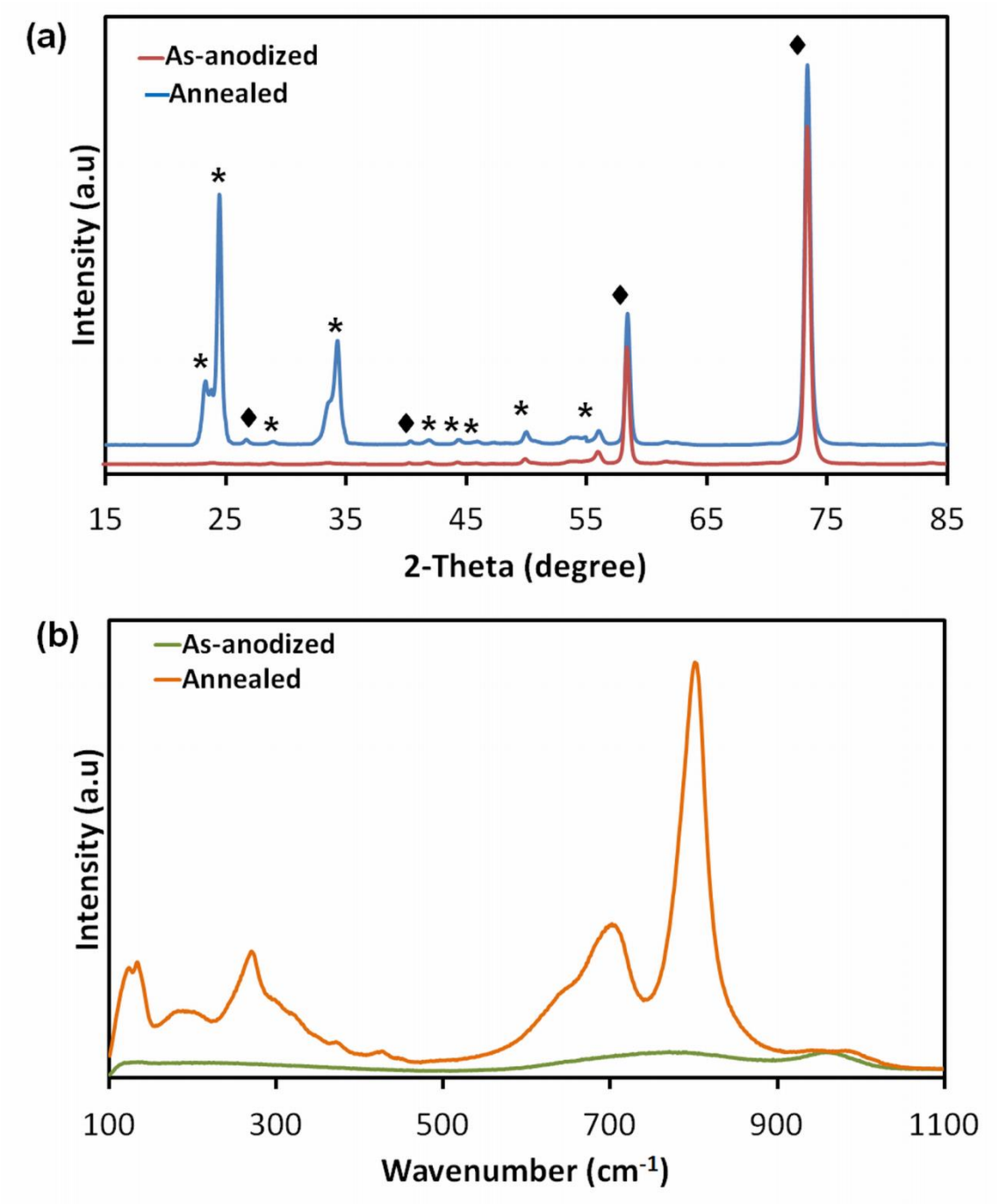

Figure 5.4: (a) (a) The XRD patterns of nanoporous WO_3 film: as-anodized and after annealing in air for 1 hour at 450 °C. The orthorhombic phase (ICDD 20-1324) is denoted by * while the as anodized film is amorphous as only the tungsten peaks exist (ICCD 04-0806) (denoted by ♦) and (b) the Raman spectra of the as-anodized and annealed nanoporous WO_3 films

5.3.2 Gas sensing performances

The current–voltage (I–V) characteristics were obtained in the presence of air alternately with 1% hydrogen gas (Figure 5.5(a)) or ethanol vapour (Figure 5.5(b)), respectively at temperatures ranging from 50 °C to 300 °C.

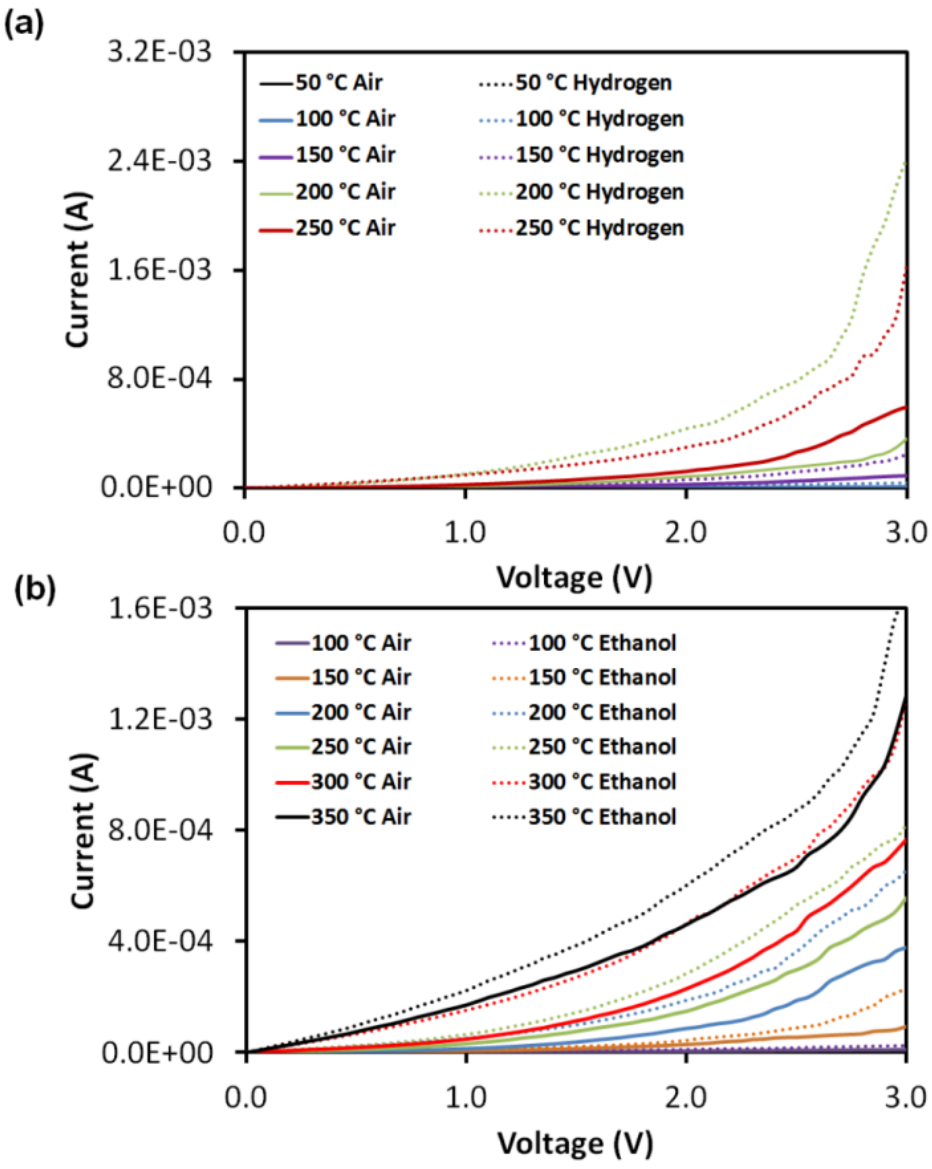

Figure 5.5: (a) The I–V characteristics of the nanoporous WO_3 gas sensor upon exposure to (a) hydrogen gas and (b) ethanol vapour.

As the operating temperature increased, the relative change in the I–V characteristics was observed with a very good non-linear curve. The I–V curve obtained showing a comparatively low current at near room temperature since the charge carriers have insufficient energy to overcome the barrier height energy [47]. However, as the temperature was increased, a larger current flow as result of augmentation in the carrier's energy. The increase in current can also be due to increase of electron-hole pair as the result of higher thermal energy [6-8]. Furthermore, the changes in currents were larger upon exposures to hydrogen gas and ethanol vapour. This is because hydrogen molecules atoms which diffuse and intercalate with WO_3 contributed to the decrease of Schottky barrier height (SBH) [9], which allow the doping of the material and also the formation of dipoles near the junction. The joint effect can result in more carriers with sufficient energies to flow over the lowered barrier easily *via* the thermionic emission mechanism [10, 11]. The mechanism of the gas sensing will be discussed in detail in the following section.

The voltage shift of each sensor is attributed to the reduction of SBH, which can be calculated using the thermionic emission equation. The dependence of forward current on the applied voltage of Schottky diode is given by the expression [7]:

$$I_F = I_s\left\{\exp\left(\frac{qV_F}{kT}\right)-1\right\} \tag{5.1}$$

where I_s, q, V_F, T and k are the saturation current in ampere, charge of one electron in Coulomb, forward applied voltage in volt, absolute temperature in Kelvin and the Boltzmann's constant, respectively. The I_s is defined by:

$$I_s = AA^{**}T^2\exp\left(-\frac{q\Phi_B}{kT}\right) \tag{5.2}$$

in which A is the diode area in m^2, A** is the Richardson constant and Φ_B is the Schottky barrier height in eV. Using equation [5.2], the SBH can be determined. The SBH change in hydrogen, $\Delta\Phi_{B(H_2)} = \Phi_{B(H_2)} - \Phi_{B(Air)}$ or SBH change in ethanol, $\Delta\Phi_{B(Eth)} = \Phi_{B(Eth)} - \Phi_{B(Air)}$ at different temperatures were calculated and shown in Table 5.1.

Table 5.1
Barrier height change at different temperatures.

Temperature	Barrier height change (eV)	
(°C)	$\Delta\Phi_{B(H_2)}$	$\Delta\Phi_{B(Eth)}$
50	0.029	0.011
100	0.039	0.018
150	0.047	0.022
200	0.065	0.028
250	0.035	0.032
300	-	0.041
350	-	0.033

As can be seen from Figure 5.5, the largest lateral voltage shift of the sensor towards hydrogen gas was observed at 200 °C, while for the exposure towards ethanol vapour, the largest voltage shift occurred at 300 °C. It is suggested that, ethanol vapour dissociated by catalytic metals at higher temperatures as compared to hydrogen. Optimum operating temperature for the maximum voltage shift of hydrogen being lower compared to ethanol agrees well with the other previously reported Schottky-based sensors [2, 12, 13].

As the largest lateral voltage shifts upon exposure to hydrogen and ethanol were observed at 200 and 300 °C, respectively, the dynamic responses of the sensor were investigated at these temperatures. The dynamic responses of the sensor with the constant bias current of 100 μA towards different concentrations of hydrogen gas and

ethanol vapour, in air background, are shown in Figure 5.6(a) and (b). The device demonstrated a very good response to hydrogen and ethanol at its respective optimum temperature, where the sensor's output returns to the baseline after recovery.

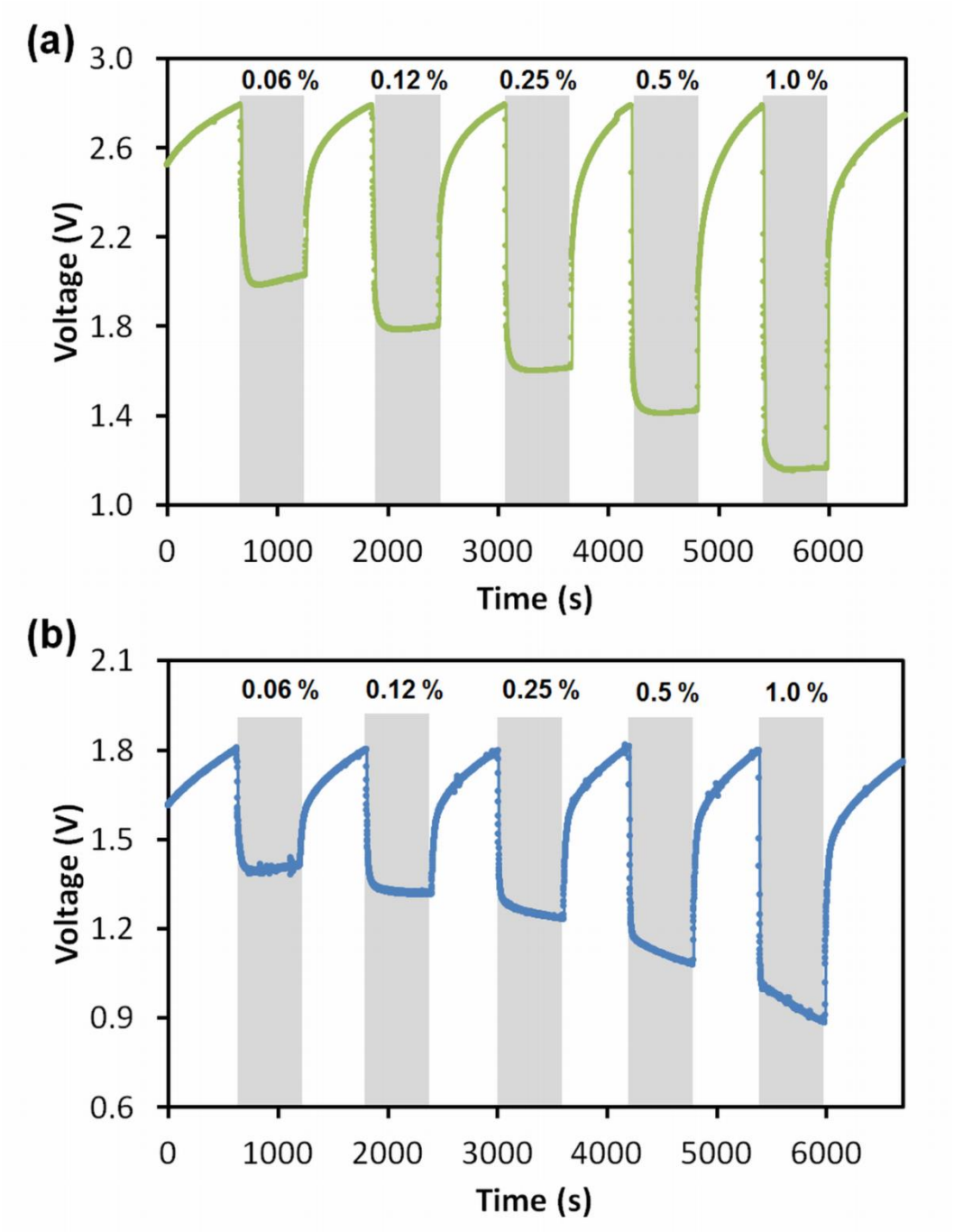

Figure 5.6: (a) The dynamic response of nanoporous WO_3 gas sensors measured with different concentrations of (a) hydrogen gas at 200 °C and (b) ethanol vapour at 300 °C with a constant bias current of 100 μA.

The stability of the sensor was investigated by repeatedly switched from air to 1 % hydrogen over a few cycles and presented in Figure 5.7. The sensor was found to have stable response and recovery characteristics, indicating high repeatability and stability were achieved. The measurements were all conducted in no humidity environment. Humidity will certainly deteriorate the response of the device as reported previously [12, 14].

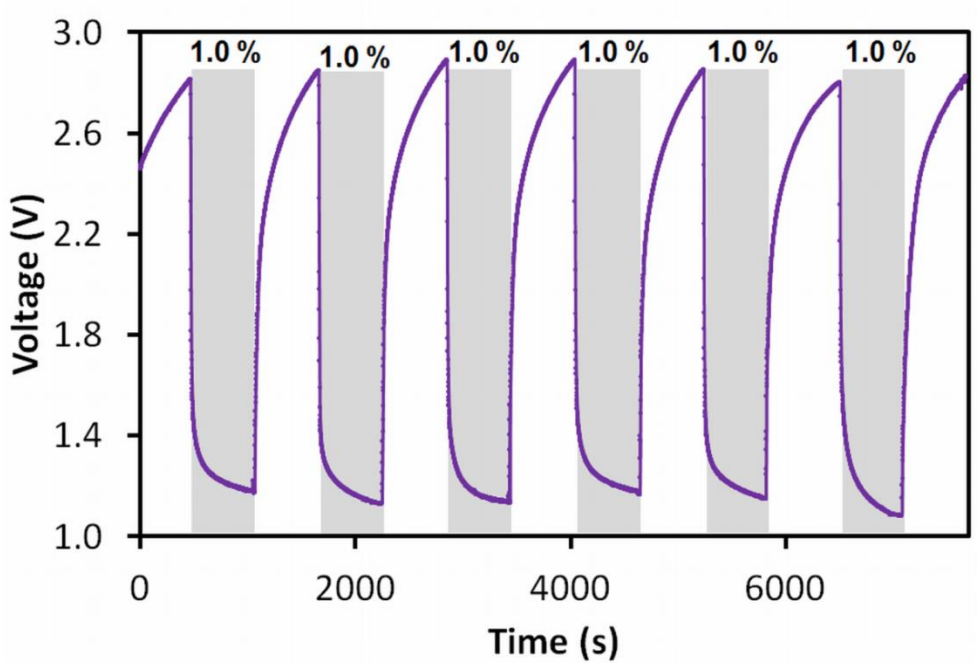

Figure 5.7: Sensors' repeatability of the sensor upon exposure to hydrogen gas at 200 °C for 6 cycles.

The voltage shift towards both hydrogen gas and ethanol vapour *vs* their different concentrations are presented in Figure 5.8. Voltage shift of 0.77, 0.99, 1.18, 1.38 and 1.63 V were measured for 0.06, 0.125, 0.25, 0.5 and 1 % hydrogen gas, respectively. However, the same set of ethanol vapour concentration resulted in smaller voltage shift which are 0.4, 0.46, 0.55, 0.68 and 0.79 V, respectively, as discussed previously. As the concentration of the hydrogen gas or ethanol vapour increases, more hydrogen

molecules will be adsorbed on the Pt catalytic surface. Consequently, a lower barrier height was observed resulting higher voltage shift. Additionally, it can be clearly seen that the sensor is more sensitive to hydrogen as compared to ethanol.

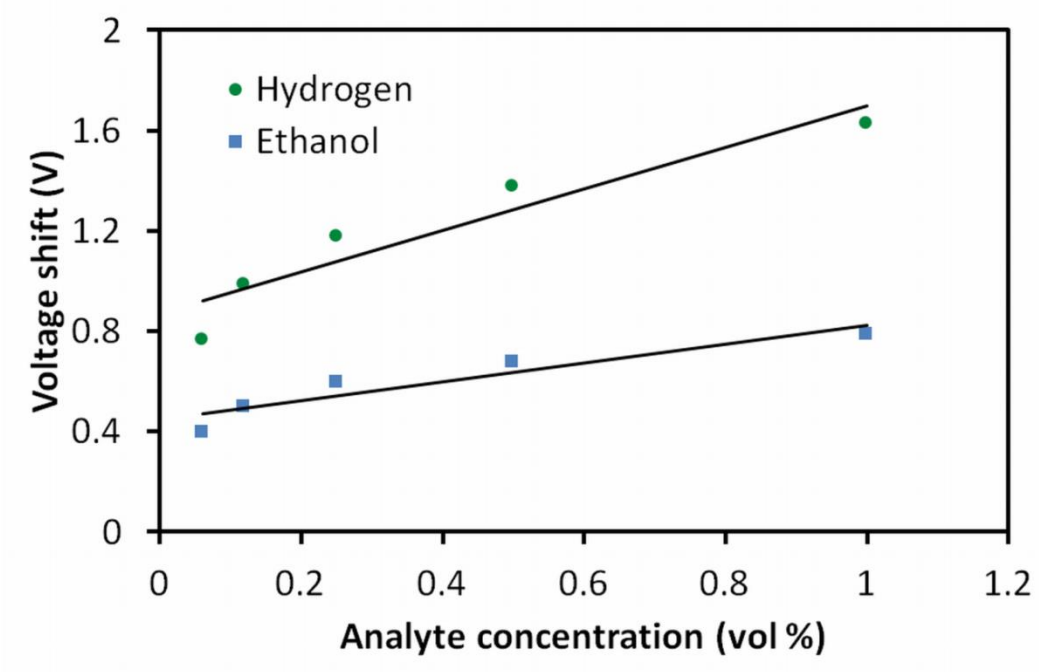

Figure 5.8. Voltage shifts of nanoporous WO_3 gas sensors at different concentrations of target gas.

The PhD candidate further evaluated the performance of the WO_3 gas sensor in terms of the response and recovery time. The response time is defined as the time for 90% of the total voltage change. Conversely, the recovery time is the time for 90% recovery of the total voltage change. Response and recovery time were obtained for the nanoporous WO_3 Schottky diode sensor when exposed alternately to synthetic air with a hydrogen or ethanol balance concentration in the order of 0.06 - 1% and shown in Table 5.2. The sensor's recovery time is about 4 times longer than the response time. The same trend of response and recovery time of other nanoporous metal oxide gas sensors have been reported where the recovery time is generally longer than response

time upon exposure to varieties of analyte [2, 15]. As the concentration of gas analyte increases, faster response is demonstrated. Conversely, the recovery time increases as the gas analyte concentration increase. It is suggested that, at higher concentrations of the target gas, a larger number of target gas molecules dissociate onto catalytic metal and adsorb inside the porous film [16]. As a result, faster response is observed as compared to response of target gas at lower concentration. However, purging the target gas out from the nanoporous films takes longer time as the concentration of the target gas in the films results in a deeper stoichiometry changes within the films, which requires longer recovery time to return to its initial condition.

Table 5.2
Response and recovery time of the sensor at different analyte concentrations.

Analyte concentration (vol %)	Hydrogen		Ethanol	
	Response time (s)	Recovery time (s)	Response time (s)	Recovery time (s)
0.06	43	108	55	128
0.12	38	111	42	139
0.25	29	124	32	153
0.5	23	151	27	172
1.0	20	180	25	185

Shorter response time is observed upon hydrogen exposure in comparison with response to ethanol. Hydrogen gas dissociated directly to produce hydrogen ions, while ethanol vapour needs an additional dehydrogenation step where ethanol dissociated into ethoxides and acetaldehyde before generates the hydrogen ions [17, 18]. Thus, the device demonstrated longer response time upon ethanol vapour exposure.

The mechanism of the nanoporous WO_3 gas sensor is further discussed. Dissociative chemisorption of molecular hydrogen onto Pt, forming hydrogen ions (H^+) and electrons charge (e^-) is described as [19]:

$$H_2(g) \rightarrow 2H^+ + 2e^- \quad (5.3)$$

Similarly, on the catalyst surface, ethanol molecules start to dissociate into ethoxides and further oxidize into acetaldehyde as in equation (4) and (5) when the temperature increases [20]:

$$C_2H_5OH(g) \rightarrow CH_3CH_2O + H(a) \quad (5.4)$$

$$C_2H_5O(a) \rightarrow CH_3CHO(g) + H(a) \quad (5.5)$$

in which (g) and (a) stand for the gaseous and adsorbed species, respectively. The H atoms produced from equation (5.4) and (5.5) are further broken down to H^+ and an electron e^- , resulting in adsorbed H^+.

The accumulated absorbed H^+ ions from equation (5.3) to (5.5) further spills through the catalytic metal and intercalate with WO_3 pore wall that can be described according the following formula [21]:

$$WO_3 + xH^+ + xe^- \leftrightharpoons H_xWO_3 \quad (5.6)$$

The released electrons in equation (5.6) reduce the length of the depletion region in the oxide film, which decreases the resistance of the film and also the barrier height that corresponds to the voltage shift for the gas sensor [19].

As the system is maintained at an elevated temperature, it is also possible that H_xWO_3 breaks down into reduced WO_3 producing H_2O vapour [22].

$$2H_xWO_3 \leftrightharpoons xH_2O + 2WO_{3-x/2} \quad (5.7)$$

Exposing the sensors back to air (oxygen rich environment) the reduced oxide restores its stoichiometry to form WO_3.

$$WO_{3-x/2} + (x/4)O_2 \leftrightharpoons WO_3 \quad (5.8)$$

This allows the repeatability of the gas sensor.

5.4 Summary

In this chapter, the PhD candidate presented her investigations on highly ordered nanoporous WO_3 Schottky-based gas sensor synthesized *via* electrochemical anodization of W. Pt was deposited as a Schottky forming contact, which also provided catalytic properties for sensing hydrogen gas and ethanol vapor. The structural properties of WO_3 films were investigated using SEM, XRD, XPS and Raman spectroscopy demonstrating the existence of an orthorhombic crystal phase made of pores in the order of 10 to 30 nm in dimensions. The Pt/WO_3 Schottky-based gas sensor was tested towards hydrogen and ethanol molecules in gaseous environments. The porosity of WO_3 structure resulted in a high surface to a volume ratio sensitive film that facilitated the gas molecules adsorption/desorption. Gas sensing measurements for the device exhibited the best performance towards hydrogen obtaining a voltage shift of 1.67 V for 1% hydrogen, when the device was biased at a current of 100 μA and operated at 200 °C. The WO_3 nanoporous Schottky gas sensor also produced good reproducibility and repeatable responses with a stable baseline.

In the next chapter, the author will present the summary and concluding remarks of her PhD thesis. In addition, the author will highlight her achievements and elaborate on the future outlooks for this research.

References

[1] H. Zheng, A. Z. Sadek, K. Latham, and K. Kalantar-Zadeh, "Nanoporous WO_3 from anodized RF sputtered tungsten thin films," *Electrochem. Commun.,* vol. 11, pp. 768-771, 2009.

[2] R. A. Rani, A. S. Zoolfakar, J. Z. Ou, M. R. Field, M. Austin, and K. Kalantar-zadeh, "Nanoporous Nb_2O_5 hydrogen gas sensor," *Sens. Actuators B Chem.,* vol. 176, pp. 149-156, 2013.

[3] J. Z. Ou, M. H. Yaacob, M. Breedon, H. D. Zheng, J. L. Campbell, K. Latham, *et al.*, "In situ Raman spectroscopy of H_2 interaction with WO_3 films," *Phys. Chem. Chem. Phys.,* vol. 13, pp. 7330-7339, 2011.

[4] K. Kalantar-zadeh, A. Vijayaraghavan, M.-H. Ham, H. Zheng, M. Breedon, and M. S. Strano, "Synthesis of atomically thin WO_3 sheets from hydrated tungsten trioxide," *Chem. Mater.,* vol. 22, pp. 5660-5666, 2010.

[5] J. Z. Ou, R. A. Rani, S. Balendhran, A. S. Zoolfakar, M. R. Field, S. Zhuiykov, *et al.*, "Anodic formation of a thick three-dimensional nanoporous WO_3 film and its photocatalytic property," *Electrochem. Commun.,* vol. 27, pp. 128-132, 2013.

[6] J. P. Xu, P. T. Lai, D. G. Zhong, and C. L. Chan, "Improved hydrogen-sensitive properties of MISiC Schottky sensor with thin NO-grown oxynitride as gate insulator," *IEEE Electron Device L.,* vol. 24, pp. 13-15, 2003.

[7] S. M. Sze and K. K. Ng, *Physics of semiconductor devices*, 3rd ed. John Wiley & Sons, Inc: Hoboken, NJ, USA, 2007.

[8] M. Shafiei, J. Yu, R. Arsat, K. Kalantar-zadeh, E. Comini, M. Ferroni, *et al.*, "Reversed bias Pt/nanostructured ZnO Schottky diode with enhanced electric field for hydrogen sensing," *Sens. Actuators B Chem.,* vol. 146, pp. 507-512, 2010.

[9] I. Lundström, S. Shivaraman, C. Svensson, and L. Lundkvist, "A hydrogen−sensitive MOS field−effect transistor," *Appl. Phys. Lett.*, vol. 26, pp. 55-57, 1975.

[10] S. Pitcher, J. A. Thiele, H. Ren, and J. F. Vetelino, "Current/voltage characteristics of a semiconductor metal oxide gas sensor," *Sens. Actuators B Chem.*, vol. 93, pp. 454-462, 2003.

[11] T.-H. Tsai, J.-R. Huang, K.-W. Lin, W.-C. Hsu, H.-I. Chen, and W.-C. Liu, "Improved hydrogen sensing characteristics of a Pt/SiO_2/GaN Schottky diode," *Sens. Actuators B Chem.*, vol. 129, pp. 292-302, 2008.

[12] R. A. Kadir, R. A. Rani, A. S. Zoolfakar, J. Z. Ou, M. Shafiei, W. Wlodarski, *et al.*, "Nb_2O_5 Schottky based ethanol vapour sensors: Effect of metallic catalysts," *Sens. Actuators B Chem.*, vol. 202, pp. 74-82, 2014.

[13] L.-L. Xing, B. He, Z.-H. Chen, and X.-Y. Xue, "Schottky barrier and catalytic effect induced high gas sensing of one-step synthesized Pd-SnO_2 nanorods," *Solid State Sci.*, vol. 15, pp. 42-46, 2013.

[14] L. Talazac, F. Barbarin, C. Varenne, L. Mazet, S. Pellier, and C. Soulier, "Gas sensing properties of pseudo-Schottky diodes on p-type indium phosphide substrates - Application to O_3 and NO_2 monitoring in urban ambient air," *Sens. Actuators B Chem.*, vol. 83, pp. 149-159, 2002.

[15] G. Yamamoto, T. Yamashita, K. Matsuo, T. Hyodo, and Y. Shimizu, "Effects of polytetrafluoroethylene or polyimide coating on H_2 sensing properties of anodized TiO_2 films equipped with Pd–Pt electrodes," *Sens. Actuators B Chem.*, vol. 183, pp. 253-264, 2013.

[16] Y. Liu, J. Yu, and P. T. Lai, "Investigation of WO_3/ZnO thin-film heterojunction-based Schottky diodes for H_2 gas sensing," *Int. J. Hydrogen Energ.*, vol. 39, pp. 10313-10319, 2014.

[17] M. Ivanovskaya, D. Kotsikau, G. Faglia, P. Nelli, and S. Irkaev, "Gas-sensitive properties of thin film heterojunction structures based on Fe_2O_3-In_2O_3 nanocomposites," *Sens. Actuators B Chem.,* vol. 93, pp. 422-430, 2003.

[18] G. Han, Q. Lu, G. Liu, X. Ye, S. Lin, Y. Song, *et al.*, "Enhanced ethanol sensing properties based on α-Fe_2O_3/In_2O_3 hollow microspheres," *J. Mater. Sci-Mater. El,* vol. 23, pp. 1616-1620, 2012.

[19] T. Hübert, L. Boon-Brett, G. Black, and U. Banach, "Hydrogen sensors – A review," *Sens. Actuators B Chem.,* vol. 157, pp. 329-352, 2011.

[20] B. A. Sexton, K. D. Rendulic, and A. E. Huges, "Decomposition pathways of C_1-C_4 alcohols adsorbed on platinum (111)," *Surf. Sci.,* vol. 121, pp. 181-198, 1982.

[21] J. Z. Ou, S. Balendhran, M. R. Field, D. G. McCulloch, A. S. Zoolfakar, R. A. Rani, *et al.*, "The anodized crystalline WO_3 nanoporous network with enhanced electrochromic properties," *Nanoscale,* vol. 4, pp. 5980-5988, 2012.

[22] M. H. Yaacob, M. Breedon, K. Kalantar-zadeh, and W. Wlodarski, "Absorption spectral response of nanotextured WO_3 thin films with Pt catalyst towards H_2," *Sens. Actuators B Chem.,* vol. 137, pp. 115-120, 2009.

Chapter 6

Conclusion and Future Works

6.1 Concluding remarks

The PhD candidate commenced her PhD research with the vision of creating novel gas sensing devices with enhanced performance based on selected nanoporous and nanotubular (filled or empty tubes) metal oxide films. The author chose electrospinning and anodization methods in order to produce desired nanostructures that enabled remarkable enhancement in their sensing properties as shown in the previous chapters of this thesis.

In the course of carrying out this research, the author investigated and critically assessed numerous literatures on semiconductor metal oxide gas sensors. Upon this critical review and analysis, the PhD candidate chose to focus on metal oxides with nanoporous and nanotubular morphologies. These morphologies were selected due to the fact that they could naturally provide the best pathways for the diffusion of gas molecules in and out of the sensitive films and also their continuous structures along the nano-walls could enable the facile passage of free carrier charges for fast response and highly sensitive performance of the sensors. SnO_2, Nb_2O_5 and WO_3 were chosen as the target sensitive metal oxide films.

SnO_2 was identified as the most common gas sensitive metal oxide, also as an invaluable platform for benchmarking. The author demonstrated that she could greatly control the synthesis of nanotubular fiber morphologies of SnO_2. These nanofibers with granular walls and controlled oxygen vacancies were synthesized by electrospinning using a cocktail of solutions containing stannous chloride, polyvinyl pyrrolidone,

polyacrylonitrile and dimethylformamide. The electrospun nanofibers applied as sensing layers and were proved to offer significant enhancement in the operation of SnO_2 based gas sensors by reducing their operating temperatures.

The PhD candidate focused on the anodization procedures to create nanoporous Nb_2O_5 films. These sensing films were synthesized by anodizing Nb foils at elevated temperatures using ethylene glycol and ammonium fluoride as the electrolyte, which resulted in highly nanoporous Nb_2O_5 structures. She investigated the concept of ethanol vapour Schottky-based gas sensors by depositing a thin layer of platinum layer with a dual functionality; as a catalyst and Schottky establishing contact.

Next, the author of this thesis, for the first time, presented the idea of intercalating ionic species generated from gas molecule interactions with Nb_2O_5 films. She used modified anodization parameters with the intention of accelerating the etching process and obtaining more robust and high density nanoporous films. The anodization process of Nb film sputtered on FTO glass was carried out in glycerol mixed with dipotassium phosphate at a high temperature. The PhD candidate showed that the interaction with hydrogen containing gas species could efficiently modulate anodized Nb_2O_5 films' transparency. Hence, the system could be used as an optical gas sensor.

The PhD candidate conducted research on nanoporous WO_3 based systems, as the final section of the thesis. Gas sensors were developed based on the Schottky contacts of WO_3 and used for gas sensing that had not been demonstrated before. The sensing films were synthesized *via* anodization of W foils at room temperature. The author of this thesis successfully developed nanoporous WO_3 Schottky-based ethanol and hydrogen sensors and presented their unique advantages over previously reported works based on nanoporous WO_3.

In order to achieve the objectives of this PhD research, the candidate divided her investigation into four stages. The major findings of each stage are summarized as follows:

6.1.1 Stage 1

- In the first stage, the author demonstrated electrospin synthesis process for the fabrication of SnO_2 nanofibers. The electrospinning process resulted in nanofibers with corrugated surface composed of many aggregated grains that contained significant oxygen vacancies.
- Nanofibers with different morphologies and diameters could be achieved by manipulating the applied stirring speed of pre-cursor solutions.
- The author assessed their gas sensing performance and found that nanofibers with the smallest diameter, containing the highest oxygen vacancies, demonstrated the best sensing capability at low operating temperatures.

6.1.2 Stage 2

- In the second stage, the PhD candidate sought to investigate the potential of nanoporous Nb_2O_5 films which were fabricated *via* anodization as ethanol Schottky-based gas sensing devices. The author showed that nanoporous sensing films greatly enhanced sensing performances.
- The author focused her investigation on the effect of catalytic metals on sensing performances. The catalytic metals such as Pt, Pd and Au were chosen in this study due to their relatively large work function in comparison with Nb_2O_5.

- The author found that sensing device equipped with a Pd catalyst demonstrated the highest sensitivity as well as relatively short response and recovery times as compared to the devices equipped with Pt and Au catalysts.
- The excellent performance of the Pd–Nb_2O_5 gas sensor was attributed to the properties of Pd catalyst allowing efficient breakdown of ethanol molecules and better solubility of the H atoms, in comparison to Pt and Au.
- The author also demonstrated the selectivity of the developed sensing device towards hydrogen and methane. It was found that, the sensor exhibited a strong selectivity to ethanol and hydrogen and was less sensitive to methane.

6.1.3 Stage 3

- Despite being widely used as electrochromic devices, the potential of Nb_2O_5 nanoporous for optical gas sensing was less investigated. The author postulated that Nb_2O_5 nanoporous could potentially be used as an optical gas sensing system due to its intercalation capability. Hence, for the first time, the PhD candidate developed optical gas sensing devices based on nanoporous Nb_2O_5 films.
- Nanoporous Nb_2O_5 with a large surface-to-volume ratio coated with a thin layer of Pt provides enhanced pathways for efficient hydrogen adsorption and dissociation.
- The presence of a thin Pt layer facilitated the dissociation of hydrogen gas molecules into H^+ ions from the hydrogen gas. The H^+ ions further intercalated into the nanoporous films, thereby resulted in an energy bandgap change of the material that induced an optical response.

- The author found that the devices demonstrated excellent absorbance changes at 100 °C with a response factor of 12.1 % at 1% hydrogen in ambient air, as well as a rapid response and recovery.

6.1.4 Stage 4

- In this final stage, the PhD candidate for the first time developed nanoporous WO_3 Schottky-based gas sensors. The nanoporous films obtained by an anodization method provided a high surface-to-volume ratio, enhancing the gas adsorption and desorption.
- The PhD candidate investigated the performance of nanoporous WO_3 Schottky-based gas sensors in the presence of ethanol vapour and hydrogen gas.
- Analysis of the current–voltage characteristics and dynamic responses of the sensors indicated that these devices were more sensitive to hydrogen gas compared to ethanol vapour at an optimum operating temperature of 200 °C.
- The WO_3 nanoporous Schottky gas sensors also produced good reproducibility and repeatable responses with stable baselines.

6.2 Journal publications

The work conducted by the author of this dissertation during her candidature resulted in four journal publications, as the first author, and four as the co-author. The list of author's scientific manuscripts is as follows:

1. **R. Ab Kadir**, R. A. Rani, A. S. Zoolfakar, J. Z. Ou, A.F. Chrimes, A. Z. Sadek and K. Kalantar-zadeh, "Electrospun granular hollow SnO_2 nanofibers

hydrogen gas sensors operating at low temperatures", *The Journal of Physical Chemistry C*, 2014, 118, 3129-3139.

2. **R. A. Kadir**, R. A. Rani, A. S. Zoolfakar, J. Z. Ou, M. Shafiei, W. Wlodarski, *et al.*, "Nb_2O_5 Schottky based ethanol vapour sensors: Effect of metallic catalysts," *Sensor and Actuators B: Chemical*, 202 (2014), pp. 74-82.
3. **R. Ab Kadir**, R. A. Rani, Manal M. Y. A. Alsaif, J. Z. Ou, W. Wlodarski, A. P. O'Mullane and K. Kalantar-zadeh, "Optical gas sensing properties of nanoporous Nb_2O_5", *ACS Applied Materials & Interfaces*, 2014
4. **R. Ab Kadir**, Wei Zhang , J. Z. Ou, W. Wlodarski, A. P. O'Mullane and K. Kalantar-zadeh, "Anodized Nanoporous WO_3 Schottky Contact Structure for Hydrogen and Ethanol Sensing", *Journal of Materials Chemistry A*, 2014 – under review
5. S. Zoolfakar, **R. Ab Kadir,** R. A. Rani, S. Balendhran, X. Liu, E. Kats, S. K. Bhargava, M. Bhaskaran, S. Sriram, S. Zhuiykov, A. P. O'Mullane and K. Kalantar-zadeh, "Engineering electrodeposited ZnO films and their memristive switching performance", *Physical Chemistry Chemical Physics*, 2013, 15, 10376-10384.
6. R. A. Rani, A. S. Zoolfakar, J. Z. Ou, **R. Ab. Kadir**, H. Nili, K. Latham, S. Sriram, M. Bhaskaran, S. Zhuiykov, R. B. Kaner and K. Kalantar-zadeh, "Reduced impurity-driven defect states in anodized nanoporous Nb_2O_5: the possibility of improving performance of photoanodes", *Chemical Communications*, 2013, 49, 6349-6351.
7. M.Z. Ahmad, A. Wisitsoraat, A.S. Zoolfakar, **R.A. Kadir**, W. Wlodarski, "Investigation of RF sputtered tungsten trioxide nanorod thin film gas sensors

prepared with a glancing angle deposition method toward reductive and oxidative analytes," *Sensors and Actuators B: Chemical*, 183(2013) 364-71.

8. S. Walia, S. Balendhran, Y. Wang, **R. Ab Kadir**, A. Sabirin Zoolfakar, P. Atkin, et al., "Characterization of metal contacts for two-dimensional MoS_2 nanoflakes," *Applied Physics Letters*, 103(2013).

6.3 Recommendations for future works

Significant advancement in the field of gas sensing materials has been achieved during the course of this PhD project. However the PhD candidate has identified few other opportunities for expanding this research. In alignment with those presented in this thesis, the author recommends the followings as future works:

- The sensing devices based on electrospun SnO_2 nanofibers presented in Chapter 2 have shown to operate at 150 °C. However it is worthy to investigate the doping effect on the sensing performances. By doping the nanofibers with Pt, Pd or Au it is believed that the operating temperature of the devices will reduce significantly.
- It has been demonstrated that by controlling the volume of the precursor solutions and the stirring speed, morphology and stoichiometry of the nanofibers can be tailored. There are possibilities to produce different structures of nanofibers that will improve sensor performance by introducing different polymers in the precursor solutions as well as further adjusting electrospinning parameters.
- As presented in Chapter 3, the anodized nanoporous Nb_2O_5 Schottky-based gas sensors demonstrated remarkable performance in the presence of reducing gas

species (H_2, C_2H_5OH and CH_4). It is known that the response of oxidizing gases (NO and NO_2) is opposite to that of reducing gas species. However, the oxidizing gases don't produce any intercalation effect and the overall response behaviour is still unknown. The investigation of the gas sensor in the presence of oxidizing gas was not possible in the time frame of this thesis. Consequently, it is suggested to further study the sensing performance of the devices in the presence of oxidizing gases.

- As presented in Chapter 4, the PhD candidate observed the changed of optical absorption properties of Nb_2O_5 films due to the intercalation of H^+ ions into the nanoporous films. There are two widely accepted models for describing this response behaviour. The first one is due to the H^+ intercalation called "double injection model" and the second one is due to the stoichiometry change of the films. Hence, the PhD candidate suggests for further investigation on the composition of the final products after the interaction with H_2 gas using spectroscopic and diffraction techniques to reveal the actual model of nanoporous optical sensing mechanisms.
- Furthermore, the Nb_2O_5 nanoporous optical gas sensor films presented in Chapter 4 incorporated a thin layer of Pt catalyst to facilitate gas dissociation onto the sensitive layers. Different types of catalysts should be employed for future investigations.
- As presented in Chapter 5, nanoporous WO_3 Schottky-based gas sensors demonstrated good performances in the presence of hydrogen gas and ethanol vapour. The sensing responses were associated to the intercalating H^+ species that were generated as the result of the hydrogen and ethanol molecules breakdowns onto Pt/WO_3 contact. Therefore, it is beneficial to investigate the

effect of H^+ intercalation in the WO_3 nanoporous films and observe the changes in its optical responses. It is believed that, the utilizations of nanoporous WO_3 films can produce superior optical gas sensors, owing to the highly ordered structures that provide continuous pathways for fast transfer of electrons.

- It is also beneficial to investigate plasmonic resonance effects of nanoporous WO_3 films under different gas environments such as different volatile organic compounds, carbon oxides and hydrocarbons. The selectivity for various gases can be tuned by adjusting the stoichiometry of the films. The outcomes of this investigation can be potentially used for developing gas sensors with multi-gas detection abilities.